UNIVERSITY OF CAPE TOWN
IYUNIVESITHI YASEKAPA • UNIVERSITEIT VAN KAAPSTAD

VIBRATION BASED PERFORMANCE ASSESSMENT OF CONCRETE-CONCRETE COMPOSITE BRIDGES

By

BONGANI SIBANDA

Submitted in partial fulfillment of the requirements for the degree

MSc Eng

In the

DEPARTMENT OF CIVIL ENGINEERING

FACULTY OF ENGINEERING AND BUILT ENVIRONMENT

Supervisor: A/Prof P Moyo
Co-supervisor: Dr H D Beushausen

January 2009

DECLARATION

I know the meaning of plagiarism and declare that all of the work in the document, save for that which is properly acknowledged, is my own. I also affirm that this work has not been submitted in this, or any other university for examination, or for any other purposes.

Signature..... Date 16/01/2009

Signed by candidate

This study is dedicated to my family: Freddy, Vusa, Cliff, Charles, Mnce, Ntando and Nto for their personal sacrifices

ACKNOWLEDGEMENTS

Praise the Lord for His ever-abundant blessings and love.

The author acknowledges the following:

My supervisors, A/Prof Moyo and Dr Beushausen for the guidance, support and assistance during this study. Prof Oosthuizen and Phillip Ronne' for providing technical advice and support. Charles Nicholas, Theo Moyana, Elvino, Charles May and all the workshop and concrete lab staff, many thanks for the assistance in construction of the model and providing the much needed technical support. My warmest gratitude goes to Elly Yelverton for the motherly support she always provided. The author is also grateful to the following students for their constructive ideas throughout the study: Crispen Masuku, Goitseone Malumbela, Mike Otien , Rachel Muigai, Mmusi Mompati, David Ochan and Kungu Githachuri. I am also thankful to my girlfriend Cecilia Mpofu for the many times she assured me to have faith in myself and to keep going and never give up.

The author also acknowledges the Department of Civil Engineering for the financial assistance provided throughout the study.

ABSTRACT

Concrete composites consisting of precast pre-stressed standardized beams and a cast *in-situ* deck slab have been used for the construction of short to medium span bridges for the past four decades in South Africa and worldwide. The pre-cast beams and cast *in-situ* slab are commonly connected using shear connectors. Failure of these connectors would compromise the composite action of the structure, thus reducing the load carrying capacity and hence its efficiency. This study seeks to assess the integrity of such shear connectors using dynamic testing and Finite Element (FE) analysis. The main objective of the work is to assess the practicality of vibration-based techniques to detect damaged shear connectors using experimental and analytical modal data. A scaled bridge model was constructed and 10 mm bolts connetcted the beams and slab to simulate shear connectors in the prototype bridge. Different damage scenarios were introduced by loosening some of the connectors and vibration testing was done to detect the artificial damage. An FE model of the system was also developed. The shear connectors were modeled as non-linear spring elements capable of simulating the composite action between the slab and beams. Damage of shear connectors was simulated by reducing the spring stiffness. The updating of the FE model was done manually by adjusting appropriate spring stiffnesses.

The experimental and analytical results show that the natural frequencies are sensitive to this damage. The frequencies dropped from undamaged to severe damaged structure. Very little information was deduced from the damping ratios, modal assurance criteria (MAC) and coordinate modal assurance criteria (COMAC) values. The experimental and analytical first bending, torsion and transverse modes were sensitive to the damaged shear connectors. 65% of damaged connectors were located using these modes. Using experimental modal data, the mode curvatures and flexibility changes were able to locate the damaged region when more than 35% of shear connectors were loosened. However, using numerical data, the mode curvatures and flexibility changes were able to localize the damaged region for 6% damage introduced. 75% of the loosened connectors were identified. The stiffness change technique could only identify less than 10% of damaged shear connectors using experimental modal

data. The same technique was applied on analytical data and over 75% of damaged shear connectors were located.

The FE modeling of shear connectors used in this work was applied on an existing bridge. Van der Kloof bridge (South Africa) was constructed using precast pre-stressed beams and a cast *in-situ* slab. Extended beam web stirrups were used as shear connectors. The main aim was to develop a robust FE model for this bridge that could be used in future to investigate the condition of shear connectors. Using 6-D non-linear spring elements to model the shear connectors, a maximum difference of 0.98% was observed between the measured and theoretical frequencies after manual updating. This is quite a small difference. This model could therefore be used as a true representative of the physical structure for future investigations.

TABLE OF CONTENTS

LIST OF TABLES

LIST OF FIGURES

CHAPTER 1

INTRODUCTION

1.1 Background

Bridges constitute significant and critical components of transportation systems and are among the most expensive investment asset of any country's infrastructure. However, there is a growing number of deteriorated bridge structures owing to ageing of these structures (Parkash *et al*, 2006; Jin *et al*, 2008). Seracino *et al*, 2004 state that bridges are now subjected to increased stresses as they convey larger volumes of traffic and heavier loads for which they were not designed. This is due to growth of the economy in most countries, hence increase in axle loads (Brownjohn *et al*, 2003; Parkash *et al*, 2006). In South Africa it was estimated, in the year 2000, that the annual cost of overload road damage was R650 million and the accrued backlog for the upgrading, maintenance and repair of the over 13000 bridges was R37 billion (Sowman and Poree, 2000). In addition, a report by the Department of Public Works, the Construction Industry Development Board and the Council for Scientific and Industrial Research of South Africa (2006) states that most of the country's infrastructures build in the 1960s-1970s needs major refurbishments, or might even have to be replaced. In order to decide on appropriate refurbishment strategies an in-depth understanding of the condition of bridges is required. Owing to the above reasons, assessment of civil infrastructure including bridges for damage, service performance and load carrying capacity is required.

One of the most common type of bridges in service for short to medium spans, in South Africa and worldwide, is the concrete-concrete composite structure consisting of precast pre-stressed beams and cast in-situ slab. The use of pre-cast beams results in cost savings due to the reduction or total elimination of formwork and the rapid execution of the construction

(Gajanan, 1979; Flavia *et al*, 2005: Panandiker. 2006). Typical beam cross-sections are I, T, M, U and box sections. The beams are connected to the slab using shear connectors and this will be discussed in detail in the next chapter. These connectors resist the horizontal and vertical flexural shear stresses that develop in the structure and are responsible for the composite action and therefore the structural efficiency (Gajanan. 1979; Xia *et al*, 2006: Larose and Elwood, 2006; Queiroz *et al*, 2007). The code of practice for the design of highway bridges and culverts in South Africa TMH7 (1989) also emphasizes the importance of the composite action in concrete-concrete construction for a competent structure. The loss in composite action affects the load redistribution capabilities of the bridge deck (Ryall *et al*, 2003) and thus its efficiency. A typical concrete-concrete composite beam bridge under construction is shown in Fig 1.1.

***Fig 1.1**: Concrete-concrete composite bridge under construction*
Source: www.interactions.org/../1018/concret .mor .html [July 2007]

This work will focus on assessing the integrity of the shear connectors using vibration-based techniques.

1.2 Brief review of damage detection techniques for bridges

Visual inspection techniques are widely used for condition assessment of bridge structures (Wahab and De Roeck, 1999). These techniques are however not applicable for assessing inner damaged parts of the structure such as horizontal shear connectors due to lack of access. As a result, some problems relating to structural performance go unnoticed until they become expensive to maintain, repair, and sometimes endanger the life of the road users. Apart from the difficulty in accessing some parts of the bridge like the shear connectors, this method is hampered by the shortage of experienced personnel able to detect early signs of damage in the structure. The following is an extract clarifying the situation in South Africa. "*A major concern in South Africa is the loss of experienced professionals to other countries. Although there is a growing number of young engineers, most of them do not have the necessary experience in bridge management and condition assessment* (Moyo and Alexander, 2006). Thus it is important to investigate alternative methods.

Other alternative methods, which complement visual based techniques, are non-destructive techniques (NDT) such as acoustics, impact echo, radar, ultrasonic and the proof load tests and the destructive-coring technique. Nevertheless, these techniques are limited to small areas and are time consuming. The author did not find evidence of use of these techniques in detecting damaged shear connectors in concrete-concrete composite bridges.

During the past few decades, Vibration-Based Techniques (VBTs) have emerged as promising tools for assessing and detecting damage in structures (Yong et al 2007 and Wahab and DeRoeck, 1999). The basis of VBTs is that a change in structural stiffness due to damage results in the change in modal parameters i.e. natural frequencies, damping ratios, mode shapes and their derivatives. These parameters are used to characterize and monitor the performance of the structure (Salawu and Williams, 1995) and can therefore be used to detect internal structural damage such as damaged shear connectors.

The VBTs are divided into 'model based approach' and the 'response based approach'. The model based approach integrates both the Finite Element (FE) and experimental modal investigations to detect damage in the structure. This involves updating certain parameters of

the FE model using the measured parameters until there is correlation between the experimental and analytical results. The FE model improvement is not intended for only mimicking test results but also should improve the physical parameters upon which the stiffness and finite element masses depends (Wahab and De Roeck, 1999). An updated FE model can be used to investigate further aspects in more detail than possible in experimental work alone.

The response based approach, on the other hand, utilizes only the experimental data to detect damage in the structure.

Application of vibration-based techniques for detecting damage in bridges has been reported by many reseachers (Wahab and De Roeck, 1999, Brownjohn *et al,* 2003, Maeck et al (2000), Xia *et al*, 2006). Despite the potential of these techniques, it is surprising that the work of Xia *et al* (2006) and Dilena (2003) were the only ones found especially for this problem. However Dilena's work was focusing on a concrete-steel composite beam. Xia *et al* (2006) used the model-based approach based on measurements from a scaled model of a typical beam and slab bridge. The measurements were taken from both the deck slab and the beams. Their approach has limitations for practical applications owing to difficulties of assessing beams for testing in most bridge structures. Nevertheless, the vibration-based techniques will be used in this work and a more practical approach will be proposed.

1.3 Aim of research

Owing to limitations of visual inspection techniques used to assess bridges and to limitations of local based methods proposed by Xia *et al* (2007), it is proposed to investigate the development of a more practical approach to integrity assessment of shear connectors based on a robust FE model of the system and also on vibration measurements taken on deck slab only.

1.4 Hypothesis statement

Vibration based techniques can efficiently detect, locate and quantify the extent of damage in concrete composite bridges resulting from a reduction in stiffness as a result of loss in composite action between pre-stressed beams and cast *in-situ* deck slab.

1.5 Objective and scope of investigations

The following are the key objectives:

(i) Understand the mechanics of the composite action and the construction of beam and slab bridges.

(ii) Investigate the use of VBTs to detect loss in composite action in these structures.

(iii) Develop a robust FE model of a composite bridge that can be used for further investigations.

1.6 Limitations

This research has been limited to detection of loss in composite action in concrete beam and slab bridges using the VBTs. This does not include determining remaining service life and the effect of loss in composite action on load carrying capacity of the structure.

1.7 Organisation of the thesis

Chapter one introduces the research topic. This includes the background information, brief review of relevant research work and the aims of the study. The formulated hypothesis and objectives of study also form this chapter.

Chapter two reviews different structural systems of concrete beam and slab bridges and the mechanics of composite action. Potential problems on these bridges are described and different techniques used to assess and detect damage in bridges are also reviewed.

Theoretical framework forms Chapter three of this research. This gives in-depth discussion on dynamics of structures and experimental modal analysis. This covers the equipment used in testing, the processing of data and the checks necessary on experimental data.

Chapter four contains the methodology and plan of action. This details the work to be done and includes the construction of a scaled model of beam and slab bridge, description of instrumentation and vibration testing. The FE modeling of the system is also described in this chapter. The focus lies mainly on modeling of composite action between the deck slab and the beams.

The observations and findings of this research are reported in chapter five. Both results from experimental and the FE analysis of the system are discussed.

Chapter six describes the practical application of modeling shear connectors in concrete-concrete composite structures. An FE model of an existing bridge was developed. Spring elements were used to model the shear connectors. The resulting modal parameters were compared to the measured parameters. A manual updating process described in Chapter four was used to correlate the measured and theoretical parameters.

The last chapter (Chapter seven) concludes and proposes steps that can be followed to assess the condition of shear connectors in concrete-concrete composite bridges. Recommendations for future work are found in this chapter.

CHAPTER 2

LITERATURE REVIEW

2.1 Introduction

The beam and slab arrangement is the most common and simple form of a bridge deck (Nigel, 2003). This design utilises pre-cast pre-stressed concrete beams with a cast in-situ deck slab. This type of construction is well suited for short to medium span bridges where the beam weights are small enough for placing using available machinery, such as cranes. (Nigel, 2003). With the slab cast on site and the beams pre-cast, this type of bridge is a composite structure because the concrete properties are different. In composite structures, the different components are assumed to act together as a single unit under load and the composite behaviour significantly increases both the flexural strength and stiffness of the structure (Garajan, 1979; Sameh *et al*, 2002; Panandiker, 2006). Apart from the increased flexural strength and stiffness and reduction in member sizes, the primary appeal of composite construction is that of economy. This is due to minimised formwork leading to a faster construction process (Gajanan, 1979).

There are two factors governing the composite action that needs to be considered in order to understand concrete-concrete composite bridges and possible potential problems. These are:

(i) Structural form or geometry of the bridge and the detailing process.

(ii) Mechanics of the composite action.

The following sections discuss factors governing the composite action.

2.2 Typical concrete-concrete composite bridge geometry

Standardised precast pre-stressed beam sections are used for the construction of these bridges. Typical beam sections commonly used are shown in Table 2.1. These are I, T, M,

U, Y and box. The choice of section to be used is determined by the span of the bridge. Y and I beam sections are used for construction of medium (12-36 m) span bridges. They are usually spaced at 1.5-2.0 m centre to centre. The M (inverted T) and box sections are used for short span (7-12 m) bridges whereas the U and T sections are suitable for long span (>36m) bridge decks (Somerville and Tiller, 1975).

***Table 2.1**: Standardised beams used in concrete-concrete composite bridges*

Type of beam section	***Application***	***Geometry***
I and Y	Used for medium length spans (12- 36m) and these are usually spaced at 1.5-2.5 m (Nigel 2003)	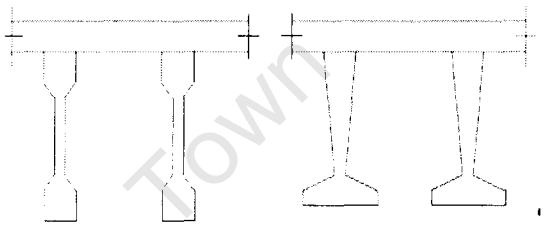
M (or inverted T) and Box beams	These are suitable for short length spans (7-12m). Box beams have the added advantage of reduced weight	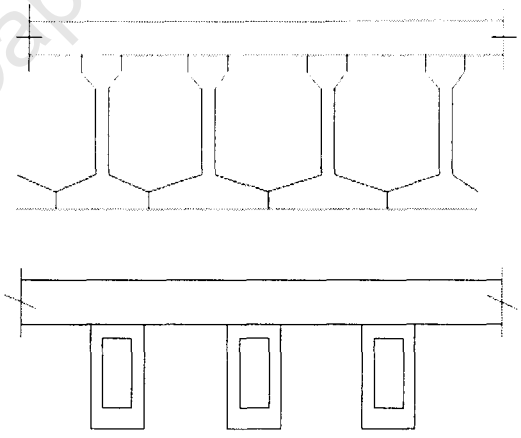
U and T	These beam sections are mostly used for long span (> 36m) bridge decks (Nigel 2003 and Ryall *et al* 2003)	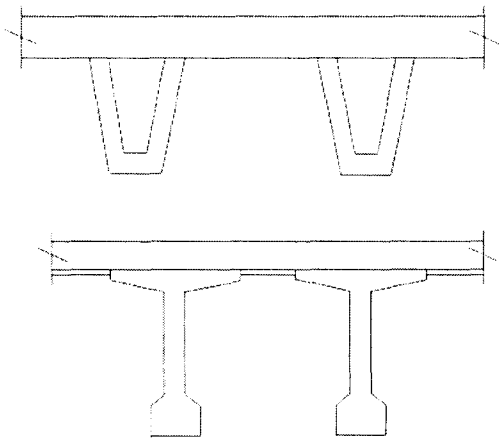

This research will focus on a bridge system constructed using I-section beams. A survey carried out in Cape Town that showed that these beams were the most commonly used for constructing these bridges.

The deck slab is connected to the beams using shear connectors. Typical connection details for an I-section beam and slab are shown in Fig 2.1. The girder web stirrups extend into the deck slab thus providing connection between beams and the slab. These connectors resist the horizontal and vertical flexural shear stresses that develop in the structure.

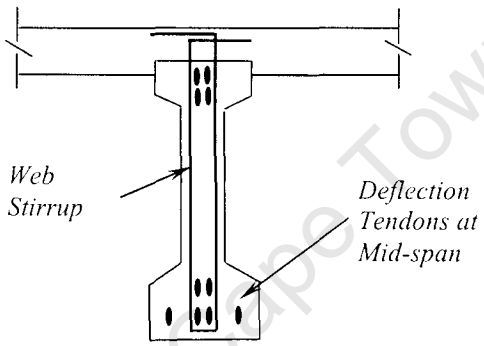

Fig 2.1: *Beam - slab connection details*

Ryall *et al*, (2003) noted that the beam and slab arrangement has poor load distribution in the transverse direction. *In-situ* transverse diaphragms are therefore cast through the beams and in integral with the *in-situ* concrete deck slab to improve the load distribution and transverse stiffness of the structure. The diaphragms are cast directly on pier positions and within the span. Typical reinforcement layout for a diaphragm is shown in Fig 2.2.

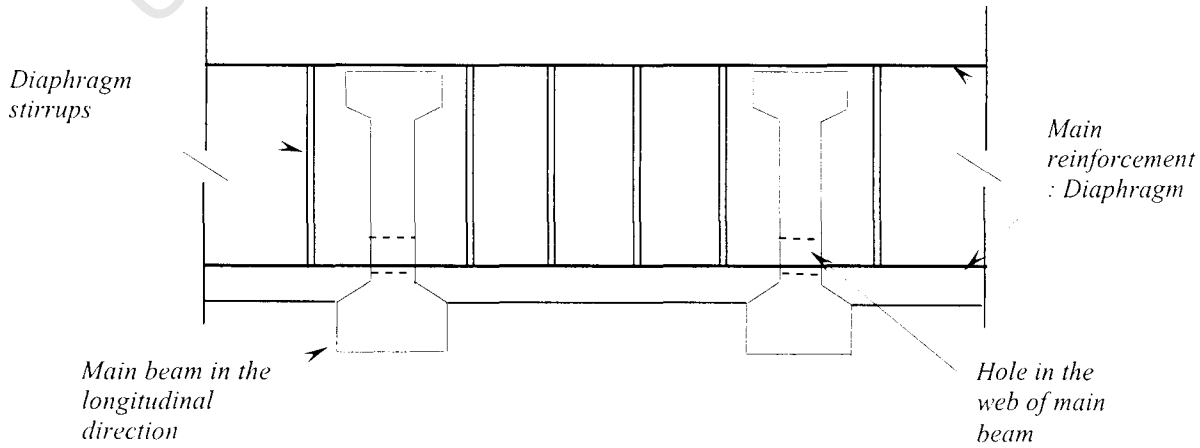

Fig 2.2*: Details of diaphragm reinforcement*

The main reinforcement of the diaphragm passes through the web openings provided in the precast pre-stressed beams and above the main beams as shown. Kumar (1988) noted that sometimes pre-stressing may be used for the diaphragms to ease congestion of reinforcement and help shear transfer at this location. However in most cases ordinary reinforcement was found to be adequate. The author did not find evidence of how these diaphragms are spaced. It is assumed that the spacing of the diaphragms is a function of the overall span of the bridge and required load distribution factor.

The following sections present the behaviour of the whole system.

2.3 Behaviour of composite action

The two primary factors that govern the behaviour of a composite structure are (Gajanan, 1979 and Xia *et al*, 2006):

(i) The difference between material properties.

(ii) Shear connection between the two components.

(iii) Transverse stiffness.

The differences between strength and stiffness of the materials acting compositely affect the load distribution in the structure (Gajanan, 1979). The stiffer material resists proportionally more load than the less stiff material. The difference in the materials is integrated in design by using the modular ratio. The modular ratio transforms the properties of one material into the other (Nigel, 2003; Ryall *et al*, 2003). When the structure is at its elastic limit at service loads, the modular ratio is the ratio of the elastic modulus of the materials (Nigel, 2003; Ryall *et al*, 2003; Gajanan, 1979). However, at ultimate limit, the modular ratio is the ratio of the ultimate strengths. Nigel (2003) and Ryall *et al* (2003) indicate that in concrete-concrete composites, the complication of modular ratio should not be neglected since the age difference in the pre-cast beams and cast *in-situ* slab results in a complete change in stress distributions. This is because of differential shrinkage and creep of the concrete of the members.

As mentioned in Section 2.2, the efficiency of a concrete-concrete composite bridge depends largely on the composite action. The composite action is a function of the integrity of shear connection provided by shear connectors. The failure of these connectors therefore results in poor load distribution and loss of stiffness of the structure. The load

carrying capacity of the bridge will obviously be reduced (Xia *et al*, 2006). This is because loss in composite action may result in slip and the assembled structural members behave independently under load. On the other hand, when members act as a composite unit, the structure has an increased section for resisting loads. This results in lower deflections as compared to that of non-connected members or when the structure has lost its composite action (Ryall *et al,* 2003; Queriroz *et al*, 2006; Panandiker, 2006).

In a concrete-concrete composite bridge, shear connectors through the interface provide the composite action. The shear connectors transfer the horizontal shear stresses between the interfaces of the members. The connectors also resist both torsional and vertical shear stresses (Kumar, 1988). The ability of the shear connectors to transfer the longitudinal forces depends on their strength as well as the resistance of concrete to longitudinal crushing induced by the high concentration of the shear force (Denis, 2006). Horizontal shear transfer in concrete composites is usually of little consequence at service load levels, but it is important in the overload range and at ultimate load (Gajanan, 1979; Ryall *et al*, 2007). This is because the bond at the interface is strong enough to take loads. The increase in allowable loads over bridges therefore means concrete-concrete bridges that have been in service for more decades might be under ultimate service conditions. This may compromise the composite action.

2.4 Longitudinal shear stresses between the beam and slab interface

The shear strength of the interface between the members is a function of the amount of steel crossing the joint, concrete strength and the bond between the precast pre-stressed beams and cast *in-situ* slab. Ryall *et al*, (2003) states that an efficient composite action is obtained when:

(i) At working loads slip does not occur.
(ii) At ultimate conditions the interface has sufficient strength.

At ultimate conditions, the shear plane must have sufficient capacity to resist shear flow. The capacity of the shear plane is estimated as the lesser of (Ryall *et al*, 2003):

(a) $Q_p = k_1 f_{cu} L_s$ or *(2.1a)*

(b) $Q_p = v_1 L_s + 0.7 A_e f_y$ *(2.1b)*

Where: Q_p - Capacity of the shear plane

k_1 - A constant depending on the concrete bond across the shear plane

f_{cu} - Characteristic concrete cube strength for the slab

L_s - Width of the shear plane

v_1 - Longitudinal shear strength

A_e - Area of fully anchored reinforcement per unit length crossing the shear plane but excluding reinforcement required for coexistent bending effects

f_y - Characteristic strength of steel

The values of the longitudinal shear strength, v_1, and constant k_1 are given in Table 2.2 (Extract from TMH 7, South Africa, 1989). The shear stress v_1 depends on the type of shear plane and concrete grade. The constant k_1 is a function of type of shear plane. It is evident, from Table 2.2 that the shear stress and constant k_1 increases from the as built shear plane to the monolithic construction. Consequently, the monolithic and prepared surface construction have higher capacity of the shear plane than the as cast surface construction.

***Table 2.2**: Longitudinal shear strength, v_1 and constant k_1 for a composite system (TMH 7, South Africa, 1989)*

Type of shear plane	***Longitudinal shear stress, v_1 (MPa) as a function of concrete grade***				k_1
	20	***25***	***30***	***40***	
Monolithic construction	0.50	0.63	0.75	0.80	0.15
Prepared surface	0.50	0.63	0.75	0.80	0.15
As cast surface	0.30	0.38	0.45	0.50	0.15

A minimum area of reinforcement, A_e, of 0.15% is recommended to pass through the shear plane to ensure that there is no separation of the components. (Ryall *et al,* 2003; TMH 7 1989, South Africa).

The interface load (shear flow) and the design of shear connectors is presented in the next section.

2.4.1 Interface stresses and shear connector design

The force transfer at the interface for composite sections is related to the rate of change of the force in the slab (Ryall *et al*, 2003). The shear flow at service load conditions is given by (Ryall *et al*, 2003):

$$q_n = \frac{VAy}{I_n} \qquad (2.2)$$

Where: q_n - Shear flow at stage n

V - Vertical shear force

A - Transferred area of concrete on the interface

y - Distance between the centre of area A and the elastic neutral axis

I_n - Moment of inertia of transformed composite section about the neutral axis

The shear flow is a function of vertical shear force as shown by equation 3.2. The increase in vertical shear force resulting from an increase in service loads therefore increases the shear flow.

Based on the shear flow calculated above, the number of shear connectors per unit length at serviceability limit state is given by (Ryall *et al*, 2003):

$$N_0 = \frac{q_n}{0.55P_u} \qquad (2.3a)$$

Where: q_n - Shear flow at stage n

P_u - Nominal static strength of the shear connector

At the ultimate limit state, the number of shear connectors required is given by;

$$N_0 = \frac{\gamma q_n}{0.8P_u} \qquad (2.3b)$$

q_n and P_u are described above and γ is a constant

The load-slip characteristic is an important property of shear connectors. However, Gajanan (1979) and Seracino *et al* (2000) noted that in design, the longitudinal slip between the members is neglected as the connection is treated as rigid. The assumption that the connection is rigid might be incorrect and may have adverse effects at ultimate loadings of the structure. Moreover, Queiroz *et al* (2006) noted that in practice, slip between the members occurs. The shear connectors only come to effect when slip has occurred.

The geometry, construction and design of a concrete-concrete composite system have been reviewed. It should however be noted that not much has been done to assess the integrity of the shear connection in concrete-concrete bridges. Notably, most of these structures were built more than 40 years ago and some are still built. Moreover, any damage on the shear connectors is difficult to detect especially using visual techniques. This is due to accessibility problems. This therefore means the composite action may be a potential weak area in these structures and need to be assessed.

The following sections review typical bridge problems that may negatively affect the integrity of shear connection in these structures.

2.5 Possible failure mechanisms of the composite action

In spite of their relatively simple structural systems and well-defined supports, bridges suffer heavily from the effects of age, climate and traffic loads that often exceed the codified limits (Abdunur, 2003; Darby, 2003 and Parkash *et al* 2006). Strength and durability of a bridge depend on the type and quality of the constituent materials, structural design, construction and maintenance. The degradation of concrete structures is attributed mainly to material failure or overstressing of structural members. Nowark (1999) state that the structural capacity of a bridge depends on resistance to deformation of its components and connections. The component resistance is a function of material strength and

dimensions, whereas the connection rigidity depends on shear connectors connecting the members together. The growth of traffic and increase in allowable axle loads therefore means bridges are now heavily loaded (Dutta and Talukdar, 2002). Bridge components such as shear connectors might be overstrained. This may be true especially for bridges built long ago such as concrete-concrete composite bridges.

The following sections describe specific problems in bridges that might have adverse effects on the composite action.

2.5.1 Material Failure

Internal degradation of concrete structural elements reduces the elementary stiffness. This may compromise the global stiffness of the structure. This degradation of concrete is a function of its constituent's materials and also the location of the structure. Fulton's concrete technology (2001) lists the main causes of degradation as: (i) Steel corrosion (ii) Alkali Silica Reaction (ASR) (iii) Freeze-Thaw action (iv) Sulphate attack. The cracks that result due to steel corrosion, ASR, freeze thaw action and sulphate attack at positions of links may reduce the concrete bond between of the shear connectors. The integrity of composite action might be reduced.

2.5.2 Structural damage due to unusual loading

Structural damage in bridges is mainly due to certain loading types. These are (Hobbs, 1994):

(i) Vehicle overloads.

(ii) Vehicle impact.

(iii) Unusual stresses from faulty structural members.

2.5.2.1 Vehicle overload

The following paragraph gives an extract from a report concerning the effects of vehicle overload on the road system in South Africa.

"The events of the period 1989 to 1993, when the previous National Department of Transport (NDoT) allowed vehicle load capacities to increase by over 30 percent, in an environment of severe road under-funding, had a major effect on the road system deterioration. What substantially raised the threat of road damage at the time was that although overloading had been identified as a serious potential problem, the law-

enforcement resources of weighbridges and traffic police manpower were not in place to implement the necessary controls" (Sowman and Poree, 2000).

Ackerman (2007) noted that although much has been done to curb vehicle overloading on South African roads, not much has been done to determine the effects of these loads on the existing bridge structures. This might be important especially for in-accessible parts of the structure such as horizontal shear connectors. Furthermore, Wium *et al* (1994) in his research concluded that current design practices are realistic except for bridges in short span range and that there should be no increase in axle loads on these bridges. In addition, Wium *et al*, (1994) indicated the difficulty of assessing loading provisions and the adequacy of the existing bridges in areas where overloading of vehicles is poorly controlled. In-light of the above, FitzGerald (1998) in his research, concluded that the South African code, TMH 7 (1987) Part 2, should be revised as a matter of agency to cater for the increase in traffic loading. However, to date, no physical revisions have been made to the code.

Assessment of shear connectors in existing concrete-concrete composite bridges is therefore justified.

2.5.2.2 Vehicle impact

Vehicle impact can cause local damage to reinforcement cover and in some serious cases the reinforcement or pre-stressed strands are damaged (Ackerman, 2007). This is mainly due to illegally loaded vehicles with heights greater than the restriction clearance height or accidents. An example of impact damage on B267 bridge over N1 is shown on Fig 2.3.
Such vehicle impact can affect the internal structural elements which are usually not accessible on a naked eye such as the shear connectors, amongst others.

Fig 2.3: *Impact damage on B267 Bridge over N1, Ackerman (2007), pp 40*

2.5.2.3 Unusual stresses from faulty structural members

The most common faulty structural members are bridges bearings (Ronne, 2008). Bridges are subjected to displacements and rotations that have to be accommodated to protect the structure. Bearings are therefore designed to accommodate the vertical displacements, shear forces and rotations. An informal discussion with Ronne (2008) revealed that most bridges in South Africa have faulty bearings. As a result, some structural members are subjected to additional stresses that can affect the efficiency of the structure.

Ronne (2008) also revealed that other major problems in South African bridges are expansion joints that are filled with debris. This tends to restrain free contraction or expansion of concrete elements due to temperature changes. This may result in overstressing of bridge decks and other structural members connected to it.

The bridge problems described above may have adverse effects on the composite action of the system. Conversely, the torsional, flexural and transverse stiffnesses of the system are negatively affected. This is described in detail in the following sections.

2.6 Effect of failure in composite action on torsional stiffness of the system

Torsion stiffness in concrete-concrete bridges elements is important to achieve proper distribution of live loads. The torsional stiffness is a function of the cross-section selected and the connection between the members of a composite structure. A study by Tamberg (1968) investigated the effect of the connection between a concrete slab and a beam on the torsional stiffness of the system. In his study an AASHTO girder type III and a deck slab was used. The results are as shown in Fig 2.4.

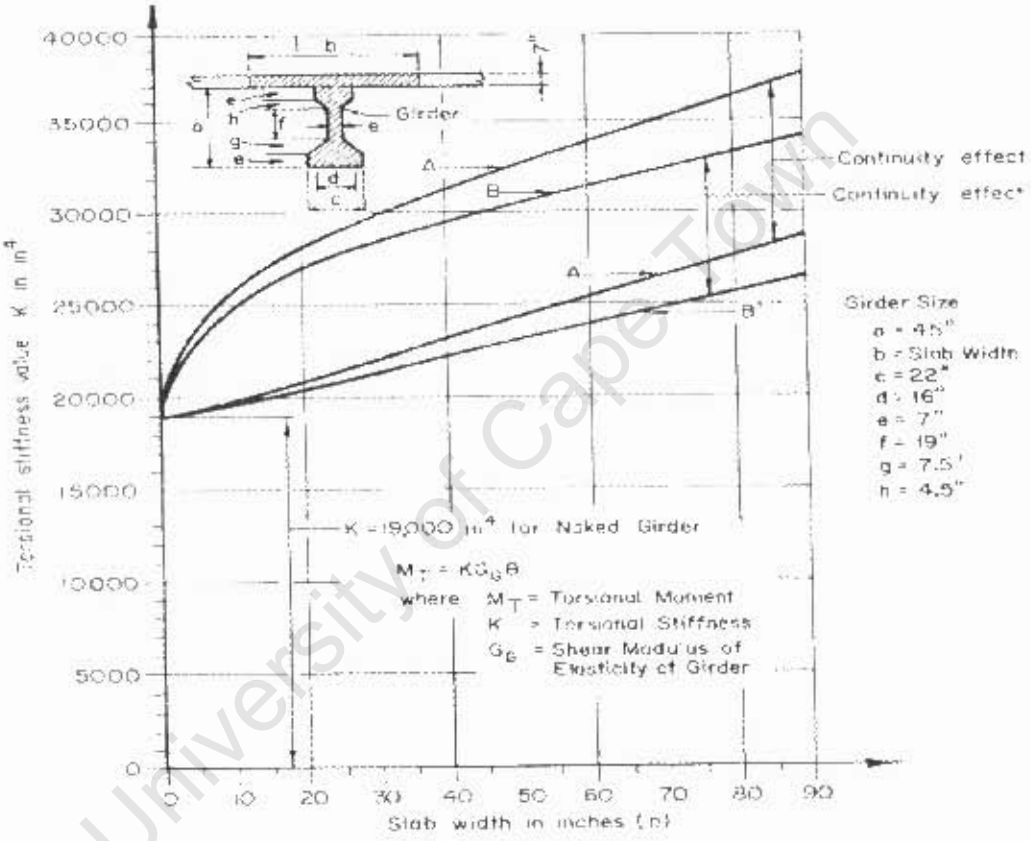

Curve A- Girder plus Slab interconnected (G-slab= G-girder)
Curve B -Girder plus Slab interconnected (G-slab= 0.77 G-girder)
Curve A` – Girder plus slab acting separately but rotating through the same angle (G-slag = G-girder)
Curve B'- Girder plus slab acting separately but rotating through the same angle (G-slag = 0.77 G-girder)

Fig 2.4: Torsional Stiffness values K for AASHTO Girder III plus slab. (Tamberg, 1968, pp36)

The results show that the torsional stiffness is dependant on the connection between the members and the shear modulus of elastic of the slab and girder. This is shown in curve A and curve B. A steady increase in stiffness with an increase in slab width for a connected system was observed and is shown in curve A. The effect of reduction is shown in curve B. The torsional stiffness reduced for the same beam and slab dimensions. The effect of loss in connection on torsion stiffness is shown on curve A' and curve B'. From the curves, a further reduction in the stiffness was observed. In light of the above observations, Taberg (1968) concluded that damage of shear connectors reduces the torsional stiffness of the system. The stiffness is also dependant on the shear modulus between the connected members.

2.7 Effect of loss in composite action on flexural and transverse stiffness of the system

Flexural stiffness of a composite structure is a function of the structure's material properties and geometry. In composite structures, failure of shear connection leads to separation of members. The effective cross-sectional area reduces and thus its flexural stiffness.

It was shown in Section 2.2 that in concrete-concrete bridges, the transverse stiffness is provided by diaphragms. The effectiveness of the deck to distribute the loads in the transverse direction is a function of the ratio of the longitudinal to the transverse stiffness (Tamberg, 1968). However there was also no research found in literature that investigates the effect of loss in composite action on the transverse stiffness on concrete-concrete composite bridges.

The following sections describe damage detection methods that are used for detecting damage in bridges. These include both destructive and Non-Destructive Techniques (NDT).

2.8 Damage detection in bridges

Bridge management is concerned primarily with existing bridge structures. The objectives are to ensure that they achieve their design life and remain open to traffic continuously throughout their life, and also ensure that the risk of failure is always very low (Vassie, 2003). Bridge management encompasses activities such as inspection, assessment for load carrying capacity and various types of testing. Frangopol and Estes (1997) and Hearn

(1998) state that bridge management involves making decisions such as when a bridge should be maintained and what type of maintenance should be carried out. However, maintenance of bridges is effective only if adequate inspections, monitoring and assessment procedures are used, facilitating an appropriate preventive action if need be. A number of damage detection techniques exist. These are reviewed in the following sections.

2.9 Assessment and testing

Assessment of load carrying capacity of a bridge is made when deterioration has reduced the strength or when the loading standard has changed (Vassie, 2003). An assessment failure implies that essential maintenance is needed. Both destructive and NDTs are used for assessment to establish the cause of deterioration, to locate defects and estimate their rate of development. There is a wide range of NDT applicable to bridges but the suitability of each method depends on precision required and accessibility of the structure. McCann and Forde (2001) emphasize the importance to undertake a feasibility study on the structure to assess the suitability of the proposed NDT techniques. Before the application of the NDT technique, a desk study is important. The study seeks to provide the historical records of the bridge, i.e. the design loads used in design, designer of the structure, FE model of the system, the constructor and type of construction amongst others (McCann and Forde, 2001). However, in most cases it is difficult to access all this information especially on bridges built a long time ago.

2.10 Principles of damage detection techniques

There are many types of techniques, each based on different theoretical principles. These techniques produce different sets of information regarding the physical properties and state of the structure. These properties include: compressional and shear wave velocities and electrical resistivity among others. These are interpreted in terms of the fabric of the structure and its engineering properties (McCann and Forde, 2001). The factors considered in design of NDT survey are (McCann and Forde, 2001):

(i) Required depth of penetration in the structure.
(ii) Vertical and lateral resolution required for the anticipated targets.
(iii) Contrast in physical properties between the target and its surroundings.

(iv) Signal to noise ratio for the physical property measured at the structure under investigation.

(v) Historical information concerning the methods used in the design and construction of the structure.

(vi) Accessibility of structural members to be assessed.

Some damage detection methods used for damage detection in bridges are shown in Table 2.3. The signatures used for damage detection, merits and demerits are described in the table as described by McCann and Forde, 2001.

***Table 2.3**: Summary of NDT used for damage detection and location in bridges*

Inspection method	***Parameter measured***	***Merits***	***Demerits***
Visual	Surface condition	Quick	Damage can only be detected when it has reached surface of the structure. Skilled personnel required
Ultrasonic	Wave velocity through structure	Relatively quick	Localised
Radar	Electromagnetic wave velocity	Quick, good penetration, give image of internal structure	Special skills required to interpret data
Coring	Internal dimensions	Simple	Scars the structure. Localised in nature
Proof load test	Load carrying capacity	Definitive	Slow and possibly dangerous. High cost
Impact testing	Mode shapes	Give some indirect measure of current condition	Difficult to quantify data
Vibration modal testing	Mode shapes, natural frequencies, Damping ratios	Give an indirect measure of current condition, simple and has no accessibility limitations	Difficult to quantify data.

Visual inspection techniques are widely used for condition assessment of bridge structures. These techniques are however not applicable for assessing inner damaged parts of the structure such as shear connectors. The other techniques listed in the table are localised in nature and are time consuming. Moreover, experienced personnel are required to analyse and interpret the measured parameters.

To date there is little work in literature related to the use of these techniques in detecting damaged shear connectors in beam and slab bridges.

This research focuses on use of vibration-based techniques (VBT) to detect and locate damaged shear connectors in a concrete-concrete composite bridge. These techniques are described in the following sections.

2.11 Vibration-based techniques (VBT)

During the past few decades, VBTs have emerged as a promising tool in assessing and detecting damage in civil structures (Yong *et al*, 2006; Alvandi and Cremona, 2005; Wahab and De Roeck, 1999). The basis of VBTs is that a change in structural stiffness due to damage results in change of modal parameters i.e. natural frequencies, damping ratios, mode shapes and curvatures. These parameters are used to characterize and monitor the performance of a structure (Salawu and Williams, 1995). They can therefore be used to detect internal structural damage such as damaged shear connectors.

The VBTs are divided into 'model based approach' and the 'response-based approach'. The model based approach integrates both finite element (FE) analysis and experimental modal investigations. This involves updating certain parameters of the FE model using the measured parameters. The response-based approach, on the other hand, utilizes change in experimental modal parameters to assess the performance of the structure.

Based on the amount of information provided regarding the condition of the structure, VBTs can provide four levels of damage detection (Farrar and Jauregui, 1997). These are:

(i) Level 1: Identify that damage has occurred.
(ii) Level 2: Identify that damage has occurred and determine the location of damage.
(iii) Level 3: Level 2 plus estimate its severity.
(iv) Level 4: Level 3 and determine the remaining service life of the structure.

The VBTs include both global and local techniques. The global parameters of the structure provide the overall condition of the structure. These are modal frequencies, damping ratios and mode shapes. These can only detect damage in a global sense and therefore form level one in damage detection levels. The following sections describe these parameters.

2.11.1 Global parameters

2.11.1.1 Natural frequencies and damping ratios

Resonant frequencies and damping ratios are modal parameters which are used to detect damage in structures in a global sense. The change in resonant frequencies and damping ratios due to damage are compared and serve as an index for damage detection. The natural frequency of a structure shows the interrelation between its stiffness and its mass using the following expression:

$$\omega_n^{\ 2} = \frac{\Phi_n^T K \Phi_n}{\Phi_n^T M \Phi_n} \qquad (2.4)$$

Where: ω_n - Natural frequency

$\Phi_n^T K \Phi_n$ – Modal stiffness

$\Phi_n^T M \Phi_n$ - Modal mass

In most damaged structures, the mass of the system remains constant before and after damage and therefore any change in natural frequency is associated with change in stiffness. The natural frequencies of any structure can be monitored and any change in stiffness due to damage can be easily detected.

Damping, on the other hand, represents the ability of a disturbed system to reduce vibrations to zero. The damping ratio is a measure of damping of the system. The damping ratio of any structure can also be measured and used to detect damage. Previous research has however shown that this parameter is difficult to measure and is also not sensitive to damage in most structures (Xia *et al*, 2007; Alampalli et al, 1995; Farrar et *al*, 1994; Mazurek and DeWolf, 1990; Spyrakos *et al*, 1990; Turner and Pretlove, 1988; Kato and Shimida, 1986; Salane, 1981).

2.11.1.2. Modal Assurance Criteria (MAC) values

MAC values serve as reliable indexes to analyse and correlate mode shapes. The method makes uses of the orthogonality properties of mode shapes to correlate two modes (Frisswell and Mottershead, 1995). The modes extracted from a structure, at different times, can be analysed using the MAC values to check for any notable changes and

therefore damage. MAC values close to zero show that the mode shapes are orthogonal and dissimilar whereas values close to one show that the modes are similar. The MAC value that compare mode *i* and *j* is calculated from (Frisswell and Mottershead, 1995):

$$MAC(i,j) = \frac{\left|\sum_{k=1}^{n}(\Phi_j)_k(\Phi_i)^*_k\right|^2}{(\sum_{k=1}^{n}(\Phi_j)_k(\Phi_i)^*_k)} \qquad (2.5)$$

Where: $(\Phi)_k$ denotes an element of mode shape vector and the asterisk denotes complex conjugate.

This technique however has some limitations. Frisswell and Mottershead (1995) noted that it is difficult to compare modes that are close in frequency or that are measured at insufficient transducer locations using MAC values.

2.11.1.3. Mode Shapes (MS)

MS show deformed shapes of the structure at a particular frequency and damping ratio. The MS of a system measured at different times can be superimposed to check for change in curvatures resulting from damage.

The global techniques described above, except mode shapes, only satisfy the first level in damage detection efficiency i.e. identify that damage has occurred in the structure but cannot localise it. Localisation of damage may be possible using one of the vibration-based algorithms (VBA) described in the next section.

2.11.2. Vibration-Based Algorithms (VBA)

VBAs try to localise the damaged regions of the structure. These are usually referred to as mode shape derivatives because they use the mode shape data to localise damage within the structure Pandey *et al*, (1991). The following section describes these algorithms.

2.11.2.1 Coordinate Modal Assurance Criteria (COMAC) values

COMAC values, unlike MAC values, compute the correlation between two similar locations of the modes. This algorithm can therefore localise damage within a structure.

COMAC values are estimated from the following algorithm suggested by Pandey *et al*, (1991):

$$COMAC(i) = \frac{\sum_{l=1}^{L} \left| (\varphi_{ud})_{il} (\varphi_{d})_{il} \right|^2}{\sum_{l=1}^{L} (\varphi_{un})_{il}^2 \cdot \sum_{l=1}^{L} (\varphi_{d})_{il}^2} \qquad (2.6)$$

Where: $\varphi_{ud}, \varphi_{d}$ - Unit mass normalised mode shape vectors for the undamaged and damaged structure respectively.

l - Represents an individual correlated pair of which a total of L are available

COMAC values greater than 0.9 show correlation between the two points on the modes whereas a value less than 0.9 means that the points are not related. This can be the case when a structure has been damaged. This technique thus can be used to localise damage in the structure.

2.11.2.2. Change in curvature method

The change in curvature method uses mode shape data from both undamaged and damaged mode shapes to localise damage. The mode curvature is computed from any differentiation schemes such as the forward difference method, central difference and backward difference methods. For a beam element subjected to bending moment, *M(x)*, the curvature at location, x, along the length of the beam is estimated from (Pandey, Biswas and Samman, 1991):

$$v'' = \frac{M(x)}{EI} \qquad (2.7)$$

Where: v - Curvature

E - Modulus of elasticity

I - Moment of inertia of the section

The curvature values are used to calculate Curvature Damage Indicators (CDI). This index computes a damage factor for all points of interest and thus can be used to localise damage

in the structure. Wahab and De Roeck (1999) used the following expression to calculate CDI values for a damaged beam structure:

$$CDI = \frac{1}{N}\sum_{n=1}^{N} | v''_{oi} - v''_{di} | \qquad (2.7a)$$

Where: N - Number of modes

v''_{oi}, v''_{di} - Curvature values for the undamaged and damaged structure at node i

In their study, Wahab and De Roeck (1999) observed that damage in some locations of the structure could be located whilst damage in other locations could not be located. False damage was also detected.

2.11.2.3. Change in flexibility method

The flexibility of a structure measures its absolute range of movement at a particular location under load. The flexibility of a system is expected to change for intact and damaged structure. The undamaged regions are expected to have higher amplitude of vibrating than the damaged sections. This phenomenon can be used to locate damage in a structure. Pandey and Biswas, (1994) estimated the modal flexibility of a structure from the following expressions:

$$[F] = \sum_{i=1}^{n} \frac{1}{\omega_i^2} \{\phi_i\} \{\phi_i\}^T \qquad (2.8a)$$

$$[F]^* = \sum_{i=1}^{n} \frac{1}{\omega_i^{*2}} \{\phi_i\}^* \{\phi_i\}^{*T} \qquad (2.8b)$$

Where: $\acute{\omega}_i$ - *i th* natural frequency of the structure

Φ - *i th* unit mass normalized mode vector.

* - Signify the damaged structure.

The change in flexibility is given by:

$$[\Delta F] = [F] - [F]^* \quad (2.8c)$$

For each column of [ΔF] matrix, the damaged locations are defined as the absolute maximum, δj_{max}, at each measurement *j*. Xia *et al* (2007) used this method to locate damaged shear connectors in a concrete-concrete composite bridge. Some damaged connectors were located and false identification was also observed. Farrar and Jauregui (1997) also used this technique to localise damage in a bridge structure. This technique was only efficient when severe damage was inflicted in the structure. Likewise some false damage was observed. This means one should use these methods carefully.

2.11.2.4. Change in stiffness method

This algorithm uses the eigen-value problem of a structure to campare eigen-vectors of damaged and undamaged structure. The general eigen-value problem for an undamped structure is given by:

$$\left(\lambda_i[M]+[K]\{\psi_i\}\right) = 0 \quad (2.9a)$$

Where: λ_i - The i^{th} eigen-value

[M], [K] - Mass and the stiffness matrix respectively

$\{\psi_i\}$ - Displacement vector

The eigen-value problem of the damaged structure is formulated from first replacing the pre-damaged eigenvectors and eigen-values with a set of post-damaged modal parameters (Farrar and Jauregui, 1997). This is shown in equation 2.9b.

$$\left(\lambda^*_i[M-\Delta M_d]+[K-\Delta K_d]\{\psi_i\}^*\right) = \{0\} \quad (2.9b)$$

Where: ΔM_d and ΔK_d - Change in mass and stiffness respectively.

The damaged vector, $\{D_i\}$ for the i^{th} mode is given by:

$$\{D_i\} = \left(\lambda^*{}_i[M] + [K]\{\psi_i\}^*\right) = (\lambda^*{}_i[\Delta M_d] + [\Delta K_d]\{\psi_i\}^* \quad (2.9c)$$

Damage is assumed to change only the stiffness of the structure i.e. $[\Delta M_d] = 0$, therefore the damage vector reduces to:

$$\{D_i\} = [\Delta K_d]\{\psi_i\}^* \quad (2.9d)$$

$$[K] \approx \sum_{i=1}^{n} \omega_i{}^2 \Phi_i \Phi_i{}^T \text{ and } [K]^* \approx \sum_{i=1}^{n} \omega_i{}^{*2} \Phi^*{}_i \Phi^*{}_i{}^T \quad 2.9(e)$$

Where: [K] and [K]* are stiffness matrices for undamaged and damaged structure respectively.

$$[\Delta K] = [K] - [K]^* \quad (2.9f)$$

As in the flexibility method, the modal stiffness can be calculated for all measured locations on a structure. The resulting damage vectors can be used to localize damaged sections in a structure.

2.11.4.5. Change in strain energy method

This method uses the principle of change in strain energy to locate damage in a structure. The strain energy for a Bernoulli-Euler beam of length L is given as: (Zhang and Aktan, 1995; Alvandi and Cremona, 2006):

$$U_i = \frac{1}{2}\int_0^L EI_z(x)\left(\frac{\partial^2 \Phi_i}{\partial x^2}\right)^2 dx \quad (2.10a)$$

Where: EI_z - Flexural rigidity about the z-axis ad

Φ - Mode shape value

For a beam with N elements, the strain energy for an element *j* is expressed as: (Zhang and Aktan, 1995; Alvandi and Cremona, 2006):

$$U_{ij} = \frac{1}{2}\int_{a_j}^{a_{j+1}} EI_z(x)\left(\frac{\partial^2 \Phi}{\partial x^2}\right)^2 dx \qquad (2.10b)$$

Where: a_j, a_{j+1} - Bounds for element j

The fractional strain energy of the element is calculated from:

$$F_{ij} = \frac{U_{ij}}{U_i} \qquad (2.10c)$$

For N elements:

$$\sum_{j=1}^{N} F_{ij} = 1 \qquad (2.10d)$$

Similar expressions can be derived for a damaged case:

$$U_i^* = \frac{1}{2}\int_0^L EI^*(x)\left(\frac{\partial^2 \phi_i^*}{\partial^2 x}\right)^2 dx \qquad (2.11a)$$

For an element *j*:

$$U_{ij}^* = \frac{1}{2}\int_{a_j}^{a_{j+1}} EI^*(x)\left(\frac{\partial^2 \phi_i^*}{\partial^2 x}\right)^2 dx \qquad (2.11b)$$

Fractional strain energy for an element j:

$$F_{ij} = \frac{U_{ij}^*}{U_i^*} \qquad (2.11c)$$

For small damage in a structure: $F_{ij}^* = F_{ij}$ + *higher order terms*

$$\frac{F_{ij}^*}{F_{ij}} = \frac{U_{ij}^* U_i}{U_{ij} U_i^*} = \frac{\int_{a_j}^{a_{j+1}} EI^*(x)\left(\frac{\partial^2 \phi_i^*}{\partial x^2}\right) dx \int_0^L EI(x)\left(\frac{\partial^2 \phi_i}{\partial x^2}\right) dx}{\int_{a_j}^{a_{j+1}} EI(x)\left(\frac{\partial^2 \phi_i}{\partial x^2}\right) dx \int_0^L EI^*(x)\left(\frac{\partial^2 \phi_i^*}{\partial x^2}\right) dx} \qquad (2.11d)$$

For small damage, $\frac{F_{ij}^*}{F_{ij}} = 1$:

$$1 = \frac{EI_{ij}^*}{EI_{ij}} \frac{\int_{a_i}^{a_{j+1}} \left(\frac{\partial^2 \phi_i^*}{\partial x^2}\right)^2 dx}{\int_{a_i}^{a_{j+1}} \left(\frac{\partial^2 \phi_i}{\partial x^2}\right)^2 dx} \frac{EI^*}{EI} \frac{\int_0^L \left(\frac{\partial^2 \phi_i}{\partial x^2}\right)^2 dx}{\int_0^L \left(\frac{\partial^2 \phi_i^*}{\partial x^2}\right)^2 dx} \qquad (2.11e)$$

For light damage, EI is assumed to be approximately constant, therefore $EI^* \approx EI$:

$$\frac{EI_j}{EI_j^*} = \frac{\int_{a_i}^{a_{j+1}} \left(\frac{\partial^2 \phi_i^*}{\partial x^2}\right)^2 dx}{\int_{a_i}^{a_{j+1}} \left(\frac{\partial^2 \phi_i}{\partial x^2}\right)^2 dx} \frac{\int_0^L \left(\frac{\partial^2 \phi_i}{\partial x^2}\right)^2 dx}{\int_0^L \left(\frac{\partial^2 \phi_i^*}{\partial x^2}\right)^2 dx} \qquad (2.11f)$$

For a mean set of mode shapes:

$$\beta_j = \frac{EI_j}{EI_j^*} = \frac{1}{n} \sum_{i=1}^{n} \frac{\int_{a_j}^{a_{j+1}} \left(\frac{\partial^2 \phi_j^*}{\partial x^2}\right)^2 dx}{\int_{a_j}^{a_{j+1}} \left(\frac{\partial^2 \phi_j}{\partial x^2}\right)^2 dx} \frac{\int_0^L \left(\frac{\partial^2 \phi_j}{\partial x^2}\right)^2 dx}{\int_{a_j}^{a_{j+1}} \left(\frac{\partial^2 \phi_j^*}{\partial x^2}\right)^2 dx} \qquad (2.11g)$$

Where: β_j - Damage index for element j

For any structure, a normalised index is expressed as:

$$z_j = \left(\beta_j - \beta_{mean}\right) / \sigma_\beta \qquad (2.11h)$$

Where: β_{mean} - Mean of sample value β_j

σ_B - Standard deviation of sample value β_j

This normalisation leads to negative values for undamaged elements and positive values for potential damaged elements. The authors noted that it is however difficult to classify a positive value as damage.

2.12 Summary

One of the most common types of bridges in service for short to medium spans in South Africa and worldwide is the concrete-concrete composite structure consisting of pre-cast pre-stressed beams and a cast in-situ slab. The slab is connected to the girders using shear connectors which are responsible for the composite action and therefore the efficiency in the structure. The girder webs stirrups extend into the deck slab thus provide the shear connection. Increase in allowable axle loads and age effect might affect the horizontal shear connection and therefore the composite action in these bridges. Furthermore material degradation resulting might affect the integrity of shear connection in these bridges. Other structural problems likely to weaken the composite action include failure in bridge bearings and effect of vehicle impact during accidents, amongst others.

Despite the technological advancements, most BMS still rely on visual inspections for condition assessment. This means that damage in inaccessible parts of the structure such as shear connectors may go undetected until it is expensive to repair or catastrophic failure occurs. Other methods used to detect and locate damage in bridges include ultrasonic techniques, the radar method, impact testing, magnetic based methods and proof load tests amongst others. Nevertheless, these techniques are limited to small areas and are time consuming.

During the past few decades, vibration-based damage detection techniques (VBDDT) techniques have emerged as a promising tool in assessing and detecting damage in structures. These techniques include both global and localising methods. Global parameters detect damage in a global sense while the local algorithms can locate the damaged region of a structure. The global parameters include the natural frequencies, damping ratios and mode shapes. The local techniques are COMAC values, change in

curvatures, flexibility change algorithm and change in strain energy algorithms. Farrar and Jauregui (1995) compared these methods using damage inflicted on I-40 bridge in Rio Grande. It was discovered that these methods were able to locate damaged regions for severe damage scenario. Varying levels of success were observed. False damage locations were also observed. This was also observed by Xia *et al* (2006) when they used these techniques to locate damaged shear connectors in a concrete-concrete composite bridge. They took measurements from both the slab and the beams. Xia *et al* (2007) did not take into account that it is difficult, if not impossible, to access girders in these structures. This research therefore aims at comparing these techniques based on data measured from the top of the slab, which is accessible.

CHAPTER 3

THEORETICAL FRAMEWORK: MODAL ANALYSIS

3.1 Introduction

Modal analysis is a process of determining the modal parameters (frequencies, modal damping, damping mass, mode shapes) using either experimental approach or analytical modelling. Experimental modal analysis (EMA) is based upon digital electronic gadgets such as Fast Fourier Transform (FFT) analysers, Transfer Function Analysers (TFA) and discrete data acquisition instruments. Analytical modal analysis (AMA) using a finite element model can also be used to obtain the modal parameter of a structure. Modal parameters are needed for a number of purposes:

(i) To understand the way a structure behaves and the contributions of structural elements and boundary conditions to the structural response to loads. For example curvature of mode shapes shows how support fixity works.

(ii) To provide a basis for predicting of the structure for certain types of dynamic loading, eg to predict the response of a grandstand to crowd loads or of a footbridge to pedestrian traffic.

(iii) To provide data for seismic qualification, e.g mode shapes and frequencies are used for equivalent static seismic response calculations.

(iv) To investigate the possibility of a structure being excited in resonance due to low damping and/or modal mass and coincidence of mode frequency with that of an external dynamic input, e.g. testing of as-built grandstands and footbridges

(v) Development of experimentally-based dynamic models.

Modal analysis requires a sound knowledge of structural instrumentation and signal processing.The concepts of modal analysis are well presented in most standard modal testing and analysis books. The following sections discuss the concepts of this subject.

3.2 Basic concepts of vibration analysis

The basic features of any dynamic system are its mass, elastic (stiffness) properties, damping and excitation force. The mass possesses inertia and has kinetic energy by virtue of its motion. Damping helps to dissipate energy from a vibrating system while stiffness enables it to restore potential energy by virtue of its deformation. A structure possessing these properties is therefore capable of vibrating when an excitation force is applied. A typical representation of a single degree of freedom (SDF) dynamic system is shown in Fig 3.1. Real structures however have distributed mass, damping and stiffness properties resulting in a multiple degrees of freedom system (MDF).

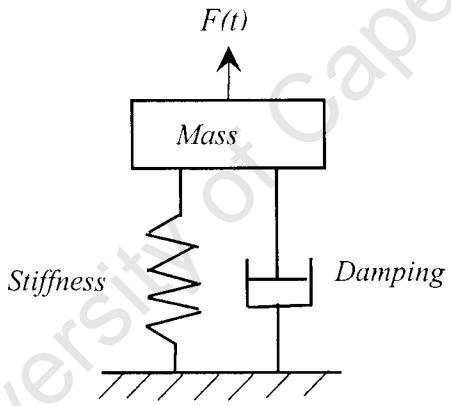

***Fig 3.1**: Idealised SDF system*

A mathematical model that describes the motion of a MDF system is given by:

$$[\mathbf{M}]\{a(t)\}+[\mathbf{C}]\{v(t)\}+[\mathbf{K}]\{x(t)\}=\{F(t)\} \qquad (3.1)$$

Where: **[M]** – Mass matrix
[K] – Stiffness matrix
[C] – Damping matrix
$F(t)$ – Applied force
$a(t)$ – Acceleration of the system
$x(t)$ – Displacement
$v(t)$ – Velocity

The solution of the general equation (3.1) of motion results in eigen-equations that result in eigen-vectors and values. These are natural frequencies, damping ratios and displacement vectors of the structure. These parameters are used to characterise the structure and are referred to as modal parameters. Detailed content on this subject is found in Ewins (2000) and Maia *et al* (1997). The modal parameters of a structure are contained on the measured frequency response functions (FRFs). This is discussed in the next section.

3.3 Frequency Response Functions (FRF)

The frequency response function (FRF) is defined as the ratio of the Fourier Transform (FT) of the output to the FT of the input. The output or response of the structure can be measured in terms of acceleration and the resulting FRF is called Inertance (acceleration divided by force). The response may also be velocity or displacement, then the FRF is called the Mobility (velocity divided by force) or the Receptance (displacement divided by force) respectively.

The general expression of FRF is expressed mathematically as:

$$H(j\omega) = \frac{X(j\omega)}{F(j\omega)} \tag{3.2}$$

Where: $X(j\omega)$ - FT of the output

$F(j\omega)$ - FT of the input

For a SDF system under forced vibration, the FRF is expressed as:

$$H(j\omega) = \frac{X(j\omega)}{F(j\omega)} = \frac{1}{(k - \omega^2 m) + i(\omega c)} \tag{3.3}$$

Where: k- stiffness

ω - natural frequency

m - mass

c - damping

It should be noted that equation 3.3 is complex and contains both magnitude and phase information (Ewins, 2000). For an MDF system, the FRF matrix also contains the magnitude and phase information for each degree of freedom and therefore the modal parameters of the structure can be estimated.

In practice, the measurements of FRFs are disturbed by noise as shown in Fig 3.2.

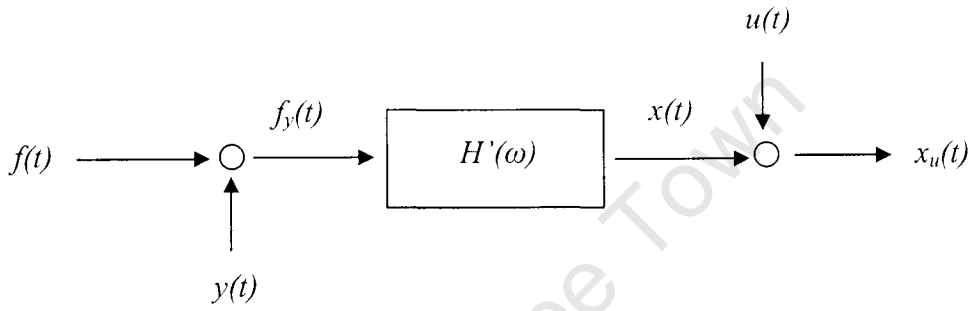

$f(t)$ – pure input signal; $y(t)$ – input noise signal; $f_y(t)$ – input signal with noise component
$H'(\omega)$ – modified FRF; $x(t)$ – output signal; $x_u(t)$ – output signal with noise

***Fig 3.2**: Signal flow diagram of test set-up*

Noise effects are introduced into the input and output signal resulting in modified FRF expression given by equation 3.2. The modified expression is given as (Qi, 2000):

$$H'(j\omega) = \frac{X_u(j\omega)}{F_y(j\omega)} = \frac{X(j\omega)+U(j\omega)}{F(j\omega)+Y(j\omega)} \qquad (3.4)$$

Where: $U(j\omega)$ and $Y(j\omega)$ are the noise on the spectra of $X(j\omega)$ and $F(j\omega)$ respectively.

It is evident that the noise effect results in unreliable measurements. However signal conditioners and filter equipment minimises this effect during the modal testing. Nevertheless, the reliability of the measured FRFs has to be checked. The necessary checks are explained later in the chapter.

3.4 Modal testing

Modal testing involves measuring the FRFs of the structure that contains its modal parameters. There are a number of testing methods and these include phase resonance techniques, phase separation testing, single point testing and multi point testing (Maia *et al*, 1998).

3.4.1 Phase resonance technique

Phase resonance, also known as the normal mode or the sine dwell testing, applies multiple exciters to excite a single mode of vibration. The use of more than one "exciter" however has a number of limitations. Firstly, the tuning of the excitation force pattern is time consuming. Secondly, the choice of excitation frequency needs to be critically selected to avoid missing important modes.

3.4.2 Phase separation testing

In contrast to the phase resonance method, this method uses a single point excitation. The following are advantages of using this method. It is cheaper, easier and quicker to implement.

3.4.2.1 Single point testing

This is the most common method and easier to implement. The impact hammer and shaker are used to excite the structure. A series of single input tests are done to obtain the overall response of the structure. Nevertheless, this method has limitations such as the localisation of the input energy. This means that some of the modes of vibration of the system cannot be excited especially for complex structures.

3.4.2.2 Multi point testing

This technique is applied to large structures where structural energising is done using a number of shakers. The shakers apply uniform loads and therefore the effect of non-linearities in the structure is reduced. However, the process of FRF extraction is a costly exercise compared to the single point testing. In addition, it has been found that the motion of the structure tends to correlate to the actual multiple forcing inputs. This is believed to affect the resulting FRF's at resonance.

3.5 Experimental measurement and modal testing

An experimental setup for modal testing consists of three major processes to extract the modal data (Fig 3.3). These are:

(i) An excitation mechanism

(ii) A transducer mechanism to record the response of the structure

(iii) An analyser to extract the desired information

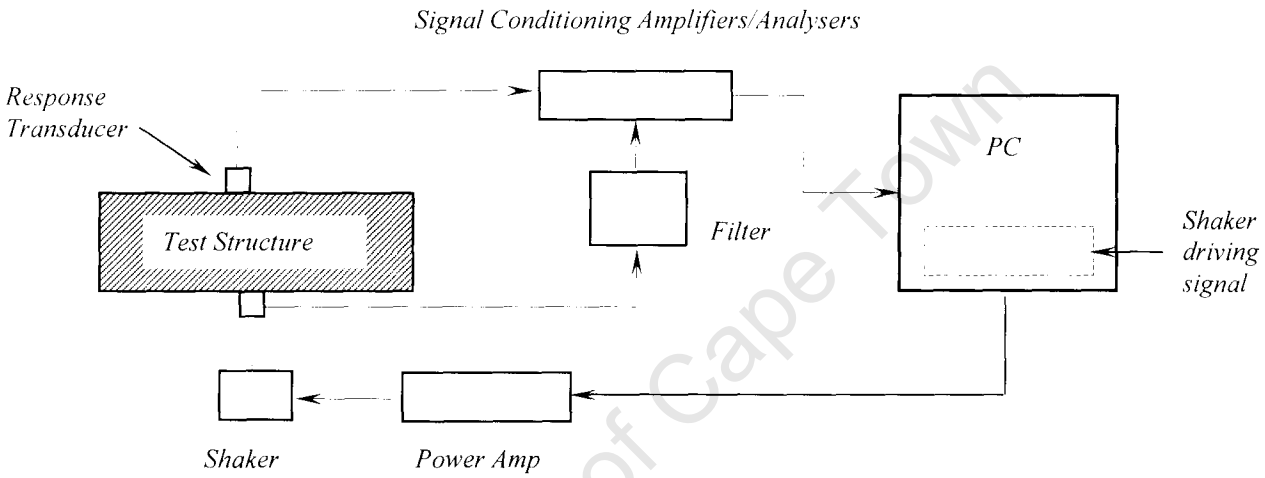

Fig 3.3: *Schematic representation of components for modal testing*

3.5.1 Excitation mechanism

The position of the excitation force is of importance in dynamic testing. The optimum location of an exciter should be such that all modes of interest are excited. In practice, preliminary testing and FE analysis of the system is used to find the optimum location of the exciter using the driving point residue (DPR) (Richardson and Schwarz, 2003). DPR is the measure of how much a point participates in the overall response of a mode. Maia *et al* (1998) describe DPR mathematically as follows:

$$|r_{ik}| = \frac{v_{ik}^2}{2m_k\omega_{dk}} \qquad (3.2)$$

Where: v_{ik} - Mode shape coefficient for DOF i and mode k. It is given as the amplitude of mass i expressed as a ratio of the amplitude of one of the masses of the system for any particular mode k

m_k - Modal mass for mode k

ω_{dk} - Damped natural frequency of the system for mode k

The optimum position is one having the largest DPR averaged for a set of modes. This means all modes of vibration for the structure that fall in the range of excitation frequencies will be excited.

Shakers and impact hammers are commonly used structural exciters in modal testing. Two common types of shakers are the electromagnetic (Fig 3.4) and an electro-hydraulic shaker. Shakers can be positioned on top of a structure and allowed to vibrate freely. In some cases, a drive rod is used to couple the shaker to the structure. As mentioned earlier in this section, the positioning of the shaker on the structure should be such that all modes of interest are excited.

***Fig 3.4**: Typical electromagnetic shaker*

Impact hammers on the other hand do not need to be coupled to the structure. As with the shaker, the position of impact should be so as to excite the required modes. The type of impulse force from the hammer is varied by changing hammer/tip heads. The amount of force applied is varied by changing drop heights. Unlike shakers that need a driving signal, impact hammers need no driving signal.

3.5.1.1 Types of excitation signals

Structural excitation forces can be classified as either narrow band or broad band (Richardson and Schwarz, 2003). The broad band signals include the chirp signals,

transient (impulsive) and the ambient forces. These are characterised by non-zero frequency spectrum over a broad range of frequencies whereas the narrow band signal contains a single non-zero frequency. The broad-band signals are preferred in most vibration or modal investigations because of the following merits (Richardson and Schwarz, 2003):

(i) They can be designed to minimise a signal processing error caused by leakage
(ii) Many modes of the structure are excited at a time
(iii) They are controlled to minimise non-linear response of the structure
(iv) They are used with spectrum averaging to effectively linearise the non-linear response of the structure.

Driving signals can further be classified into periodic, transient and random. Periodic signals include stepped sine, slow sine sweep, pseudo random and periodic random. The transient signals include the burst sine, burst random, chirp and impulse. Typical random signals include the white noise and narrow-band signals.

Stepped sine testing uses a discrete sinusoid signal with a fixed amplitude and frequency to drive the exciter (Maia *et al*, 1997). In order to encompass a frequency range of interest, the command signal is stepped from one value to another in such a way as to provide the necessary density of points on the frequency response plot (Ewins, 2003). Using this technique, measurements are taken when steady-state conditions are attained. One advantage of this method is the convenience of taking measurements where and when they are required.

Slow sine sweep testing involves the use of a sweep oscillator to provide a sinusoidal signal to the exciter. The frequency of this signal is changed slowly but continuously through the range of frequencies. As in stepped sine testing, steady state conditions should be attained before measurements can be taken. The suitability of sweep rate is checked by comparing the measurements from sweeping up and then sweeping down. The same curve should be obtained.

Random excitation uses a random signal to drive the exciter. This signal is usually produced by a noise generator.

Transient excitation signals are the most widely used form of signals for driving the exciter in modal testing. These signals are divided into burst, rapid sine sweep (chirp) and the impact from a hammer blow. The first two are used to drive the shaker as in periodic and random testing. The principle which all these signals share is that the excitation and response are completely contained within a single sample measurement made (Ewins, 2003).

Ewins (2003) describes burst signals as consisting of short sections of an underlying continuous signal which may be a sine wave, sine sweep or a random signal followed by a zero output. The resulting response shows a transient build-up followed by decay. The duration of the burst is selected so as to provide the ideal signal processing conditions. The conditions are that the response signal has died away by the end of measurement period. Leakage and poor signal may result if the above conditions are not met.

In a chirp signal, the frequency content is chosen by the starting and finishing frequencies of the sweep. As with the burst signal, the period of excitation is controlled to optimise conditions for signal processing.

Impulsive signals are produced by impact hammers. A similar energy distribution as in a chirp excitation is also produced using impulsive signals. The main difference is that the amplitude and frequency content of the chirp input signal can be controlled whereas the signal from the hammer is difficult to control. The resulting spectrum of the hammer is detected by the tip or head materials but difficult to control (Maia *et al*, 1997).

The response of the structure under these excitation forces is recorded using response transducers. This is described in the following sections.

3.5.2 Response transducers

The response of the structure to excitation force and the magnitude of the applied force are measured using transducers. Common response transducers include: accelerometers, displacement transducers, velocity transducers, piezoelectric accelerometers, capacitive accelerometers and force balance accelerometers. A typical example of an accelerometer is shown in Fig 3.5.

***Figure 3.5**: Accelerometer*

Displacement transducers include Linear Variable Differential Transformers (LVDTs), potentiometers, Rotary Variable Differential Transformers (RVDTs) and laser optical range sensors. The functioning of these tranducers and accelerometers is well explained in standard modal analysis books (Ewins, 2000; Maia *et al* 1997) and will not be discussed here.

Transducers need to be calibrated before they can be used. This is because the measured values are terms of in voltage and therefore a scaling factor is needed to translate the voltage to force, velocity and accelerations. Transducers are used with lead lengths and these tend to affect signal quality due to their resistance, capacitance variation and their tendency to pick up noise. This tends to affect the quality of the measured data. Unfortunately, this cannot be avoided in practice.

3.5.3 Filters and analysers

Signal conditioners strengthen and filter the response signals before being sent to the analyser. A number of filters are used and these include low pass, high pass, broadband, narrow band and the notch filter. These filters have a cut-off-frequency over which they function properly.

Signal analysers, on the other hand, measure specific parameters of interest i.e. force and response levels. Two types of analysers in common use nowadays include Frequency Response Analysers (FRA) and Spectrum Analysers (SA). These analysers mainly convert the analogue signal to digital signal to produce strings of discrete values. The main difference between the FRA and the SA is that the SA simultaneously measures all the

frequency components in the time signal whereas the FRA extracts a single frequency at a time.

Analysers estimate the Fourier Transforms (FT) or Spectral Densities (SD) of signals which are supplied as inputs for analysis (Ewins, 2000).

3.6 Signal processing

Signal processing is the representation of the signals by a series of numbers and or symbols. It is divided into tuned–sinusoidal (TS) and non-sinusoidal methods (NS). TS technique uses the multi-point vibration excitation to extract measured FRFs'. This method has the advantage of determining modal parameters of a structure with high modal density. However, to apply this method, the properties of the desired modes should be known. The other limitation with this method is that it is time consuming. Moreover, the measurement and analysis is mixed.

NS methods, on other hand, have a clear distinction between measurement and analysis. Further more, the modes of interest are excited using one excitation mechanism.

The response signals are processed digitally using different transform algorithms called signal analysers to yield the FRFs or Impulse Response Functions (IRFs). A simplified procedure for signal processing in dynamic equipment is detailed in Fig 3.6. A sampler samples the input time signal and keeps it until the Analogue to Digital Convetor (ADC) has completed converting the analogue input signal to a digital signal. The digitised signal is sent to a Fast Fourier Transform (FFT) to produce a spectrum.

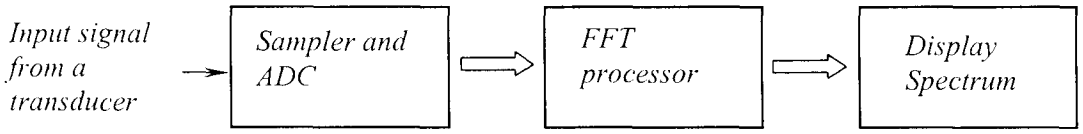

ADC- Analogue to Digital convetor

FFT- Fast Fourier Transform

***Fig 3.6**: Schematic process for computing a spectrum*

Basic knowledge of functioning of transforms is needed to understand the processing. The following sections describe the basics of analysers as explained by Ewins (2000) and Maia *et al* (1997).

3.6.1 Fourier analysis

For a pure response sine signal resulting from a sinusoidal excitation, the output displacement is represented by a Fourier series as:

$$x(t) = a_0 + 2\sum_{n=1}^{\infty}(a_n \cos\frac{2\pi nt}{T} + b_n \sin\frac{2\pi nt}{T}) \qquad (3.3)$$

Where - a_0 is the mean value of $x(t)$ over period T and,

$$a_n = \frac{1}{T}\int_{-T/2}^{+T/2} x(t)\cos\frac{2\pi nt}{T}dt \qquad (3.4)$$

$$b_n = \frac{1}{T}\int_{-T/2}^{+T/2} x(t)\sin\frac{2\pi nt}{T}dt \qquad (3.5)$$

For complex functions, the displacement is:

$$x(t) = \sum_{n=-\infty}^{+\infty} c_n e^{-2\pi nt/T}dt \qquad (3.6)$$

Where $|c_n| = \sqrt{(a_n^2 + b_n^2)}$ (3.7)

For an impulse signal, the Fourier theorem gives:

$$X(f) = \int_{-\infty}^{+\infty} x(t)e^{i2\pi nt}dt \quad \text{, or} \qquad (3.8)$$

$$x(t) = \int_{-\infty}^{+\infty} X(f)e^{i2\pi nf}df \qquad \text{Where, } X(f) = \int_{-\infty}^{+\infty} x(t)e^{i2\pi nt}dt \qquad (3.9)$$

Equations *3.9* allow the measured time domain signal to be converted to frequency domain signal. The resulting signal is digitised using Discrete Fourier Transforms (DFT) analysers.

3.6.2 Basis of Discrete Fourier Transform (DFT)

Input signals are digitised and recorded as a set of N-discrete values evenly spaced in the period T during which the measurement is made (Ewins, 2000). The sample (N-discrete values) is assumed to be periodic in time T and Finite Fourier Series (FFS) are computed using equation *3.4* to estimate DFT. A DFT approximates a Fourier Transform (FT)which is otherwise difficult to compute. The number of samples, N, the period T and sampling rate and range and resolution of frequency spectrum (ω_{max}) are related using the expression below (Maia *et al*, 1997):

$$\omega_{max} = \frac{1}{2}\left(\frac{2\pi N}{T}\right) \qquad (3.10)$$

N is generally fixed for a particular analyser and is in powers of 2 (2: 512: 1024: 2048: 4096: etc).

Discretisation approximation and the limit of the length of time history may lead to poor results. These may be due to aliasing, leakage and may be avoided using windowing, filtering and averaging processes.

3.6.2.1 Aliasing

Aliasing is the misinterpretation of a signal by a sinusoid at lower frequencies. To eliminate this problem, the sampling rate should be twice the signal frequency. Furthermore, an anti-aliasing filter may be necessary.

3.6.2.2 Leakage

Ewins (2000) describes leakage problem as a direct consequence of the need to take only a finite length of time history coupled with the assumption of periodicity. This problem is minimised by one or all of the following options:

(i) Modifying the signal sample through windowing

(ii) Increasing duration of measurement period and increasing sampling rate to refine the frequency resolution

(iii) Using the duration of measurement sample that match the periodicity in the signal

(iv) Zero padding .i.e. adding zeros to the measured sample

3.6.3 Windowing

As mentioned earlier in this section, windowing minimises the leakage of the signal, as mentioned earlier. The time signal is multiplied by a window to obtain a smooth decay to zero at the limits of the recorded time period. The resulting signal therefore approximates an exactly periodic one. The windows incorporated in FFT and other analysers include the Hanning, Rectangular, Blackman, Barlett, Kaiser-Bassel windows amongst others. Use of these windows requires rescaling to compensate for the attenuation of the signals by the application of the window. Nevertheless, no scaling should be done if the response and the excitation signals are using the same window for calculating the FRF's (Ewins, 2000).

3.6.4 Increasing the duration of measurement

Increasing the transform size reduces leakage and gives a finer resolution around the region of interest.

3.6.5 Zero padding

The resolution may also be increased simply by adding a series of zeros to the short sample of the actual signal to create a new sample which is longer. However, the limitation of this method is that the resulting spectrum is not finer but is made coarser instead.

3.6.6 Averaging

Averaging is applied in analysis of random signals since FFT's of these signals do not exist. The analysis therefore yields estimates of SD that characterise this signal. The number of averages required is mainly determined by the statistical reliability and the removal of random noise from the signal. The peak holds, exponential and linear are some of the types of averages incorporated into analysers for averaging.

3.7 Modal parameter extraction

Modal extraction is a process of extracting modal parameters of the structure from the response data. These parameters can be extracted from time domain or measured FRF's. Before these methods are described, the next section deals with preliminary checks that need to be done on FRF so as to check validity of the measured data and therefore the accuracy of modal parameters of the structure.

3.7.1 Preliminary checks on FRF data

The response data is usually affected by noise, resistance of lead wires and their capacitance. For this reason, preliminary checks are necessary to avoid analysing poor data resulting in incorrect modal parameters. The following checks are done on measured FRF (Ewins, 2000):

(i) Low frequency asymptotes
(ii) Anti-resonances
(iii) High frequency asymptotes
(iv) Shape of FRF skeleton
(v) Nyquist plot

The characteristic of FRF's at low frequencies i.e. below the first resonance indicates the degree of reliability of the data. This is the region that gives the behaviour of the support conditions of the test. For grounded systems, stiffness characteristics that appear as an asymptotic to the stiffness line at the lowest frequency is expected (Ewins, 2000). The magnitude of this stiffness should equal the static stiffness at that point.

The incidences of anti-resonances also indicate the quality of the measured data. Anti-resonaces are expected to occur between two adjacent resonances, instead of minima for a point FRF. Conversely, for a transfer FRF's between two points separated on the structure, a minima is expected (Ewins, 2000). The antiresonance troughs for point FRF should have the same sharpness as the resonance peaks. These problems are chiefly due to inadequate vibration or limitations of the spectrum analyser resolution.

A check on the upper end of frequency range that reveals an asymptotic curve to mass or stiffness line of mobility measurements indicates a high probability of unreliable data (Ewins, 2000). The author suggests that this reflects a situation where the excitation is

applied at a point of very high mass or flexibility. Such a tendency results in considerable difficulties for modal analysis process. This problem may be minimised using different excitation points.

The shape of FRF's is also used for checking reliability of measured data. In this case, relative positions of resonances, unti-resonances and the ambient levels of FRF curve are used to check validity of measured data. A mass and stiffness lines through the FRF curve should pass through the middle of the FRF plot for consistence resonance and anti-resonances frequencies.

If all the checks on measured FRF's are satisfied, modal parameters of the system can be extracted, otherwise re-testing will be necessary.

3.7.2 Modal extraction methods

Modal extraction methods are split into time-domain based and frequency-domain based methods. The time domain methods are suitable for large frequency range, whereas the frequency techniques give the best results for limited frequency range where the number of modes is relatively few (Maia *et al*, 1998). The time domain based methods are further split into direct and indirect techniques. The indirect methods means that the identification of FRF's is based on modal parameters (i.e. natural frequencies, damping ratios and modal constants) whereas the direct techniques refer to the identification based on the general matrix equation of dynamic equilibrium (Maia *et al*, 1997).

Both time and frequency techniques are further classified into Single-Input Single Output based, Single-Input-Multiple-Output methods (SIMO) and Multiple-Input-Multiple-Output (MIMO) methods. The Single-Input-Single-Output (SISO) methods use a single FRF at a time from a single excitation point to compute modal parameters. On the other hand, Single-Input-Multiple-Output (SIMO) methods analyse multiple FRF's simultaneously with responses taken from different positions but using one excitation point. The Multiple-Input-Multiple-Output (MIMO) processes all the available FRF's from multiple excitation points.

These methods are well described in Ewins (2000) and Maia *et al* (1997) and this next section only discusses the Rational Fractional Polynomial method (RFP) which is mostly used by many commercial packages of modal analysis software.

3.7.2.1 Rational Fractional Polynomial method (RFP)

The RFP method is a curve fitting technique and widely used MDOF frequency domain method. Curve fitting is a process of matching a parametric model of an FRF to experimental data. The unknown parameters of the model are the natural frequencies, damping ratios and residues for each mode. Using the RFP method, the formulation of the FRF is expressed in rational fractional form and the error function to be minimised is established in such a way that the system of equations is linear, without requiring initial estimates for the modal parameters (Maia *et al*, 1997).

The FRF, in terms of receptance, for a linear system with N-DOF and viscous damping is expressed by the following partial fraction (Maia *et al*, 1997):

$$\alpha(\omega) = \sum_{r=1}^{N} \frac{A_r + i\omega B_r}{\omega_r^2 - \omega^2 + 2i\xi_r\omega_r\omega} \qquad (3.11)$$

Where: Ar and Br are constants

ω_r - Eigen frequency for mode r

ξ - Damping ratio

Equation 3.11 can be written as a ratio of two fractions i.e. rational fraction as below:

$$\alpha(\omega) = \frac{\sum_{k=0}^{2N-1} a_k (i\omega)^k}{\sum_{k=0}^{2N} b_k (i\omega)^k} \qquad (3.12)$$

An error function between the analytical FRF ($\alpha(\omega)$) and the experimental values, $\alpha'(\omega)$, at each frequency, ω_j, is defined as:

$$e_j = \frac{\sum_{k=0}^{2N-1} a_k (i\omega_j)^k}{\sum_{k=0}^{2N-1} b_k (i\omega_j)^k} - \alpha'(\omega) \qquad (3.13)$$

Let $e_j^{'}$ be a modified error function given by:

$$e_j^{'} = e_j \sum_{k=0}^{2N} b_k (i\omega_j)^k \text{ and making } b_{2N} = 1 \qquad (3.13a)$$

$$e_j^{'} = \sum_{k=0}^{2N-1} a_k (i\omega_j)^k - \alpha'(\omega)\left[\sum_{k=0}^{2N-1} b_k (i\omega_j)^k + (i\omega_j)^{2N}\right] \qquad (3.13b)$$

This leads to a system of linear system of equations avoiding the necessity of initial estimates of the modal parameters (Maia *et al*, 1997).

An error vector for all the measured frequencies is expressed as:

$$\{E\} = \{e_1^{'} \quad e_2^{'} \quad \ldots \quad e_L^{'}\}^T \qquad (3.14)$$

Substituting equation *(3.14)* into *(3.13b)* results in equation *(3.15)* expressed in compact form as:

$$\{E\} = [P]\{a\} - [T]\{b\} - \{W\} \qquad (3.15)$$

The polynomial coefficients $\{a\}$ and $\{b\}$ are calculated from a least-squares procedure that results in:

$$[P]=\begin{bmatrix} \varphi_{1,0} & \varphi_{1,1} & \cdots & \varphi_{1,2N-1} \\ \varphi_{2,0} & \varphi_{2,1} & \cdots & \varphi_{2,2N-1} \\ \cdot & \cdot & & \cdot \\ \cdot & \cdot & & \cdot \\ \cdot & \cdot & & \cdot \\ \varphi_{L,0} & \varphi_{2,1} & \cdots & \varphi_{L,2N-1} \end{bmatrix}=[\vartheta] \qquad (3.16)$$

Where $\varphi_{j,i}$ means a polynomial of order *i* evaluated at frequency ω_j. Likewise [T] is given as:

$$[T]=\begin{bmatrix} \alpha'(\omega_1)\theta_{1,0} & \cdots & \alpha'(\omega_1)\theta_{1,2N-1} \\ \cdot & & \cdot \\ \cdot & & \cdot \\ \cdot & & \cdot \\ \alpha'(\omega_L)\theta_{L,0} & \cdots & \alpha'(\omega_L)\theta_{L,2N-1} \end{bmatrix} \qquad (3.17)$$

This can be expressed as:

$$[T]=\begin{bmatrix} \alpha'(\omega_2) & & & \\ & \alpha'(\omega_2) & 0 & \\ 0 & & \cdots & \\ & & & \alpha'(\omega_2) \end{bmatrix}\left[\theta_{i,j}\right] \qquad (3.17a)$$

Where:

$$\left[\theta_{i,j}\right]=\begin{bmatrix} \theta_{1,0} & \theta_{1,1} & \cdots & \theta_{1,2N-1} \\ \theta_{2,0} & \theta_{2,1} & \cdots & \theta_{2,2N-1} \\ \cdot & \cdot & & \cdot \\ \cdot & \cdot & & \cdot \\ \cdot & \cdot & & \cdot \\ \theta_{L,0} & \theta_{L,1} & \cdots & \theta_{L,2N-1} \end{bmatrix} \qquad (3.17b)$$

Or $$[T]=\begin{bmatrix} & \alpha' & \end{bmatrix}[\Theta] \qquad (3.17c)$$

and $$\{W\}=\{\alpha'(\omega_1)\theta_{1,2N} \quad \alpha'(\omega_2)_{2,2N} \quad \ldots \quad \alpha'(\omega_1)\theta_{1,2N}\}^T \qquad (3.17d)$$

Solution for the unknown coefficients is achieved by minimising the error function, J, defined by:

$$[F]=-\mathrm{Re}\left(\left[T^*\right]^T[W]\right) J=\{E^*\}\{E\}$$

(3.18)

This leads to: $$\begin{bmatrix} [Y] & [X] \\ [X]^T & [Z] \end{bmatrix}\begin{Bmatrix} \{b\} \\ \{a\} \end{Bmatrix}=\begin{Bmatrix} \{G\} \\ \{F\} \end{Bmatrix} \qquad (3.19)$$

Where: $[Y]=\mathrm{Re}\left(\left[P^*\right]^T[P]\right)$; $[X]=\mathrm{Re}\left(\left[P^*\right]^T[T]\right)$; $[Z]=\mathrm{Re}\left(\left[T^*\right]^T[T]\right)$;

$[G]=\mathrm{Re}\left(\left[P^*\right]^T[W]\right)$; $[F]=-\mathrm{Re}\left(\left[T^*\right]^T[W]\right)$

The polynomials φ and θ should be calculated such that $\mathrm{Re}([P^*]^T[P])=[I]$ and $\mathrm{Re}([T^*]^T[T])=[I]$ and this is possible if the polynomials are complex orthogonal polynomials (Maia *et al*, 1997).

Using the calculated φ and θ, the modal parameters are calculated from equation *(3.12)*. The modal parameters (natural frequencies and damping ratios) are given by solving the polynomial denominator for equation *(3.12)*.

Ewins (2000) noted that this method results in both genuine and computational (non-existent) modes due to the assumption that the order of the model is N. To separate the real and computational nodes, it is essential to run the analysis for a given model order using different subsets of the data contained within the frequency range and comparing the

results. The real modes will be consistent while the computational modes are likely to change.

3.8 Summary

The main aim of this chapter was to understand use of modal testing for damage detection in civil structures. This chapter introduced the basics of dynamics in structures and various methods of modal testing. The testing equipment used in modal testing was also described. The processing of modal data was presented. Under this section, the key factors discussed include necessary configurations of the equipment to get quality results. The necessary critically checks on measured FRFs to ensure the reliability of measured data forms this chapter. The RFP method widely used by many commercial packages of modal analysis software is also described.

CHAPTER 4

METHODOLOGY AND PLAN OF ACTION

4.1 Introduction

Various vibration-based damage detection techniques used for detecting and locating damage in bridges and other civil structures were described in Chapter two. Different researchers (Xia *et al*, 2006; Farrar and Jauregui, 1995) investigated how these techniques can be used to detect and locate damage in bridges. Both positive and negative results were observed using these techniques. However, to date, these techniques have not been used for detecting and locating damage on beam and slab concrete bridges based on vibration data measured on top of the accessible deck slab only. This research therefore seeks to assess the integrity of shear connectors on beam and slab bridges using the aforementioned dynamic-based techniques described in Chapter two. The work consists of experimental and numerical study. The experimental work involved building a scaled model of a bridge and introducing artificial damage. The vibration techniques are then applied in an attempt to detect and locate the damage. Shear connector damage in beam and slab bridges is also investigated using analytical methods. A robust FE model of the structure was developed by integrating both FE modelling and experimental results. The FE model developed was applied to an existing concrete-concrete composite bridge. The following sections discuses this work in detail.

4.2 Model selection

Firstly, an appropriate bridge representation was required for this work. Two systems described in literature are used to idealise bridge systems i.e. a scaled model and a system of a single beam and slab. Literature shows a strong trend by researchers, in the 80's and 90', to idealise a bridge structure using the latter system (Thambiratnam and Brameld, 1994). The latter representation assumes an infinite stiffness in the transverse direction.

This however is not a true representation of prototype structures because the stiffness in the transverse direction is finite. The other idealisation of a bridge structure is using a scaled model. This is a more practical way of idealisation especially for damage detection works. This is because transverse vibrations and transverse modes can be used for damage detection within the structure. This research therefore uses a scaled model of a beam and slab bridge.

4.3 Research approach

The following flow-chart describes in detail the approach and scope of work carried out in this investigation. Aforementioned, this work consists of experimental and numerical study component. The integration of the two is explained using the flowchart below (Fig 4.1).

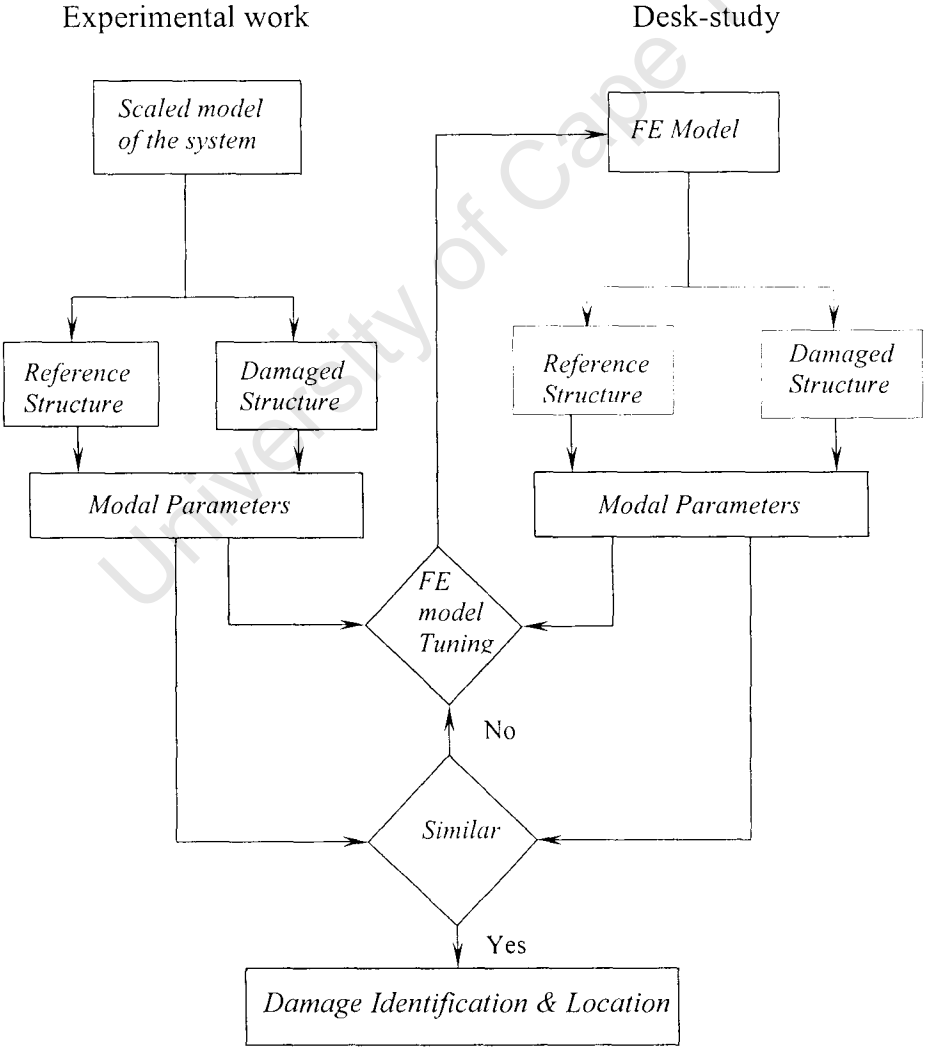

***Fig 4.1**: Flowchart of a typical dynamic investigation*

An FE model is required to design a robust experimental set-up. Firstly, the model is used to locate an optimum position of the exciter on the structure so as to excite all the modes of vibration. This is done using DPR values described in chapter three. Secondly, results of the model give an estimated range of frequencies expected during testing. Nonetheless, it is important to note that this FE model may not predict the modal behaviour of the structure and will have to be updated using experimental results if it is to be used for further investigations.

The updating or model tuning process is a two-part process i.e. prevalidating for an undamaged structure and post validating for a damaged structure. The model updating procedure is as follows (Brownjohn *et al*, 2003):

- Selection of responses as reference data.
- Selection of physical and geometrical parameters which affect the selected response data.
- Model tuning using the selected parameters.

However the reliability of a validated model depends on the precision of experimental results (Friswell and Motterhead, 1995). Poor results produce a corresponding poor fine-tuned model. Fine-tuning of the FE model will be described in further sections.

4.4 Model design and construction

A 1/6 scaled model of a typical 25 m long prototype concrete beam and slab bridge was selected for this research. I-section beam types were selected based on a survey carried out in Cape Town that showed that these beams were the most commonly used for constructing these bridges. However rectangular beam sections were cast to avoid use of complex moulds. The standardised dimensions of a girder for a 25 m span are found in the Somervillle and Tiller, 1975. The width is given as 510 mm and the depth is 1040mm. These girders have holes through the webs to facilitate the erection of diaphragms. The girders are spaced at 1500 - 3000 mm centre to centre. The deck slab depth ranges from 200 – 300 mm. Using these dimensions, the resulting dimensions for the scaled model are shown in Fig 4.2 and Fig 4.3. The deck slab was 4200 mm long, 1650 mm wide and 65 mm thick. The beams were 4200 mm long and had a cross-section of 170 mm x 120 mm.

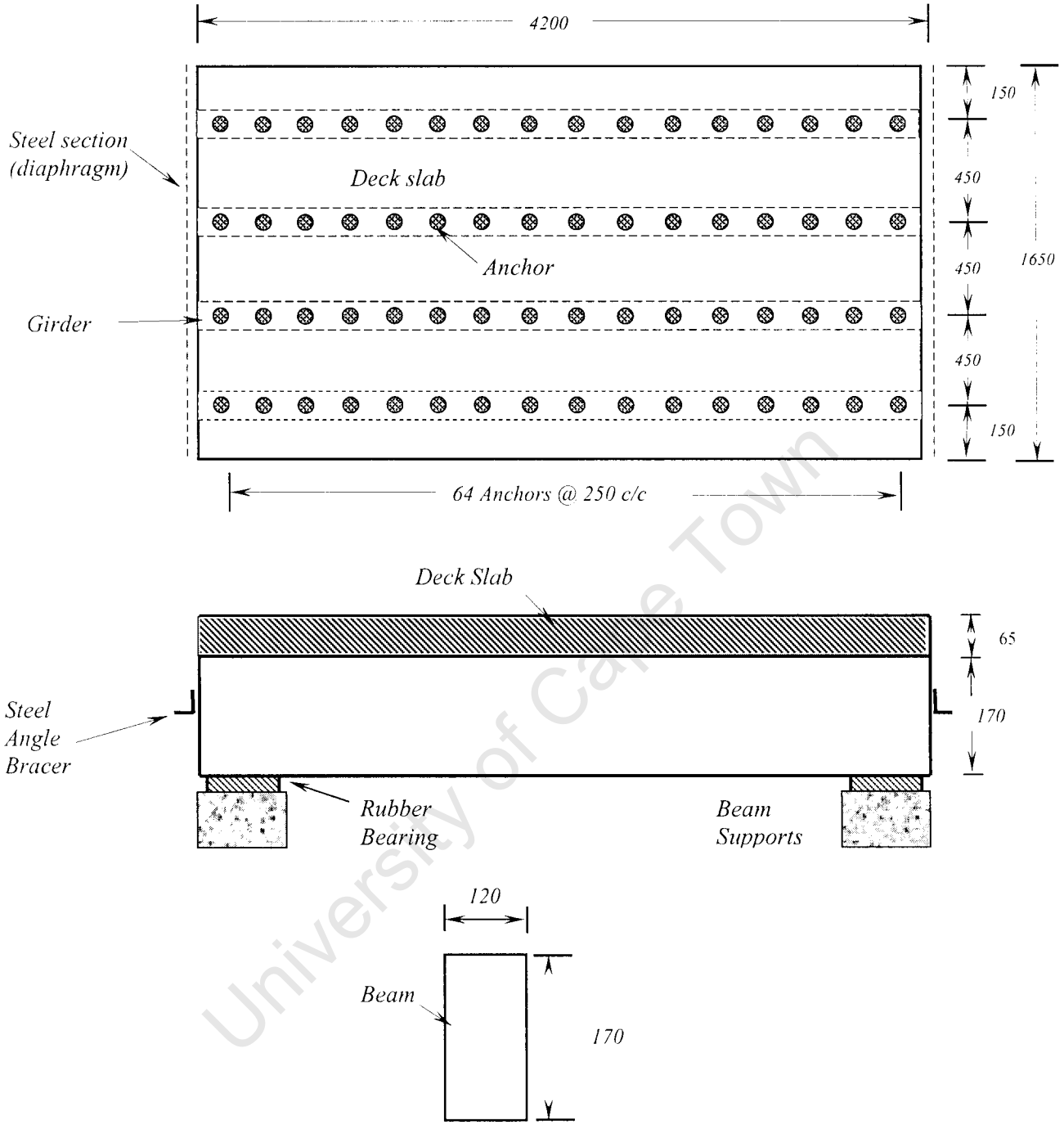

***Fig 4.2**: Plan view, cross-sections of the model and beam (all dimensions in mm)*

Because the scope of the study was to assess testing methods for reliability and practicality, with emphasis on the condition of the shear connectors, some simplifying assumptions were made. Firstly, the girders were made of reinforced concrete as opposed to pre-stressed girders used for prototype bridges. Secondly, the spacing of shear connectors in the model is uniform whereas in reality the spacing of connectors differs and finally shear connectors are protected using PVC pipes so as to have control on their

integrity. However, the selected anchor bolts that simulate the shear connectors in the real structures are modelled such that the composite action in the model is similar to that in real bridges.

In prototype bridges, diaphragms are cast across girders on piers and also in-between supports. The reinforcement for diaphragms passes through holes provided in the web of the girders for monolithic construction. These diaphragms help to distribute the loads and also act as bracers in transverse direction (Nigel, 2003). In this model, the transverse stability is provided by 50 mm x 50 mm angle steel sections bolted to the ends of beams as shown in Fig 4.2.

Fig 4.3 shows connection details between girders and the slab. 85 mm of 165 mm long, 10 mm diameter bolts with two nuts were cast into the girders at 250 mm c/c. The bottom nut, A, was used for anchorage while the top nut, B, was used for alignment purposes. 20 mm diameter PVC pipes were cast into the deck slab to protect the connectors and facilitate easy removal of deck slab and form work from the beams. However, this arrangement differs from reality where the connectors have direct bond to the deck slab concrete. A torque of 35 Nm was applied to all bolts.

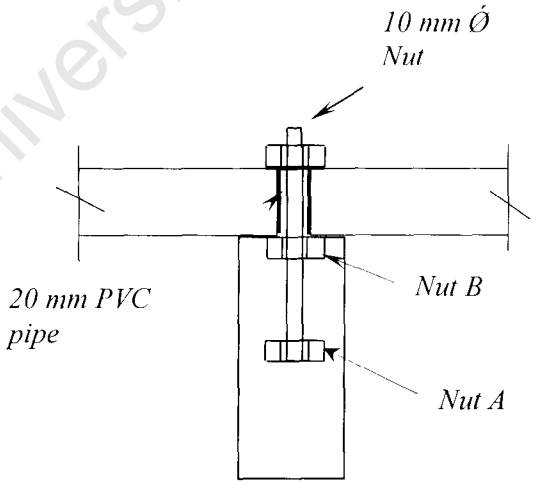

***Fig 4.3**: Slab-beam connection details*

4.5 Materials used

The design mix used consists of CEM (cement) 142,5N cement, Greywacke stones and Klipheuwel sand. Target concrete compressive strengths for the slab and beams were 25

MPa respectively. In prototype bridges, the beams are made stronger than the deck slab because they support imposed load and the self-weight of the slab in addition to their self-weight. This explains the different grades of concrete used. The mix design for the beams consists of water to binder ratio of 0.65, 19 mm Greywacke stones and Klipheuwel sand. For the slab, a water binder ratio of 0.7 was used. Klipheuwel sand and 13 mm Greywacke stone was used for the slab concrete. 13 mm stones were used in this case because of the small slab thickness and also a 20 mm cover used. Klipheuwel sand was selected because of its good grading and improved workability.

The construction process of the model is detailed in Fig 4.4.

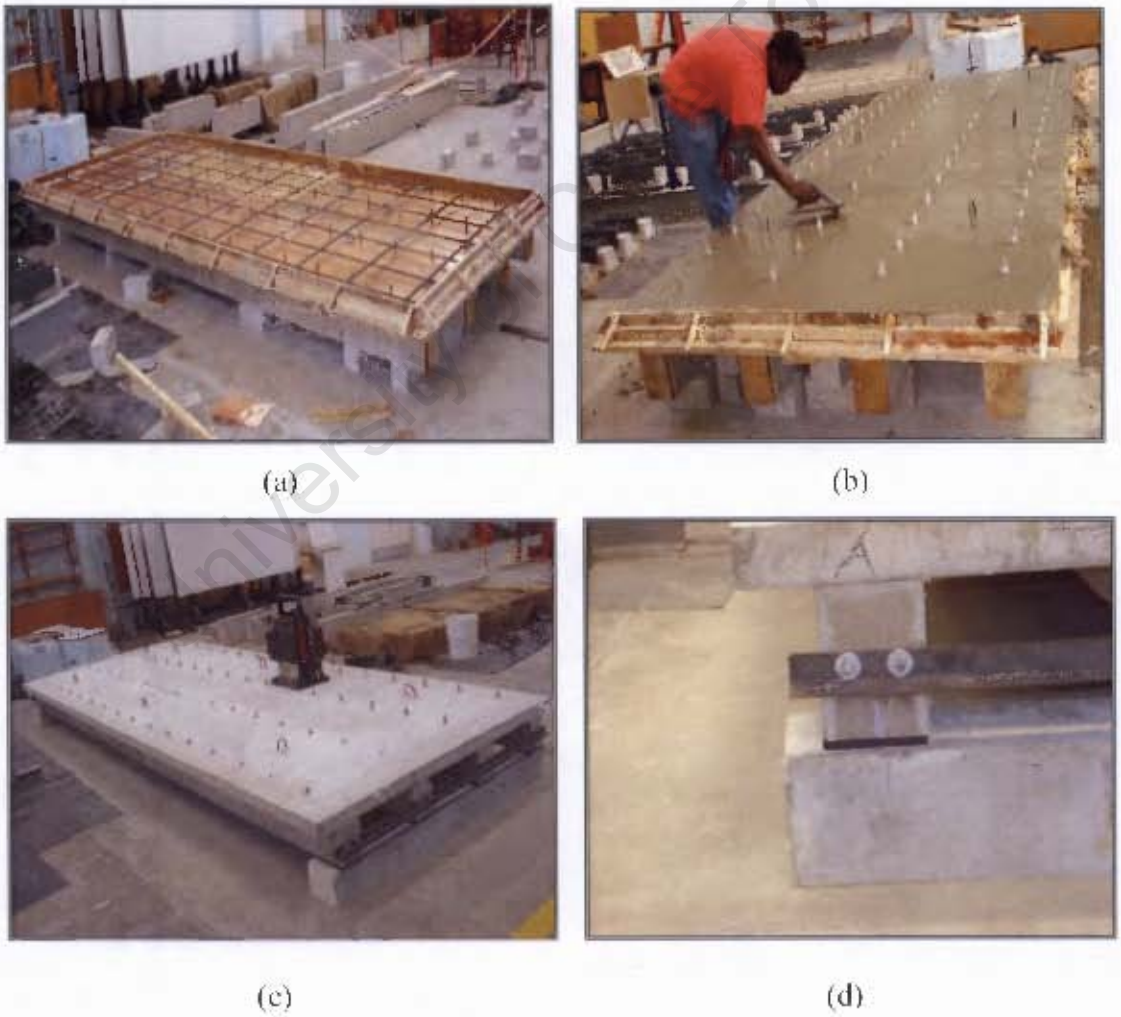

Fig 4.4: Construction process for the model

Firstly, four beams were cast with shear connectors at 250 mm spacing as discussed in section 4.4. The slab formwork was positioned on top of the beams as shown in Fig 4.4(a). However since bolts (shear connectors) were cast into the girders, holes were drilled in the formwork directly on positions of these bolts (Fig 4.4a). A mesh made of 10 mm reinforcement bars was used for the slab. The beams were spaced at 450 mm centres. Fig 4.4(b) shows shear connectors protected by 20 mm PVC pipes and protruding through the slab concrete just after casting. The PVC pipes remained within the slab concrete but were eventually cut to the same level to the slab concrete. The completed model is shown in Fig 4.4 (c). The stability of the model in transverse direction was provided by an angle steel section connected to beam edges. A typical connection detail of this bracing arrangement is shown in Fig 4.4(c). Two bolts were cast on both ends of each beam to facilitate fastening the bracer to the beams. This is shown in Fig 4.4(d). Also shown in Fig 4.4(d) are rubber bearings between the beams and beam supports. The bearings were similar to the ones used on prototype bridges.

This investigation included both experimental and FE analysis. The FE model development is detailed in following sections.

4.6 Finite Element Modelling (FEM)

Finite element models have been mostly used in the last four decade due to their computational advantages and effectiveness. They allow the user to analyse structural behaviour taking into account the connection deformability, non-linear behaviour of materials and material properties of concrete (Macorini *et al*, 2005). Nevertheless, a robust model is important for accurate and reliable results. Recently, the integration of experimental and FE models has resulted in reliable analytical models that can be used with confidence. Experimental results are used to update or fine-tune the FE model. As mentioned earlier in this chapter, the experimental results have to be reliable otherwise an FE model simulating unreliable experimental results would be produced. A suitable validated model can be utilised to investigate further aspects in more detail than is possible in experimental work.

In this study, the shear connection between the beams and slabs was critical. The shear connectors had to be accurately modelled in the FE model. The model has to take into

account the shear forces between the members, friction and the contribution of shear connectors to the integrity of the composite action.

4.6.1 Modelling composite behaviour in composite bridges

As the behaviour of composite structures presents significant non-linear effects, it is critical that the interaction of all the components and interfacial behaviour be properly modelled (Queiroz *et al*, 2007). The modelling of composite structures has received great attention in literature. However most of the work was done for steel-concrete composite structures. This representation is also believed to apply for concrete-concrete beam and slab bridge.

Various ways of modelling composite members as detailed in literature are described in the following sections.

4.6.1.1 Spring elements

Queiroz *et al* (2006) in their study to understand the behaviour of composite steel-concrete beams with full and partial connection used non-linear spring elements to model shear connectors. These connectors were modelled as shown in Fig 4.5. Two coincident nodes from the slab and the beam meshes were created at positions of shear connectors. The two nodes were connected using nonlinear spring elements as shown in Fig 4.5. These springs had vertical and horizontal stiffness and consequently accounted for the shear forces, friction and shear connectors. From their observations, a good correlation between experimental and simulated results was found.

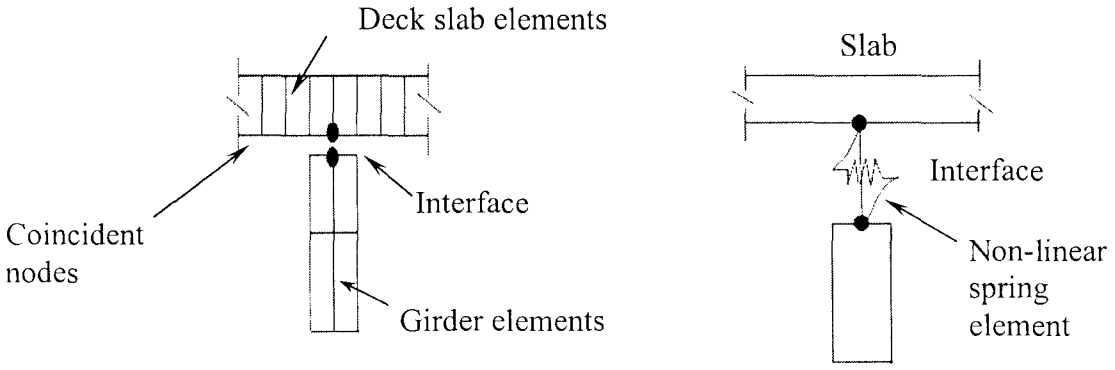

***Fig 4.5**: Representation of a shear connector using a 1-D non-linear spring element*

Wang and Chung (2008) and Macorini et al (2005) also used nonlinear springs elements to simulate shear connectors in a composite steel beam and concrete slab. Both horizontal and vertical springs were used to simulate shear, friction and axial deformation respectively. Using test data, the FE model was calibrated and the final model was able to simulate the structural behaviour well. These observations compare well with those from Queiroz *et al* (2006).

4.6.1.2 Smeared contact elements and 3-D spar elements

Another way of modelling the composite action in slab and beams is through use of smeared contact elements. These elements are capable of modelling the normal stiffness and tangential resistance to shear forces and therefore simulate the interface over an area (Clubley *et al*, 2003). The contact area has allocated stiffness properties for normal and tangential displacements. Clubley *et al* (2003) stated that these elements have an advantage because they remain a continuum which is subject to variation in stiffness so that further mesh refinement to produce an optimum surface topology is not required. Fig 4.6 illustrates a smeared element which is analogous to a spring. However, Clubley *et al* (2003) noted that it was difficult to achieve acceptable accuracy with smeared interfaces.

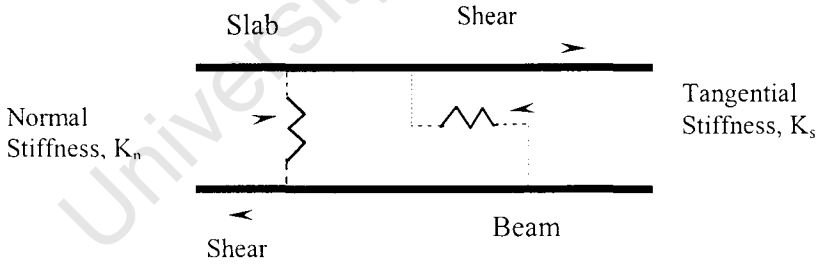

***Fig 4.6**: Contact element representation: Smeared element analogy (Clubley et al, 2003)*

Realising the limitations of a smeared element to represent the composite action, Clubley *et al* (2003) used discrete 3-D spar elements (LINK8) found in ANSYS together with smeared contact elements. These elements have mathematical properties which are representative of true physical interface actions. During simulation, stiffness values could be easily changed to required values. Surprisingly, Clubley *et al* (2003) observed that the use of these elements over the whole shear connector surface resulted in a stiffer model. Optimum configuration was found to be only three lines of discrete elements contact

between the shear connector and concrete. The authors conclude that use of combination of smeared elements and discrete element interfaces produced an accurate model of the interface.

4.6.1.3 Bar elements

Beam elements are often used to connect beams and slab together for composite action. These elements are idealised as two independent springs with stiffness in longitudinal and perpendicular directions. In general, a bar element is viewed as consisting of spring elements representing shear stresses between the interface and normal forces from shear connectors. Three researches in literature have applied these elements to model shear connectors between connecting beams and a slab. Xia *et al* (2007) used these elements to model the connection between concrete beams to a concrete slab in a bridge. It is important to note that this was the only work found dealing with concrete to concrete composite behaviour. Using this representation, Xia *et al* (2007) studied the sensitivity region for damage detection. Some loosened shear connectors were located while some were not. False damage location was also observed.

The same idealisation of shear connectors using bar elements was used by Kuan-Chen and Feng (2003) for modelling the connection of steel beams to concrete slab to analyse the behaviour of a bridge under load. As is always standard practice nowadays for engineering work, FE models are updated using experimental results to produce precise and reliable models that can be used for further investigations.

From the work of these three researches, positive observations were obtained from models using spring elements for the shear connectors. This proves to be the optimum way of modelling the composite behaviour in composite construction. Based on these observations, this research will use non-linear spring elements to represent the shear connectors and the composite behaviour of the structure.

4.7 Description of Finite Element model

Automatic Dynamic Incremental Non-linear Analysis (ADINA) was used for numerical work in this study. The program offers a wide range of options regarding element types,

material behaviour and numerical solution controls, as well as User Interfaces (UI), auto-meshes, and sophisticated postprocessors and graphics to aid in the analysis.

4.7.1 Element types and shear connector modelling

The modelling of complex structures is not trivial. Intelligent selection of elements to be used is required. Moreover, preparation of an FE model to be a candidate for updating requires some specific considerations of additional factors not normally taken into account in convectional FE model construction (Xia and Brownjohn, 2004). In this research, the resulting FE model was used for damage detection and thus parameters controlling damage needed to be modelled accurately.

The beams were modelled using eight node 3-D elastic isotropic Iso-beam elements. The deck slab was modelled using eight node 2-D elastic isotropic shell elements. The bearings were represented by non-linear spring elements catering for rotational, translational and shear rigidity. The stiffness of the springs (rotational, translational and shear) representing the bearings were provided by the manufacturer. The modelling of rubber bearings as spring elements was necessary for adequate control of the boundary conditions because vibration data is known to be sensitive to boundary conditions.

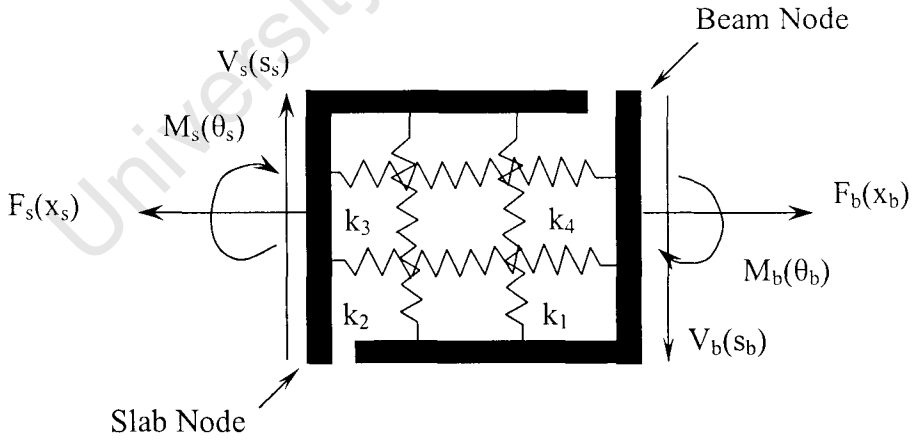

V_s - shear force on the slab node; s-displacement associated with the shear force

F_b - axial force on beam node; x- Axial displacement

M_b – moment on the beam node; θ – rotation of the beam node

***Figure 4.7**: Multi-degree spring element*

Shear connectors between the slab and beams were modelled using 3-D non-linear spring elements having rotational shear and translational stiffnesses. An exaggerated representation of a multi-degree spring element is shown in Fig 4.7 *(Li, Choo, Nethercot (1993))*. Three degrees of freedom are considered i.e. axial, shear and rotational deformations in the model. In addition, coupling effects between rotation and shear as well as rotation and axial deformations are considered. The general equilibrium equation for the element is expressed as follows:

$$\{F\} = [\mathbf{K(u)}]\{U\} + \tau \qquad (4.1a)$$

Where: $\{F\} = \{F_b, V_b, M_b, F_s, V_s, M_s\}^T$

$\{U\} = \{x_b, s_b, \theta_b, x_s, s_s, \theta_s\}^T$

τ - coupling effect

i.e.

$$\begin{Bmatrix} F_b \\ V_b \\ M_b \\ F_s \\ V_s \\ M_s \end{Bmatrix} = \begin{bmatrix} K_{ff} & 0 & K_{fr} & -K_{ff} & 0 & -K_{fr} \\ & K_{vv} & K_{vr} & 0 & -K_{vv} & -K_{vr} \\ & & K_{rr} & -K_{rf} & -K_{rv} & K_{rr} \\ & & & K_{ff} & 0 & -K_{fr} \\ & \textit{symetric} & & & K_{vv} & -K_{vr} \\ & & & & & K_{rr} \end{bmatrix} \begin{Bmatrix} x_b \\ s_b \\ \theta_b \\ x_s \\ s_s \\ \theta_s \end{Bmatrix} \qquad (4.1b)$$

Where: K_{ij} K_{ff} - Axial spring stiffness

K_{fr} - Coupled axial and rotation stiffness

K_{vv} - Shear spring stiffness

K_{vr} - Coupled shear and rotation stiffness

K_{rr} - Rotational spring stiffness

F – Axial force

V – Shear force

M - Moment

Huang *et al* (1999); Gattesco (1999) and Li, *et al* (1993) suggests that the spring constants (K_{ij}) can be obtained from test results, numerical models or calculation methods. In this work, equation 4.2 given by Chen and Lu (2003) was used to estimate the initial spring constants. The procedure for determining the optimum values for these spring constants is discussed in Section 4.7.3 under model validation.

$$k = \frac{E_s A_s}{h_s} \qquad (4.2)$$

Where: k – Axial spring stiffness: transverse and rotational stiffness were assumed based on axial stiffness

E_s - Elastic modulus

A_s - Cross-sectional area of the connectors

h_s - Height of the stud

4.7.2 Materials modelling

Table 4.1 lists concrete properties used in the model. The static modulus and density properties were determined experimentally.

***Table 4.1**: Material properties used to develop the FE model*

Property	***Value***
Static modulus of concrete: Beams	28E9 N/m^2
: Slab	26E9 N/m^2
Density of concrete: Beams	2317 kg/m^3
: Slab	2298 kg/m^3
Poisson's ratio of concrete	0.25

Figure 4.7 displays the resulting FE model. The fine tuning of the model using measured parameters is described in Section 4.7.3.

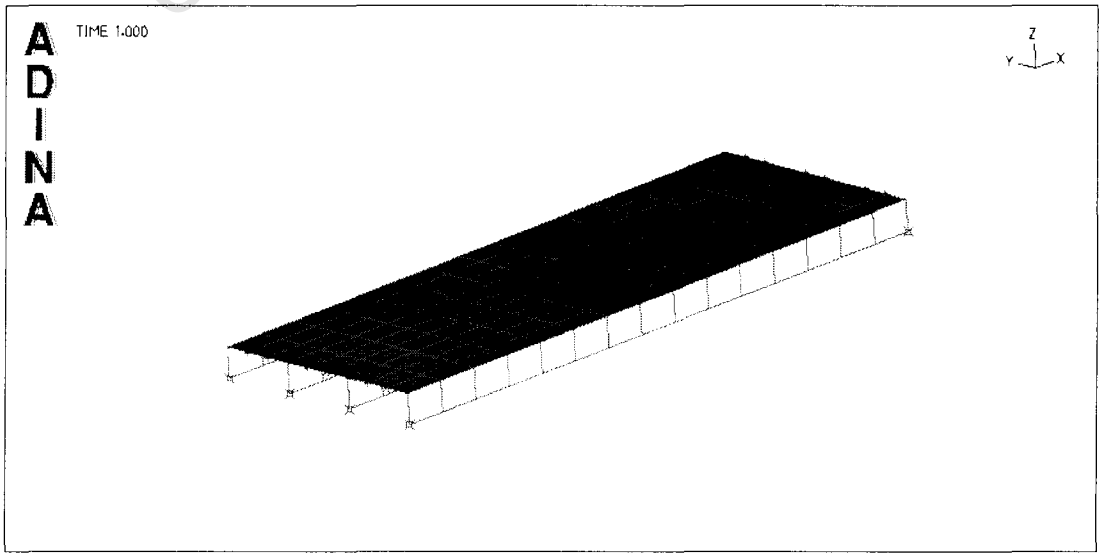

***Fig 4.8**: FE model of the bridge*

4.7.3 Validation of the FE model

Model updating techniques can produce a systematically validated FE model by correcting uncertainties from modelling, geometry, physical parameters and analysis to improve the analytical results based on vibration testing (Xia and Brownjohn, 2004). Model tuning is an iterative process that modifies selected parameters until an agreement between measured and simulated results is reached. The parameters selected for updating should describe the part of the system which is thought to be inadequately modelled such as boundary conditions and joints (Friswell and Mottershead, 1995). Using the selected parameters, the model is fine tuned and the accuracy of the resulting model is entirely dependant on accuracy of experimental measured data. The accuracy of the FE model, after fine tuning, can be checked using correlation indicators such as natural frequencies, MAC values amongst others (Xia and Brownjohn, 2004). Nevertheless, the process of fine tuning FE models may be difficult to apply for civil engineering structures because of constraints on prototype testing and experimental data analysis resulting from the nature, size, location and usage of these structures (Xia and Brownjohn, 2004). In most cases engineering intuition is applied to come up with a practical fine-tuning process.

The model updating procedure is as follows: firstly, the responses to be used as reference data are selected, secondly, physical and geometrical parameters that affect the selected response data are identified and finally the model is fine tuned using the selected parameters. This process is repeated for the damaged and undamaged structure resulting in two validating processes i.e. pre-validation and post-validation. In damage detection work, pre-validation is done for the undamaged structure which is used as a reference for post validation of the damaged structure.

The FE model updating process adopted in this work is detailed in Fig 4.8. The aim is to find optimum spring constants that will result in good correlation between the experimental and analytical results. Experimental natural frequencies were used as reference data. The initial FE model produced relatively higher natural frequencies. This means the model was relatively stiffer. However, the material properties used in the model were determined experimentally and thus were not altered so as to adjust the frequencies. The other parameter known to affect vibration data of civil structures are the boundary conditions. Spring elements were used to model all the boundary conditions. The spring

stiffnesses were therefore adjusted manually until a good correlation of frequencies was achieved. The updating process is shown in Fig 4.9. This was a manual updating process. However a more practical method based on appropriate algorithm(s) is required. This is recommended for future work.

4.7.4 Damage simulation in the model

Shear connectors were simulated using non-linear spring elements. The stiffness of these elements could easily be changed. Consequently, damage of shear connectors was simulated by reducing spring stiffness for the corresponding damaged connectors. Adjusting of spring stiffnesses was done manually since they were used as inputs

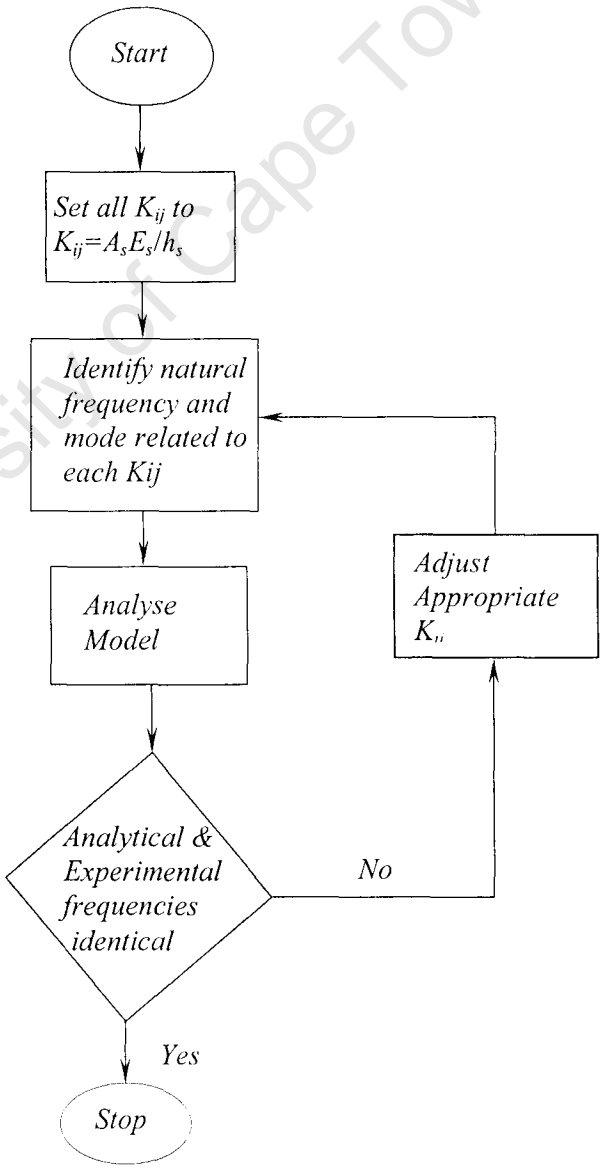

***Fig 4.9**: Flowchart for manual fine-tuning the FE model*

4.8 Experimental vibration testing

The aim of the study is to investigate the practicality of vibration based damage detection techniques (VBDDT) to detect and locate failure in composite action resulting from damage on shear connectors. Given two states of a structure, a reference state and a damaged state, the vibration data from the damage state is directly comparable to vibration data from the reference state, if data from both states were collected under similar environmental and boundary conditions. In such a case, effects of the environmental and operational conditions are eliminated. It can therefore be assumed that any changes in the vibration data are as a result of a change in structural condition.

4.8.1 Test Equipment

4.8.1.1 Excitation

Model 400 Electro-Seis Shaker (Fig 3.3) was used to excite the structure. The shaker was driven using a chirp signal. Two chirps were used, the first chirp had a frequency range of 5-64 Hz while the second chirp ranged from 55-128 Hz. Three natural frequencies were identified exited using the first chirp (5-64 Hz) and three more natural frequencies of vibrations were excited using the second chirp. Two chirps were used so as to provide adequate excitation of the structure thereby exciting all modes of vibration of the structure within the frequency band. This eliminates problems associated with processing data from an inadequate excited structure.

The shaker position is shown in Fig 4.10. This optimum location was determined based on mode shapes extracted analytically. The eccentric location of the shaker provides full harmonic excitation in the transverse direction perpendicular to the centreline of the bridge, as well as in the longitudinal direction (Womack and Halling, 1999). The force exerted on the structure was recorded using a piezoelectric accelerometer attached and was used as an input in processing the data.

4.8.1.2 Data Acquisition

Data acquisition requires careful selection of sampling points on a structure so as to capture the required response. The transducer type, sampling rate and frequency and cut-off frequency are also important. QA 700 (force balance) accelerometers (Fig 3.5) were used to measure the response of the structure. 4096 samples were recorded at a sample rate

of 500 Hz. The cut-off frequency was set at 300Hz. 112 structural responses were recorded on positions shown in Fig 4.10 for different damage scenarios to be described in Section 4.9. The accelerometers were placed directly on shear connector positions and also between the beams as shown. A more dense measurement setup could have been used but this was not necessary for this work because responses directly on shear connectors and between connectors were adequate to detect any irregularities resulting from loosening of shear connectors (damage).

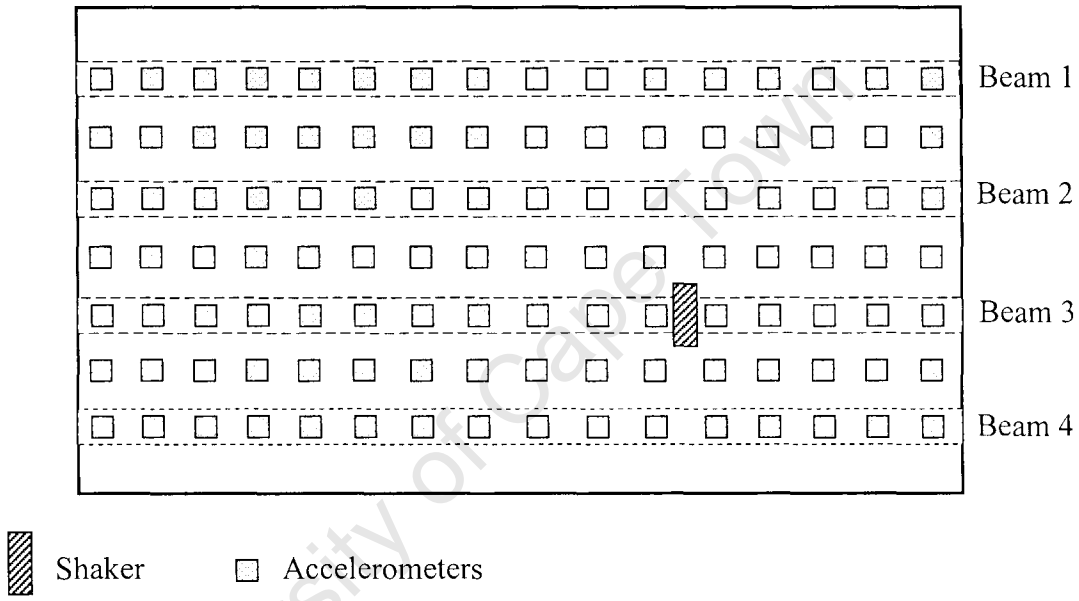

***Fig 4.10**: Position of the sensors and the shaker on deck slab*

ME'scopeVES software was used to process the modal data. This software contains an FFT and Inverse FFT that make it easy to analyse signals. It also has capabilities to remove noise from the signals and sharpen resonance peaks due to windowing integrated into the software. A number of modal extraction methods including RFP, described in chapter three, are also included into this software.

4.9. Damage configurations

Four damage scenarios, in addition to the undamaged state, were investigated. 35 Nm torque was applied to all bolts for the undamaged structure *(X0)*. The following damage cases investigated:

Case 1 (X1): This damage case simulated a light damage on the structure. Four shear connectors were loosened in the middle of the slab on two beams i.e. two on beam B2 and another two on B3 as shown in Fig 4.11(a). This result to 6.25% damage expressed as the ratio of the loosened shear connectors to the total number of shear connectors in the model.

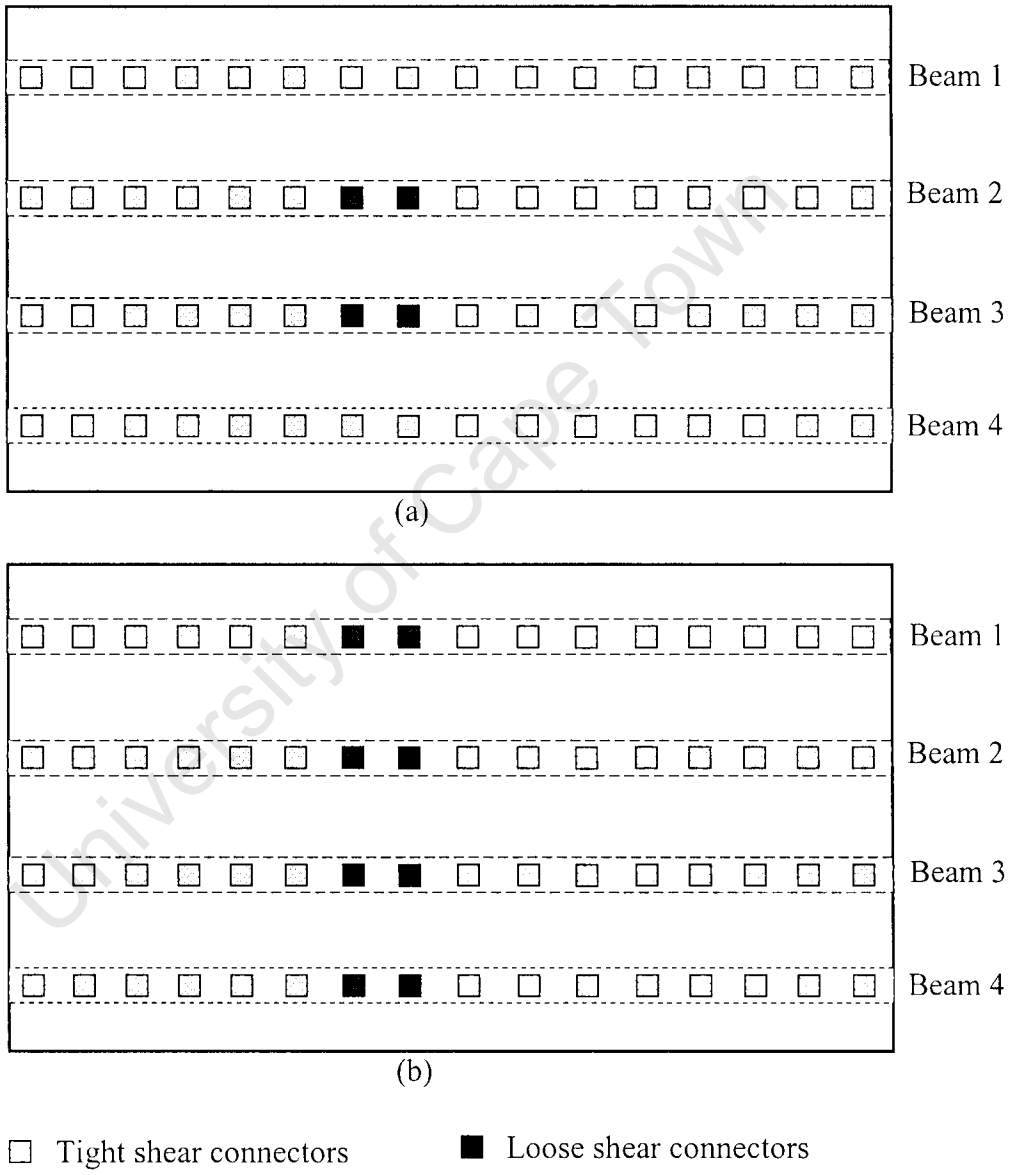

***Fig 4.11**: Damage scenarios: (a) Case one (b) Case two*

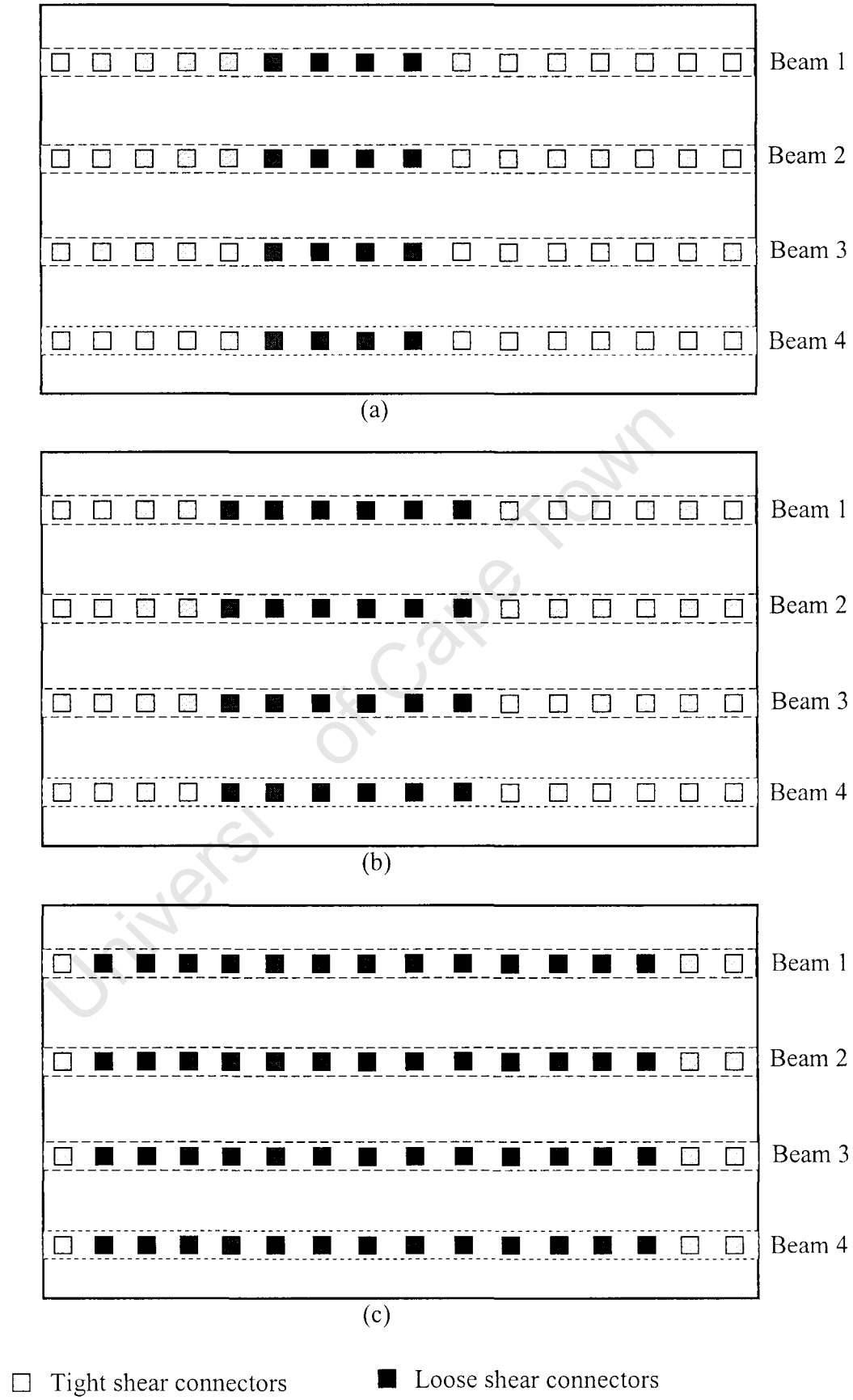

***Fig 4.12**: Damage scenarios: (a) Case three (b) Case four (c) Case five*

Case 2 (X2): For this case, four more shear connectors were loosened in addition to those for damage case *X1*. The connectors were loosened in the middle of two outside beams (Beam1 and Beam 4) as shown in Fig 4.10(b). The loosened shear connectors accounts for 12.5% damage on the structure.

Case 3 (X3): In this case 25% of shear connectors were loosened. Eight connectors, two in each beam, from the centre extending outwards were loosened. The loosened shear connectors are shown in Fig 4.12(a). This simulates a case of gradual increase in damage from the centre outwards.

Case 4 (X4): An additional eight connectors to ones in case three were loosened. The loosening was introduced in the same way as in damage scenario three. Fig 4.12(b) shows the loosened shear connectors for this damage.

Case 5 (X5): Case five is taken as the severe damage scenario. 75% of shear connectors are loosened. This damage scenario may be rare to find in any bridge. On the other hand, this might be possible especially when a natural disaster such as an earth quakes occurs. The loosened shear connectors for this damage are shown in Fig 4.12(c).

4.10 Summary

This chapter dealt with experimental and FE study done to investigate how damage in shear connectors can be detected. An important step in this research was to produce a scaled physical model of a typical concrete beam and slab bridge. The model had to simulate the bridge as accurately as possible. Using this model, vibration based tests were conducted to detect and locate the inflicted damage on shear connectors. Also described in this chapter was the integration of laboratory work with FE analysis. A robust FE model for the beam and slab was produced. The key parameter in this model was the simulation of the composite action between the beams and the slab. Spring elements were used. The resulting model, after updating using vibration modal data obtained experimentally, was able to produce the modal parameters of the structure. The FE modelling developed was applied on an existing concrete-concrete composite bridge that was closed to traffic due to serviceability problems. The shear connectors of this bridge were suspected to have failed.

This is discussed in detail in chapter six. The next chapter discusses the results of experimental and numerical investigations.

CHAPTER 5

DISCUSSION OF RESULTS

5.1 Introduction

This chapter presents and discusses findings of the investigation. This includes the global modal parameters for the undamaged and damaged systems extracted, as well as results on various localised vibration-based damage detection algorithms for both the experimental and analytical investigations. The following global modal parameters of the systems were identified:

(i) Natural frequencies
(ii) Damping ratios
(iii) Mode shapes, and
(iv) Modal Assurance Criterion (MAC)

The localised damage detection techniques investigated include the co-ordinate modal assurance criterion (COMAC), two dimensional mode shape curvature (MC) changes, change in flexibility and stiffness method. As stated in the introductory chapter, the objective of the research is to identify a practical vibration based technique(s) which can be used to detect loss of composite action in concrete-concrete composite bridges. The first stage of the work was the extraction of global modal parameters (modal signature) of the systems from response measurements. Secondly, different damage localising algorithms were then applied on modal data extracted. Detailed description of these processes now follows.

5.2 Signal processing and extraction of frequency response functions (FRFs)

The response of the structure was measured at shear connector positions along the structure and in between the connectors across the structure. A total of one hundred and twelve response readings were recorded for each damage scenario. A typical response

signal from one of the accelerometers is shown in Fig 5.1. This figure displays the accelerations or response of the system to the excitation force applied.

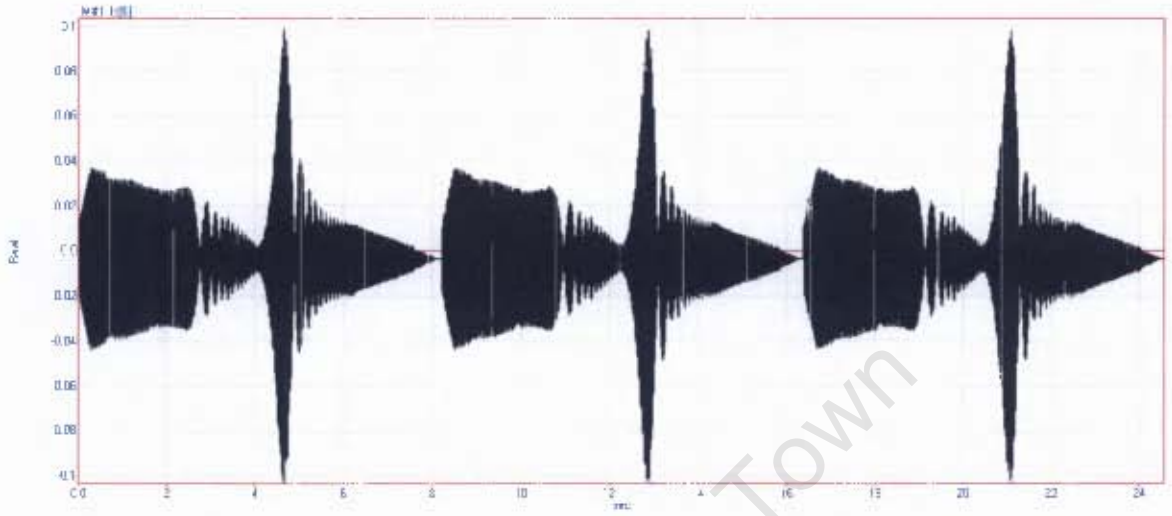

***Fig 5.1**: Response time waveform signal*

Response measurements displayed in Fig 5.1 were used to compute Frequency Response Functions (FRF's) of the system. The FRF's for one of the systems is shown in Fig 5.2 for 112 response data recorded. The peaks of this graph indicate mode of vibrations characterised by the modal frequency and damping ratio which are the modal signatures of the structure. These signatures were used to assess the service performance or condition of shear connectors.

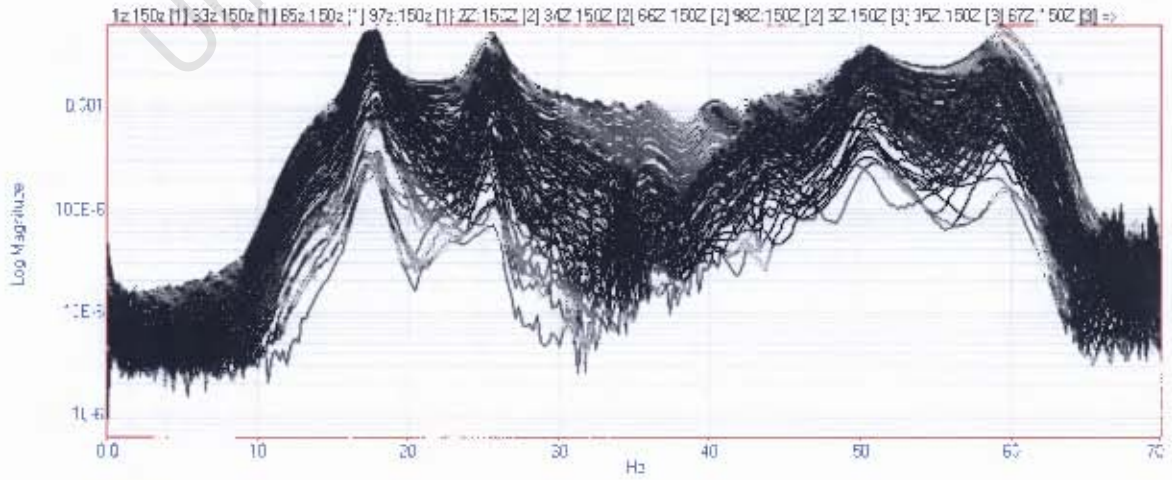

***Fig 5.2**: FRF's overlaid traces calculated from the measured response data*

5.3. Extraction of modal parameters

The Rational Fractional Polynomial (RFP) method, described in chapter three, was used to curve-fit the calculated FRF's to extract the modal parameters. RFP technique solves a set of linear equations for the unknown numerator and denominator polynomial coefficients (Richardson and Schwarz, 2003). The curve fitting technique requires three steps:

(i) Determine the number of modes represented by the data.

(ii) Estimate a pole for each mode.

(iii) Estimate residues for each mode

A pole is defined as the root of the transfer response function. The residues are directly related to the amplitude of of the impulse response function (Ewins, 2003). They represent the mode shape component for each mode.

The Complex Mode Indicator Function (CMIF) was used to determine the number of modes present in the calculated FRFs. The CMIF is defined by the single value decomposition of the FRF matrix (Ewins, 2003). The CMIF is defined as (Ewins, 2003):

$$[CMIF]_{PxP} = [\Sigma(\omega)]^{T}_{PxN} [\Sigma(\omega)]^{H}_{NxP} \qquad (5.1)$$

Where $\Sigma(\omega)$ describe the amplitude information and the number of non-zero singular values (independent modes of vibration that contribute to the measured FRFs).

The CMIF matrix results in singular values and vectors, all of which are frequency dependant (Ewins, 2003). The mode indicator values are provided by the squares of the singular values and are plotted as a function of frequency as shown in Fig 5.3 as a stability diagram for a set of calculated FRF's. A stability diagram is a plot of pole estimates for different curve fitting model sizes (numbers of modes). This diagram is useful for obtaining more accurate modal frequencies and damping estimates from a set of measurements. A stable pole confirms the availability of the mode.

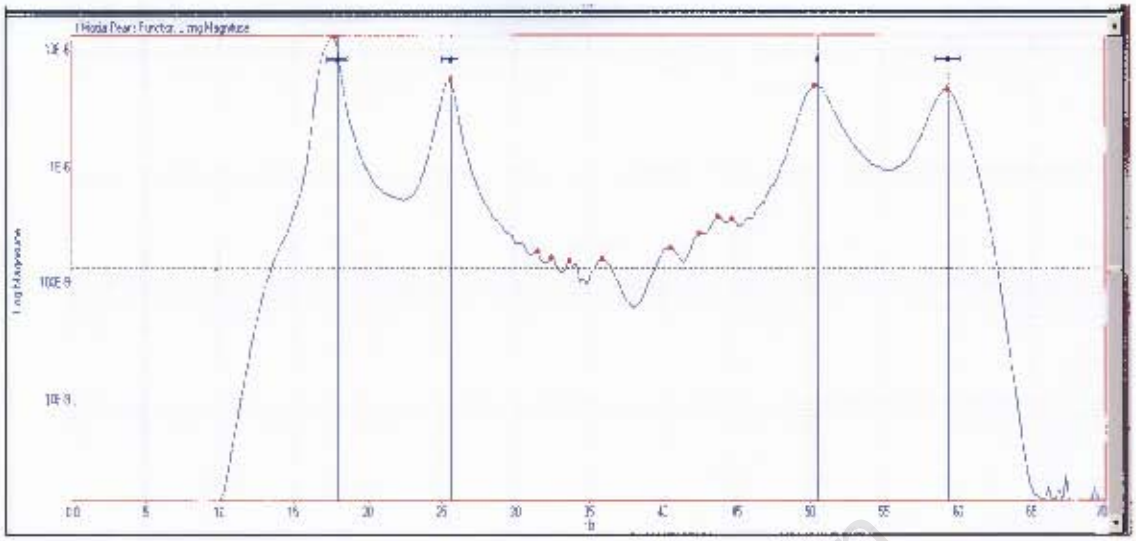

Fig 5.3: Stability diagram

The short vertical lines in the stability graph give the estimate of natural frequencies while the horizontal blue lines represent the damping ratios. From Fig 5.3, four natural frequencies where identified for one of the damaged state.

5.4. EXPERIMENTAL RESULTS

5.4.1 Global damage parameters

These include natural frequencies and damping ratios, mode shapes and the MAC values.

5.4.1.1 Natural frequencies and damping ratios

Natural frequencies represent the interrelationship between the stiffness of the system and it's mass. For this investigation, the mass of the system is assumed to remain constant and therefore any change in natural frequency is associated with change in stiffness resulting from loss of composite action. Table 5.1 shows natural frequencies and damping ratios extracted for the undamaged structure denoted (*X0*) and damaged structural systems denoted by *X1, X2, X3, X4 and X5*. As mentioned in section 4.9, 6.5% of shear connectors were loosened for damage scenario *X1*. 12.5%, 25%, 35% and 75% of shear connectors were loosened for damage scenarios X2, X3, X4 and X5 respectively. The system had relatively higher natural frequencies in comparison to those of prototype bridge structures. In real bridges, the first natural frequency can be as low as 7 Hz. The higher frequencies signify a stiffer model which is not a true replica of the actual structure. This, however, should not have a significant effect in this study since all measurements are based on the same model.

A general drop in natural frequencies was observed from the intact state *(X0)* to the most severe damage state where 75% of shear connectors were loosened. However, this was not the case for the damage state *X2*. Natural frequencies recorded for first bending, torsional and transverse modes of this damage scenario where higher than those of damage scenario *X1*.

Apart from this scenario, the trend in frequencies reveals a gradual decrease in the global stiffness of the structure resulting from loosening the shear connectors. As expected, a severe loss in stiffness was recorded on damage scenario. For prototype bridge structures, the change in frequencies below 0.1% might be attributed to environmental effects when measurements are taken on differing environmental conditions (Farrar and Jauregui, 1995). In most practical cases, however, a change of natural frequency by more than 0.1% may indicate the presence of a problem in a structure. In light of the above, a drop of natural frequencies by 25% recorded may not be encountered except in cases of natural disasters where an overhaul of the complete structure may be needed.

Table 5.1 also shows the damping ratios for different damaged systems. Damping represents the ability of a disturbed system to dissipate energy. The damping ratio therefore is the measure of damping of the system. The damping ratio values had no clear trend as seen in Table 5.1. Consequently, very little information was deduced from these values. This correlates with findings from the work by other researchers (Wahab and De Roech ,1999; Yong *et al*, 2007) who noted difficulties in measuring this property of a structural system. In conclusion, damping ratios are not suitable in the present work

Mode shapes associated with natural frequencies were also extracted. These are presented described in Table 5.2.

***Table 5.1**: Experimental natural frequencies and damping ratios*

Mode	*Case*	*Frequency, Hz*	*% Change based on X0 Frequency*	*Damping*
1st Bending Mode	*X0*	19.71	-	1.88
	X1	19.59	0.61	1.73
	X2	19.67	0.20	1.63
	X3	19.30	2.08	1.94
	X4	18.90	4.11	1.93
	X5	18.01	8.63	3.94
Torsional mode	*X0*	28.86	-	2.76
	X1	27.93	3.22	3.47
	X2	28.38	1.66	2.27
	X3	27.91	3.29	1.60
	X4	27.38	5.13	1.60
	X5	25.65	11.12	2.29
2nd Bending mode	*X0*	67.69	-	1.39
	X1	66.47	1.80	1.93
	X2	66.47	1.80	2.26
	X3	60.13	11.17	1.86
	X4	52.71	22.13	1.34
	X5	50.54	25.34	0.03
Combined Bending and Torsion	*X0*	77.85	-	0.41
	X1	75.36	3.20	2.72
	X2	74.35	4.50	2.04
	X3	71.77	7.81	1.84
	X4	69.19	11.12	1.35
	X5	59.57	23.48	2.04
Transverse mode	*X0*	86.51	-	0.89
	X1	83.93	2.98	0.59
	X2	88.41	2.20	0.21
	X3	86.71	0.23	1.25
	X4	79.68	7.90	0.58
	X5	67.62	21.84	0.98

5.4.1.2 Mode shapes

A mode shape indicates the deformed shape of the system at a particular frequency and damping ratio i.e. resonant property of the structure. Five mode shapes were extracted from the system and these are displayed in Fig 5.4.

Failure in composite action resulting from loosening of shear connectors was expected to be detected as irregularities in amplitudes of mode shapes. However, a general observation on all modes reveals that there was no difference for mode shapes between the undamaged and damaged structure, as can be seen. Further analysis of the shapes was therefore needed and this was done by plotting the mode data at each measurement point.

Table 5.2: *Comparisons of experimental mode shapes for undamaged and damaged states*

Mode	***Damage Case***			
	X0	*X1*	*X3*	*X5*
1st Bending				
Torsional				
2nd Bending			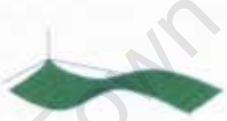	
Combined Bending and Torsion				
Transverse				

The mode shapes from the experimental data were not properly scaled to preserve the mass and the elastic properties of the structure (Schwarz and Richardson, 2003). Scaling therefore was necessary for effective comparisons of the modes. In each case, mode data from the undamaged structure was used for scaling modes for damaged systems. Figure 5.4 shows the scaled mode shapes plotted using shape vectors for different damage states.

(a) Bending Mode

A plot of this mode was done on shear connector positions along one inside beam and also on one outside beam. The shear connector positions (degree of freedom) are labelled as shown in Fig 5.4. The undamaged structure had the lowest amplitudes of vibrations and a smooth curvature on both the inside and the outside beams. This is shown in Fig 5.5. The mode curvature for the first damage state *X1* follows that of the undamaged case except at the centre of the beam where there was change in curvature. This irregularity was

observed over a region covering three shear connectors. This is the region where artificial damage was inflicted.

On the other hand, a different scenario on damage state *X2* mode could be seen from Fig 5.5. The highest amplitudes of vibrations were recorded on this damage mode. This was not expected, however. Moreover, a smooth mode curvature was observed over the entire region. These deviations on this damage mode were observed on natural frequencies.

The plot of the first bending mode for damage case *X3* reveals the same scenario as for damage case *X1*. A distinct change in curvature of the mode shape could be seen at the centre of the beam. The curvature of the mode followed that of the intact structure except at the middle span where increased amplitudes over five loosened shear connectors is observed. This localised the damage region on the system. Similarly, a clear indication of damaged indicators was evident on damage case *X4*, where 35% of shear connectors were loosened. The gradient of mode shape increased on positions of loosened shear connectors on both the inside and outside beam.

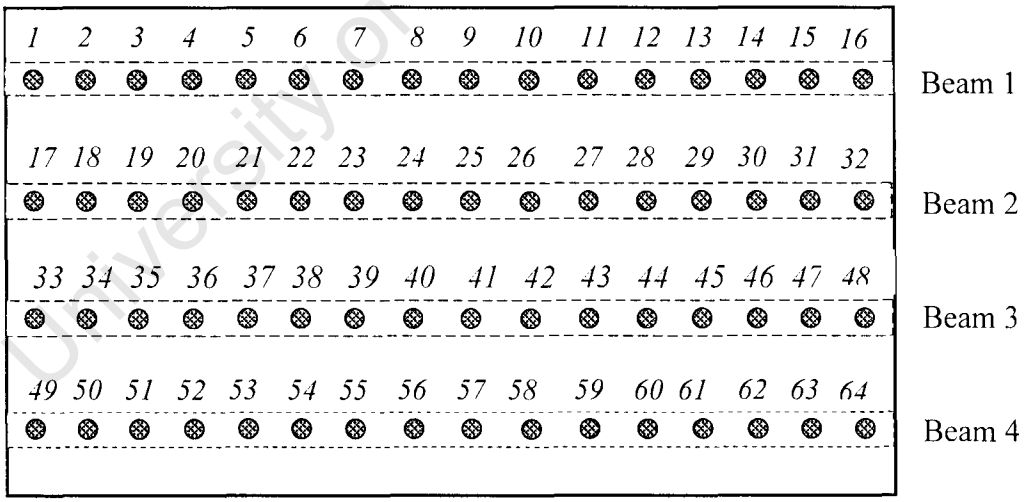

***Fig 5.4**: Degrees of freedom assigned to shear connectors*

As expected, damage scenario *X5* mode had the highest amplitudes of vibrations on most positions of the loosened shear connectors. This excludes observations on the mode shape for damage case *X2*. The change in curvature on the damaged region was more pronounced on the outside beam as can be seen in Fig 5.5. This is as a result of minimum restraint on free edge of the deck slab.

In summary, the failure in composite action in concrete beam and slab can be efficiently assessed using the first bending mode of the system. Interestingly, this mode was not expected to distinctly localise the damaged region considering that the whole mass of system moves in one direction on this mode. However, for effective detection of this damage in real bridge structures, long term monitoring and measurements on the structure should be done so as to compare the mode curvatures.

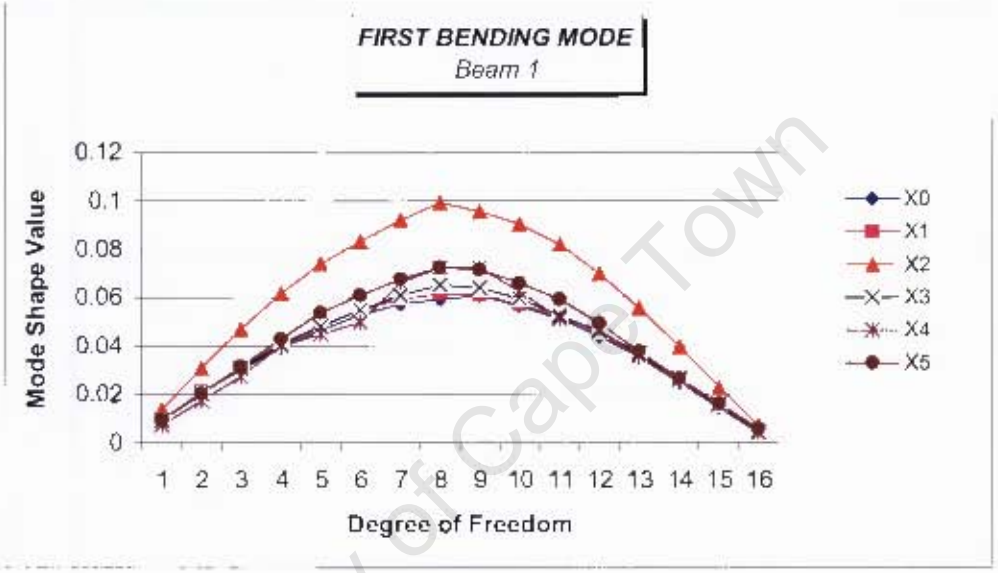

(a)

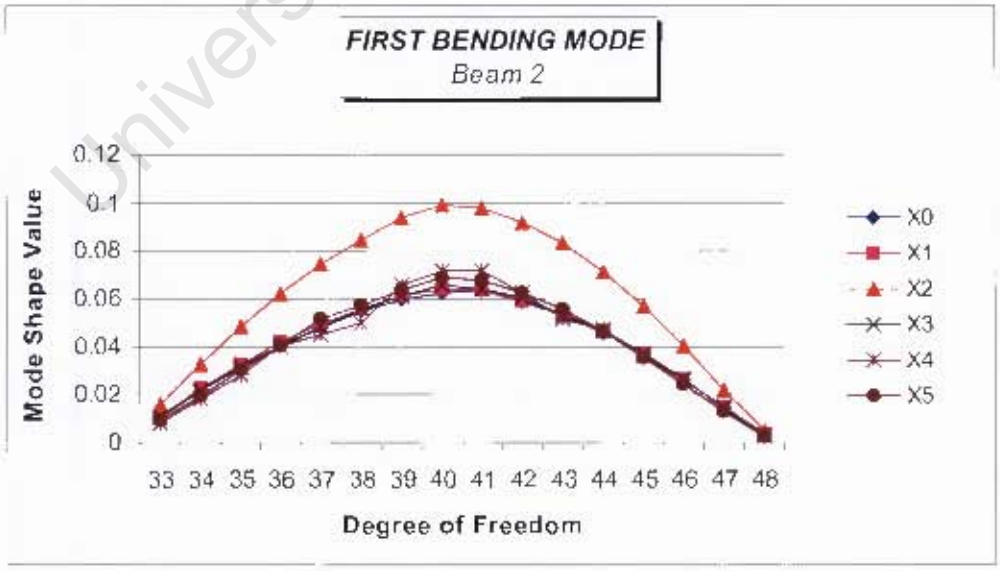

(b)

Fig 5.5: *Plot of first bending mode (a) outside beam (b) inside beam*

(b) Torsional mode shape

The plotted torsional modes for different systems are displayed in Fig 5.6 on both the inside and outside beam

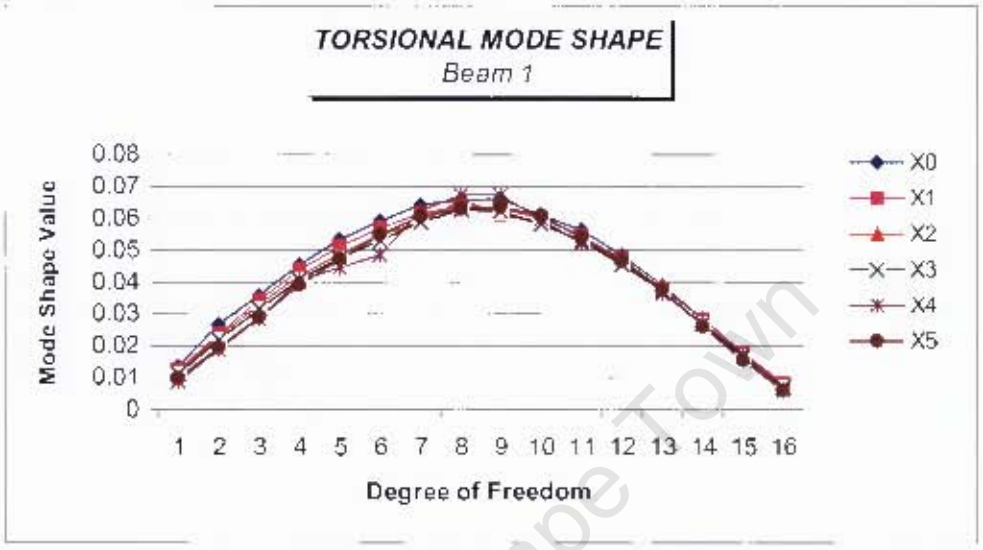

(a)

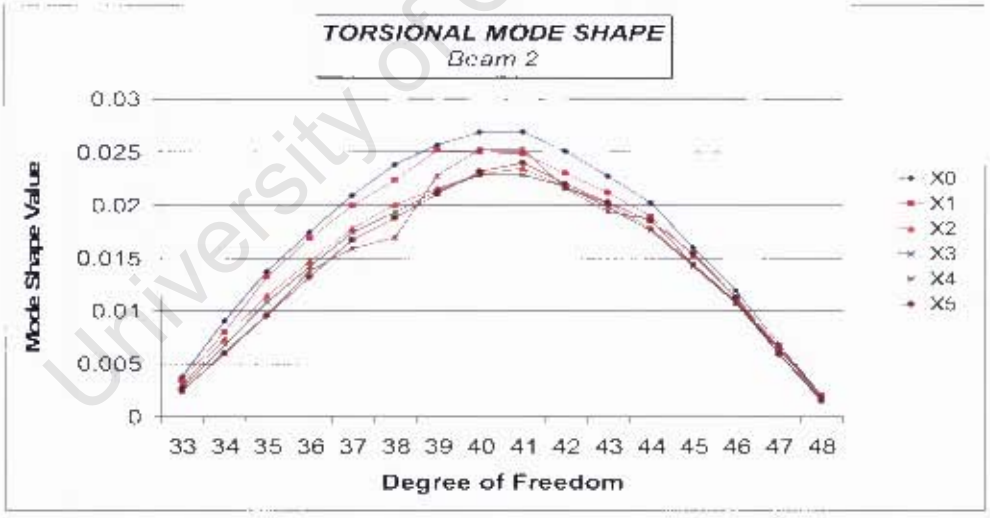

(b)

Fig 5.6: *Torsional mode: (a) Outside beam (b) inside beam*

Maximum amplitudes of vibration were recorded on the undamaged mode shape while the minimum was recorded on the severe damage case *X5*. Curvature change for the first damage case was recorded on midspan as expected. This was observed over the three loosened shear connectors. The mode plot for damage *X2* and *X3* were the same and no clear curvature change on damage regions could be observed. This was not the case on damage scenario *X4*, however. A noticeable curvature change is evident on mode plot of

this damage scenario particularly on the damaged region. Surprisingly, the loosened shear connectors could not be located on mode plot for severe damage *X5* as seen in Fig 5.6(a). This was not expected considering that 75% of the connectors were loosened on this damage case.

In general, this mode was not as effective as the first mode in detecting loss in composite action. This nullifies the assumption made earlier concerning the sensitivity of different modes to damage.

(c) Second bending mode

One of the first five modes extracted on the systems is the second bending mode. This mode is shown in Fig 5.7 for different states of the system investigated. The plot was particularly not helpful as there was no clear trend on the mode shapes. However, there was a shift in the modes at the centre. The mode shape for the undamaged case is lagging behind from the modes of damaged scenarios. This may be linked to the effect of damage in the structure.

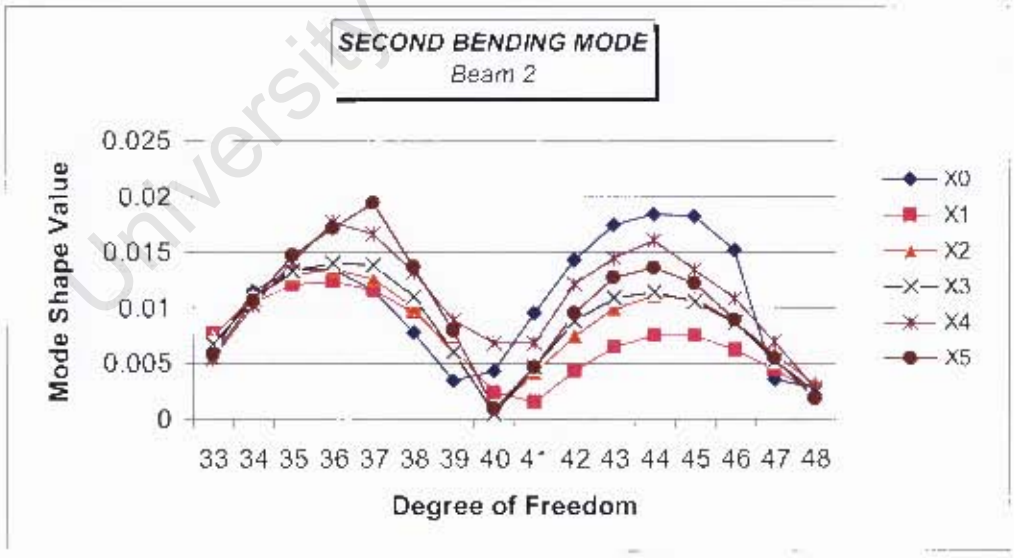

***Fig 5.7**: Plot of experimental second bending mode*

(d) Transverse and combined bending and torsion mode shape

The transverse and combined bending and torsion mode shapes are plotted in Fig 5.8 and Fig 5.9. As in second bending mode plot, it was difficult to follow the trends displayed. This made it difficult to draw any meaningful conclusions that can be linked to the damage in composite action.

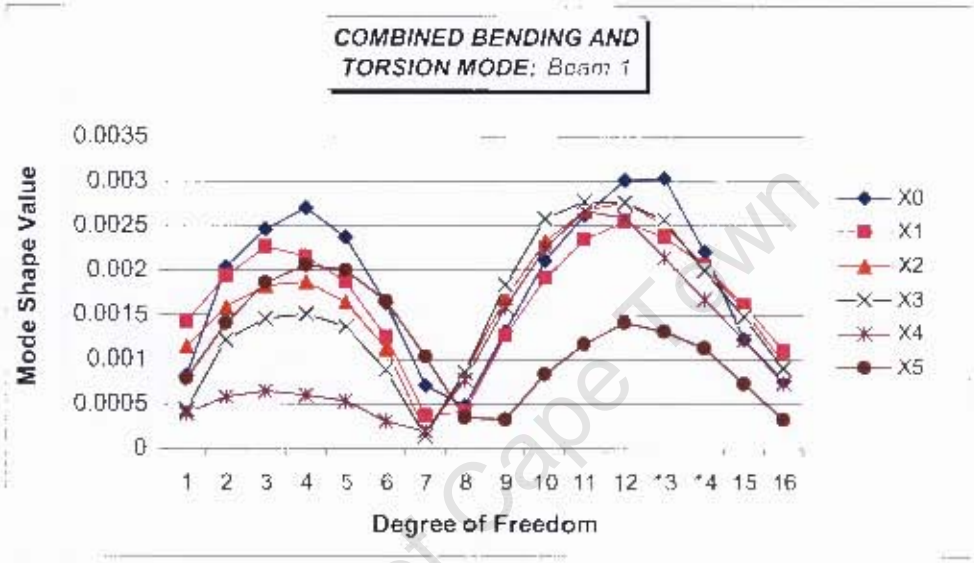

***Fig 5.8**: Plot of experimental combined bending and torsion mode*

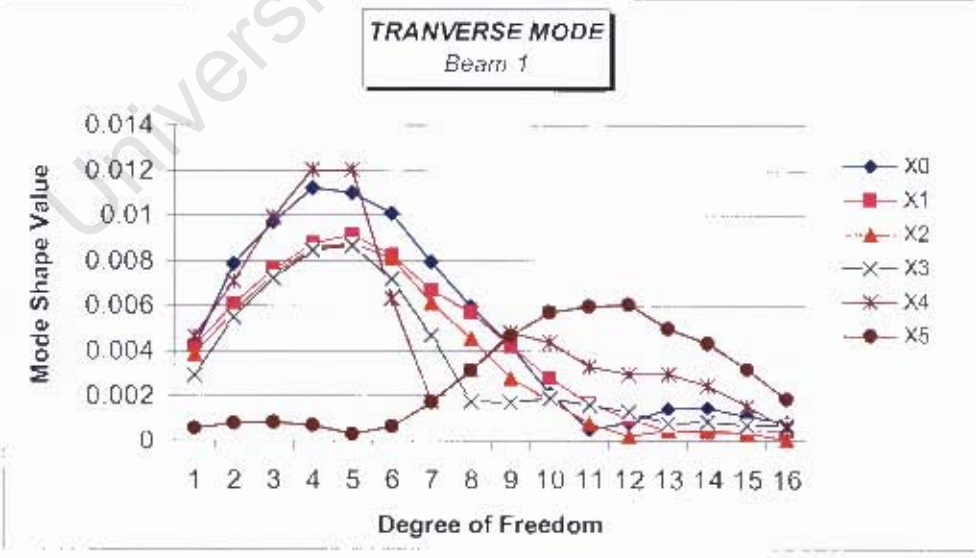

***Fig 5.9**: Transverse bending mode*

5.4.1.3 Modal Assurance Criteria (MAC)

MAC values between modes of undamaged and damaged state are shown in Table 5.3. These values quantify the correlation between mode shapes for different damage tests. A MAC value greater than 0.9 indicates a good correlation between the modes whereas dissimilar modes have MAC values below 0.9 (Friswell and Mottershead,1995). Farrar and Jauregui (1997) noted that MAC values are not sensitive to damage and hence are not widely used to detect damage in structures. Nevertheless, these were used in detecting loss in composite action of the systems.

Table 5.3: *MAC values between undamaged and damaged mode shapes*

Damage Scenario	*Mode*	*MAC Value*
X1	1	0.99
	2	0.99
	3	0.76
	4	0.81
	5	0.56
X2	1	0.99
	2	0.99
	3	0.89
	4	0.83
	5	0.53
X3	1	0.99
	2	0.98
	3	0.86
	4	0.77
	5	0.47
X4	1	0.99
	2	0.97
	3	0.72
	4	0.58
	5	0.44
X5	1	0.96
	2	0.98
	3	0.79
	4	0.60
	5	0.68

Good correlation exists between the first bending and torsional modes as shown by MAC values above 0.95. The second bending and all the other higher modes show no correlation. MAC values for these modes were less than 0.90. This finding agrees with the previous results on the plot of mode shapes where the first two modes could be compared

to identify the loosened shear connectors whereas there was little correlation from the third modes upwards.

In summary, global techniques may be used for detecting loss in composite action in this type of bridge, however a robust damage detection technique which could be used with higher confidence should include local damage indicators. These are described in following sections.

5.4.2 Vibration-based algorithms

Vibration-based algorithms try to localise damaged regions of the structure as opposed to the global indicators that assess the global damage of the system. Local damage detection algorithms use mode shape data to locate the damaged regions. The following algorithms (methods) were explored:

(i) Coordinate Modal Assurance Criterion (COMAC)
(ii) Mode shape curvature method
(iii) Change in flexibility method and
(iv) Change in stiffness method

5.4.2.1 COMAC Values

COMAC for an individual DOF, *i*, was calculated from the mode shape data using the following equation 2.6 described in Chapter 2.

Five modes were used to calculate the COMAC values for each degree of freedom and the results are shown in Fig 5.10. All the COMAC values were below 0.9. This shows the insensitivity of COMAC values to this damage. These findings correlate with work by Xia *et al*, 2007.

Another set of COMAC values was computed using only first two modes that showed good correlation earlier. The COMAC values were also below 0.9 as shown in Fig 5.11.

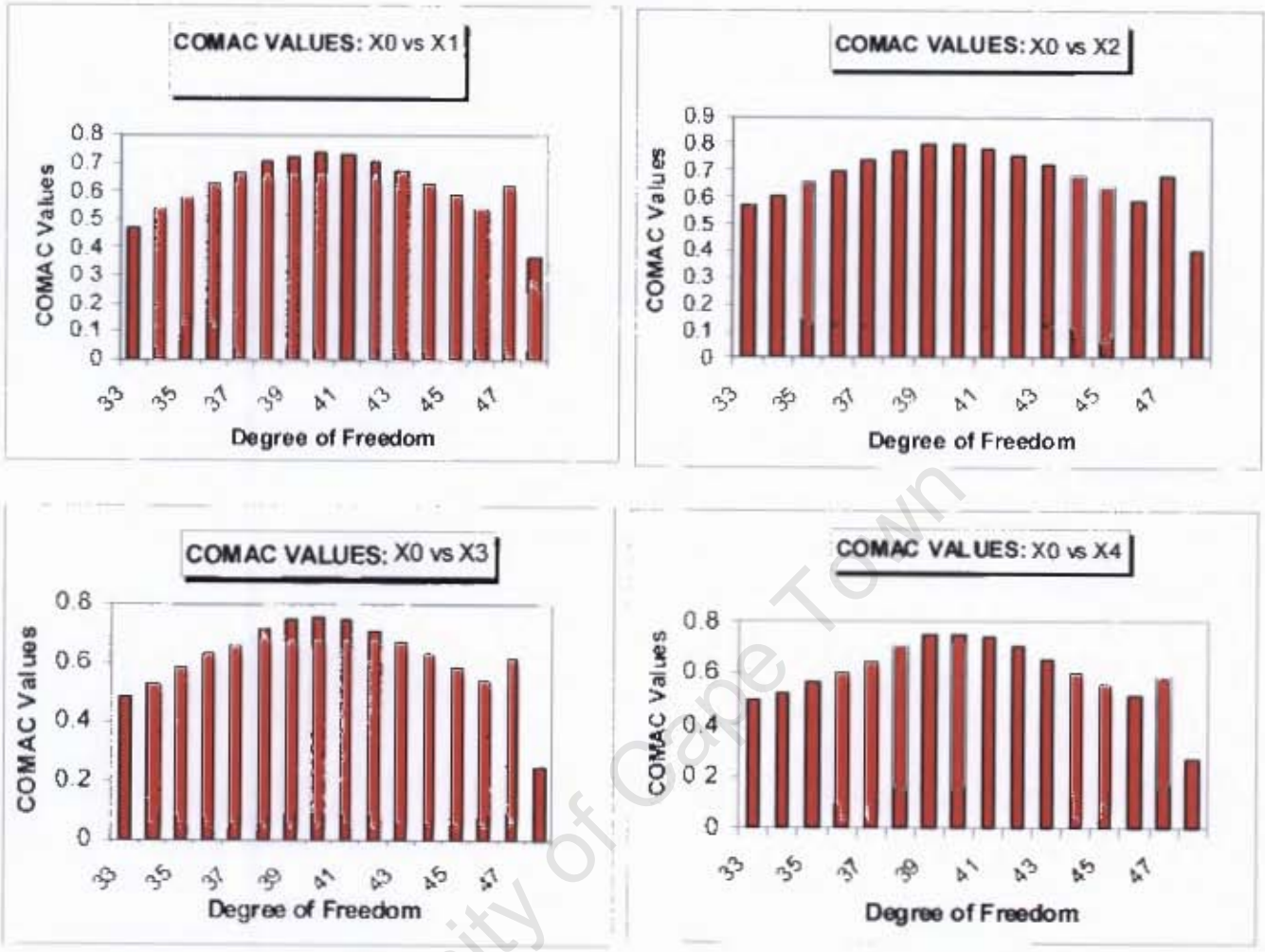

Fig 5.10: COMAC values between the undamaged and all damage states

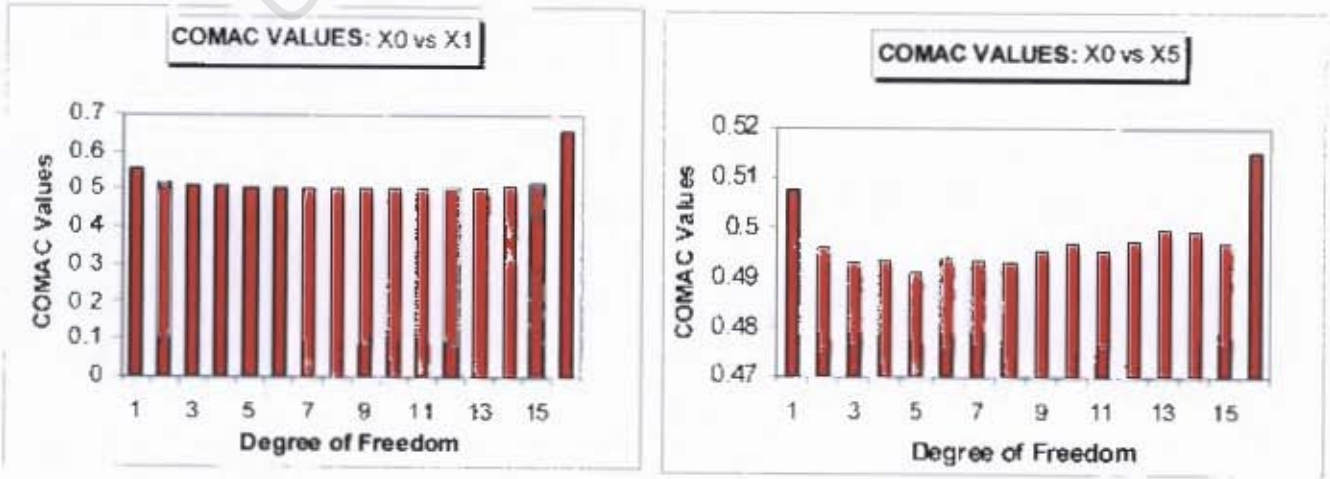

Fig 5.11: COMAC values based on data from first two modes

5.4.2.2 Mode shape curvatures

The curvatures for undamaged and damaged mode shapes were calculated from the scaled displacement mode shape values using a Central Difference Differentiation Scheme (CDDS). This algorithm was applied both longitudinally and transversely on the system and the resulting 2-D curvature value at each degree of freedom (DOF) was taken as the average of the two. The algorithm below was used to compute these curvatures:

$$v'' = \frac{(v_{i+1} - 2v_i + v_{i-1})}{h^2} \qquad (5.2)$$

Where v_i, v_{i+1}, v_{i-1} represent the displacement mode vectors at nodes *i, i+1* and *i-1* respectively

h is the distance between points of interest

The Curvature Damage Indicator (CDI) was computed for each DOF to localise damage. The CDI was estimated from equation 2.7a in Chapter 2.

The computed curvature plots for first bending mode are shown in Fig 5.12. A smooth curvature could be seen on the undamaged system. This was also evident on damage one but with reduced amplitudes. The curvatures for the second and third damages were similar to each other. These showed equal amplitudes in all DOF. The curvature amplitudes were even lower than those computed for the first damage. A different trend was observed on fourth damage as shown in Fig 5.12. Noticeable change on curvatures is observed from the fourth to the fourteenth shear connector. These connectors were loosened for this damage. Maximum curvature values were recorded for severe damage five. A distinct change in curvature is evident from the second to the fifteenth connector positions and this detects the loosened shear connectors efficiently.

Based on the experimental results it can be concluded that the first bending curvature values could detect the loss of composite action in these bridges. However, this appears to be efficient only when over 35% of the shear connectors have failed. Below this, the curvature values only reduce in magnitude and no curvature change is evident. This

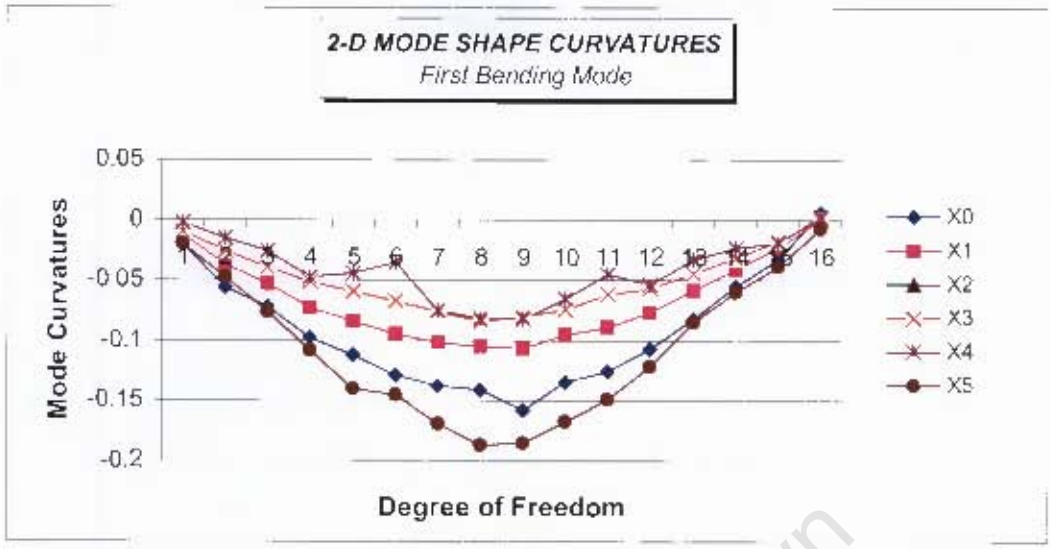

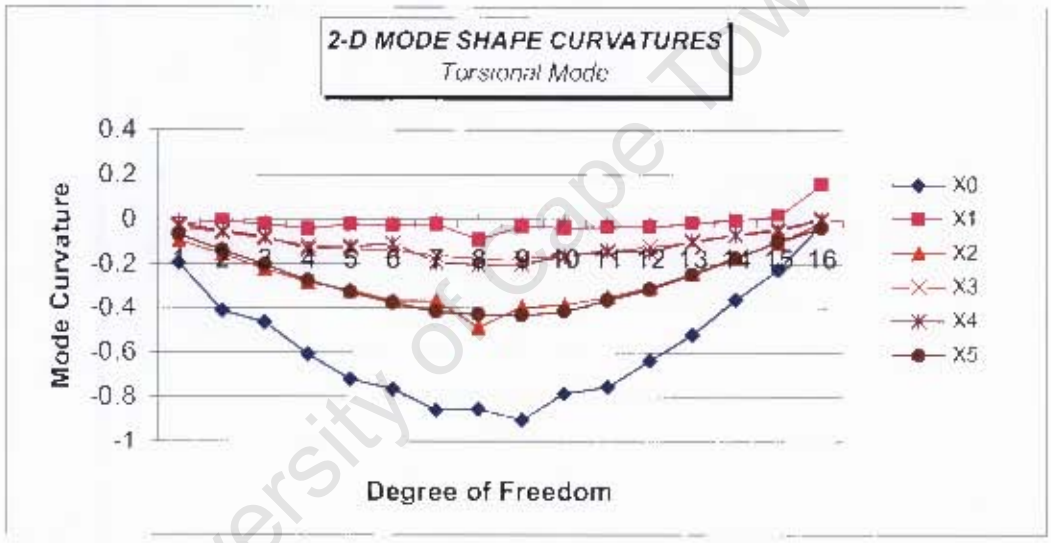

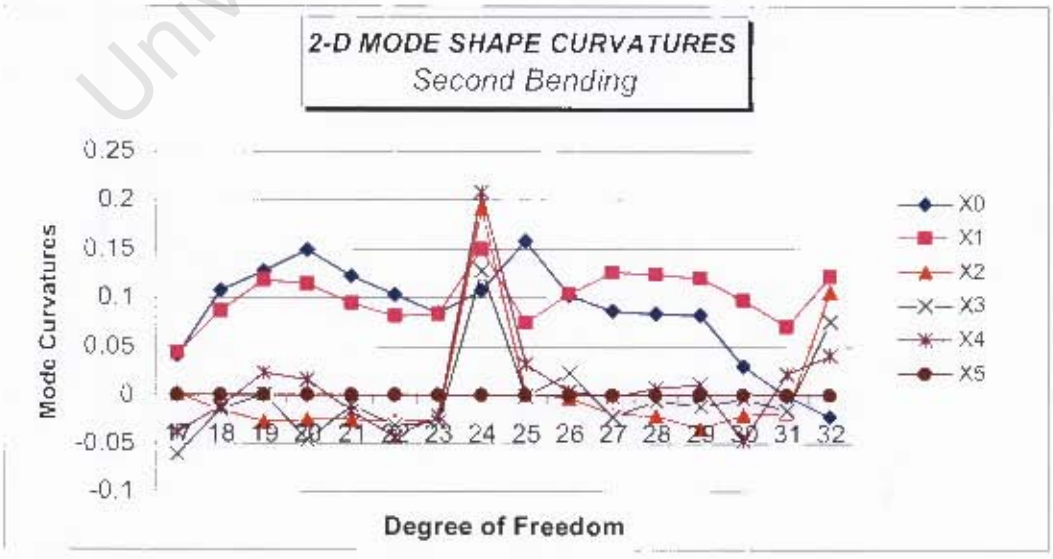

Fig 5.12: Mode Curvature plots

decrease in curvature values may be a good sign of loss in stiffness, which might trigger further investigations and possibly the localisation of the damaged region.

Also displayed on the same figure are the curvatures for the torsional and the second bending mode. The torsional mode displayed a different pattern from the first curvatures for the first mode. Firstly, maximum curvature values were recorded for the intact system and curvature changes from second to the tenth shear connector positions.

Minimum curvature values were recorded for damage one. A *kink* could be seen at the centre of the beam on three shear connectors. This gives false damage location. Curvature change was also seen on second damage cases on three connectors at the centre. Besides, this observation, a smooth curvature was obtained for the second damage.

The third and fourth damage curvatures were similar except for irregularities observed on six central connector positions for the fourth damage. A smooth curvature was recorded for the third damage, however. This perfect curvature was also observed on curvature values for severe damage five. Surprisingly, there were no visible curvature changes on loosened shear connectors.

Plotted also in Fig 5.12 are the curvature values for the second bending mode. These curvatures were difficult to interpret. This was also the case with the combined bending and torsion mode curvatures and the transverse mode curvatures. These curvatures were not plotted on this figure, however. This means that more measurements were required if the higher and more complex modes were to be used for this work. This will be recommended for future investigations.

As mentioned earlier in this section, curvature values were used to compute CDI values to detect and localise damage. These CDI are displayed in Fig 5.13 (a) and Fig 5.13(b) for damage scenario *X1*. Two sets of CDI values were computed for the inside and the outside beams. This was done to investigate how the CDI values vary from one beam to another under the same damage. Higher damage indicator values for damage one were observed at point 7, 8 and 9 on the outside beam in Fig 5.13(b). The indicators reduced gradually from the centre to the ends of the beam. This might be attributed to loosened shear connectors.

Nevertheless, the indicators on the inside beam show an opposite scenario where the lowest damage indicators where recorded at the middle points and increasing towards the edges as shown in Fig 5.13(b). Higher indicators were recorded at positions 33 and 48 on the outside beam. This might be due to the effect of the support conditions.

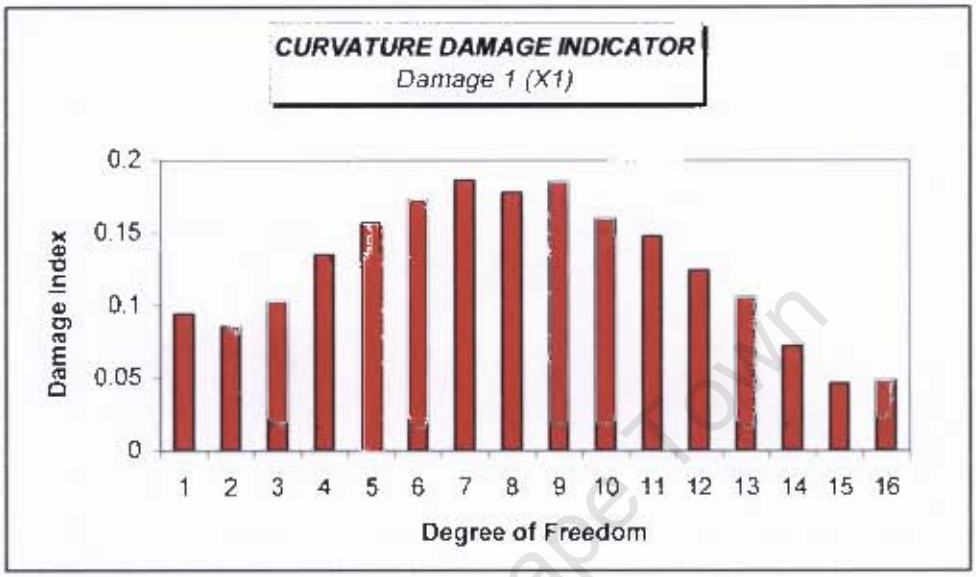

(a)

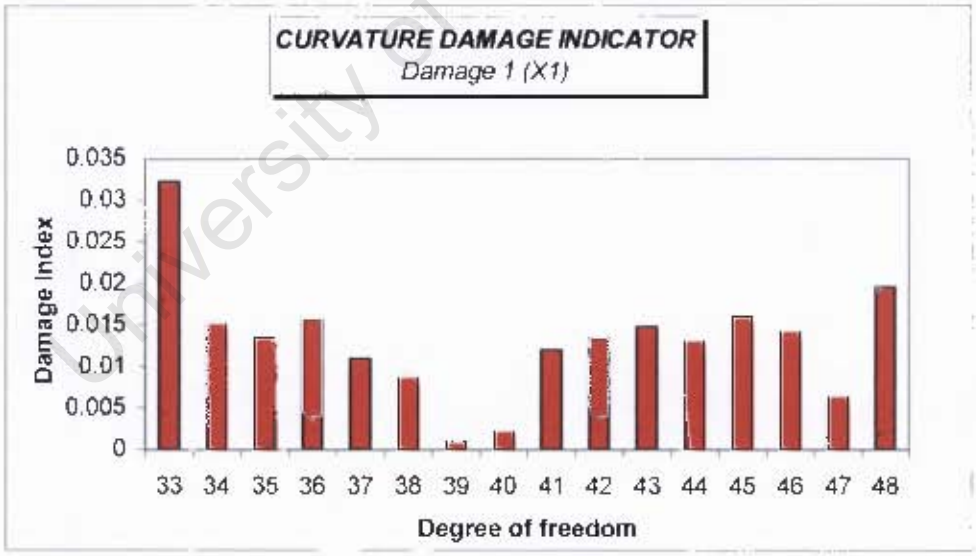

(b)

Fig 5.13: *Curvature damage indicators for damage case one*

The CDI values for second damage are shown in Fig 5.14. These were also computed for shear connectors on one internal and external beam. A similar pattern as the one on CDI values for the first damage is shown on outside beam 1. Maximum values were observed at the centre and gradually decreased towards the supports. Peak values were recorded on positions 19, 20, 21, 25, 26, 27, 28 and 29 for the inside beam. The damage on position 25

is therefore located. The peak CDI values at 19, 20, 21 and 29 are false damage indicators, however.

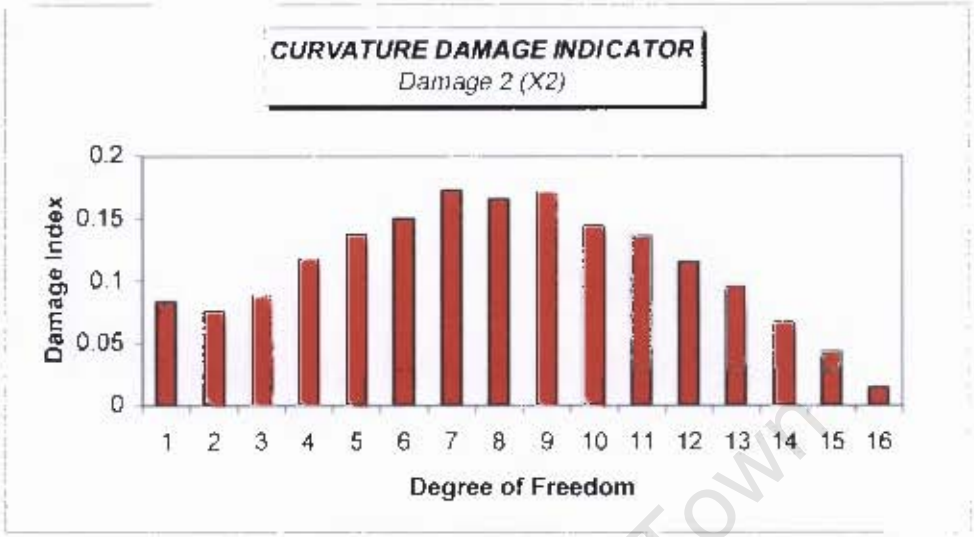

(a)

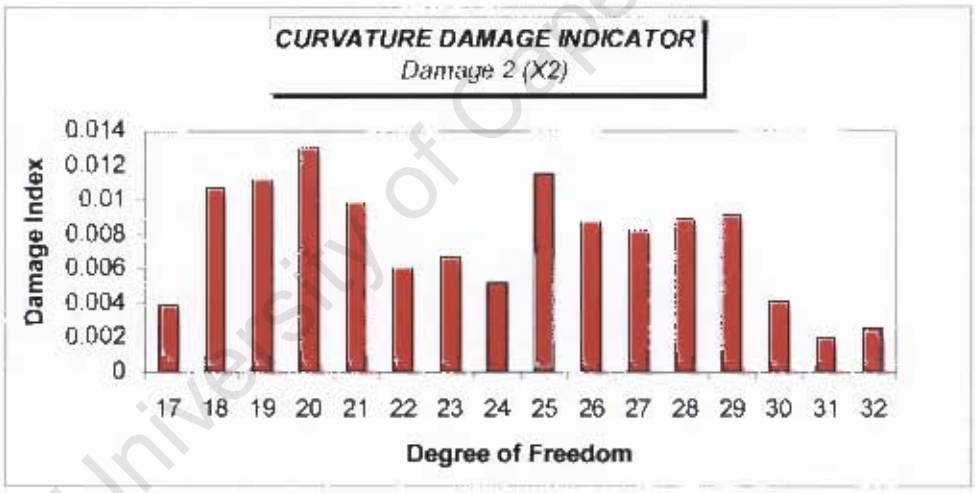

(b)

Fig 5.14: *Curvature Damage indicators for damage scenario two*

Loosened shear connectors on position 25 are located in Fig 5.15 on the inside beam for the third damage case *(X3)* investigated. This is shown by a higher CDI value at this position. The other loosened shear connectors on the beam could not be located. A minimum CDI value was observed at the centre of the beam. Three peak values could be seen at positions 6 to 9 on the outside beam one for the same damage. These values could be associated with damage inflicted on this region. In general, the CDI values on the outside beam decreased from the centre outwards. This was also observed on CDI values for the first and second damage scenarios.

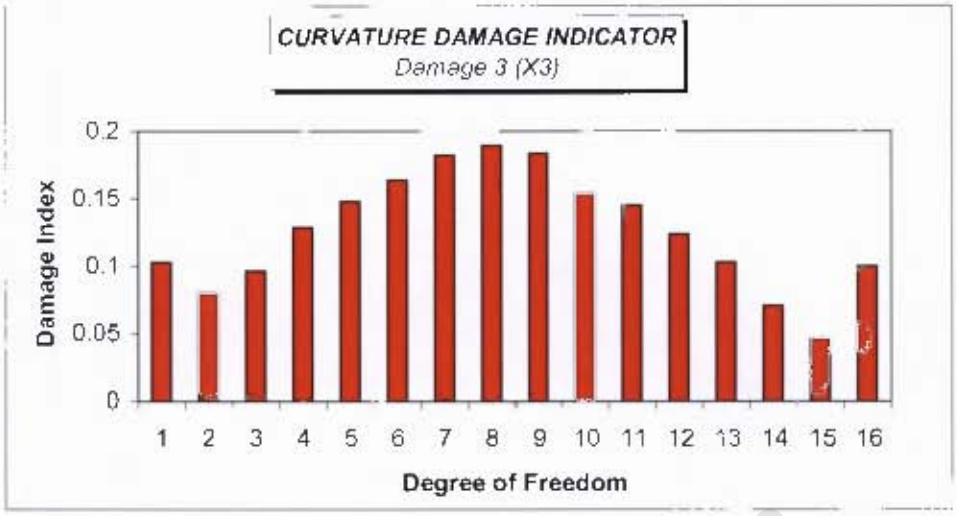

(a)

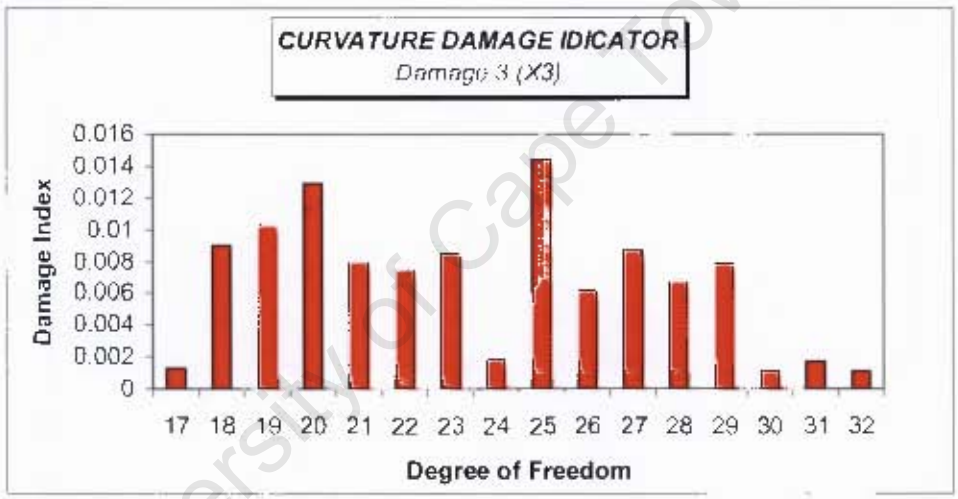

(b)

Fig 5.15: *Curvature Damage Indicator for damage scenario three*

In summary, 40% of the damaged shear connectors were identified for this damage scenario.

Fig 5.16 shows CDI values calculated for damage scenario four. As in previous values calculated for other damage cases, a similar trend was observed on CDI values for the outside beam on this damage case. Maximum values were observed at the centre on positions 6 to 10 on the outer beam. This identifies 80% of the loosened shear connectors. Higher CDI values could be seen on positions 17, 18, 23 and 25 on the inside beam. These values localise the loosened shear connectors.

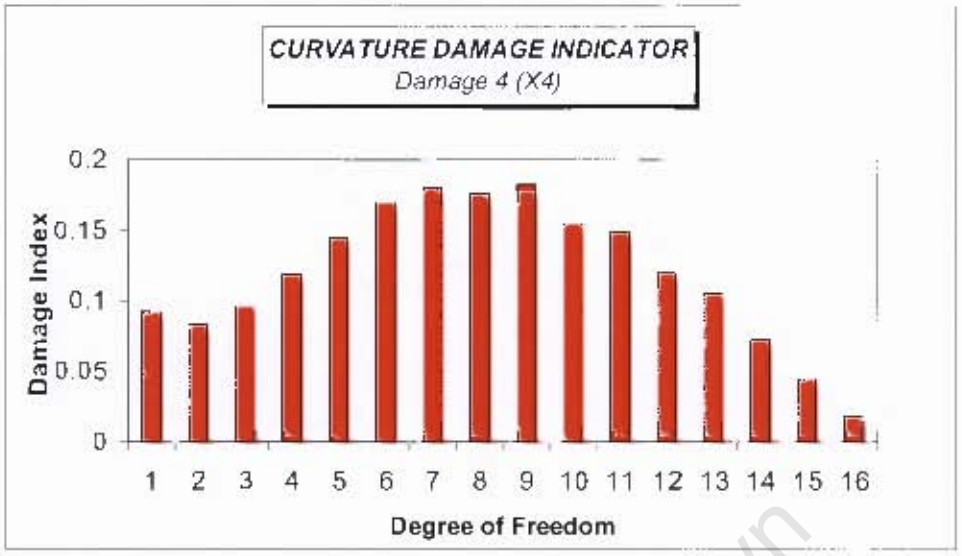

(a)

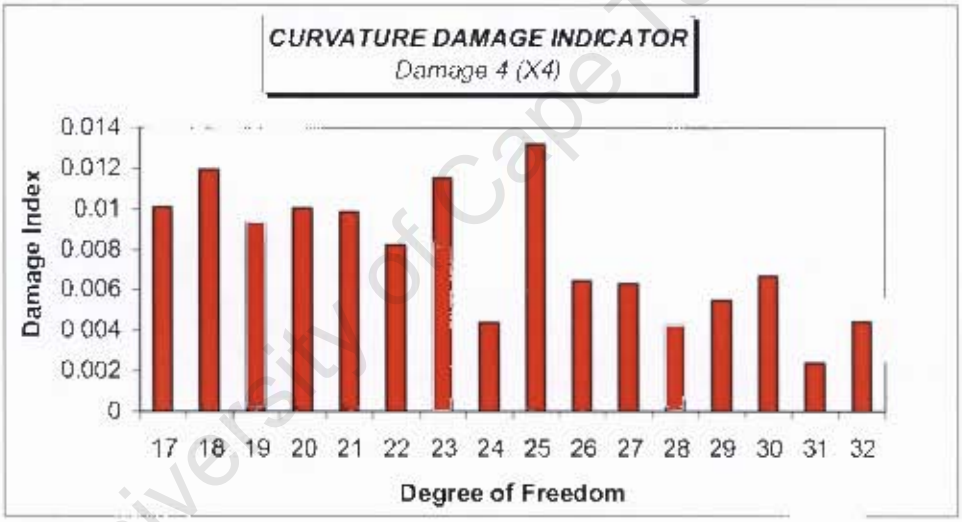

(b)

Fig 5.16: *Curvature Damage indicator for damage scenario four*

The maximum values at position 17 and 18 gives false damage detection as the connectors at these positions were intact

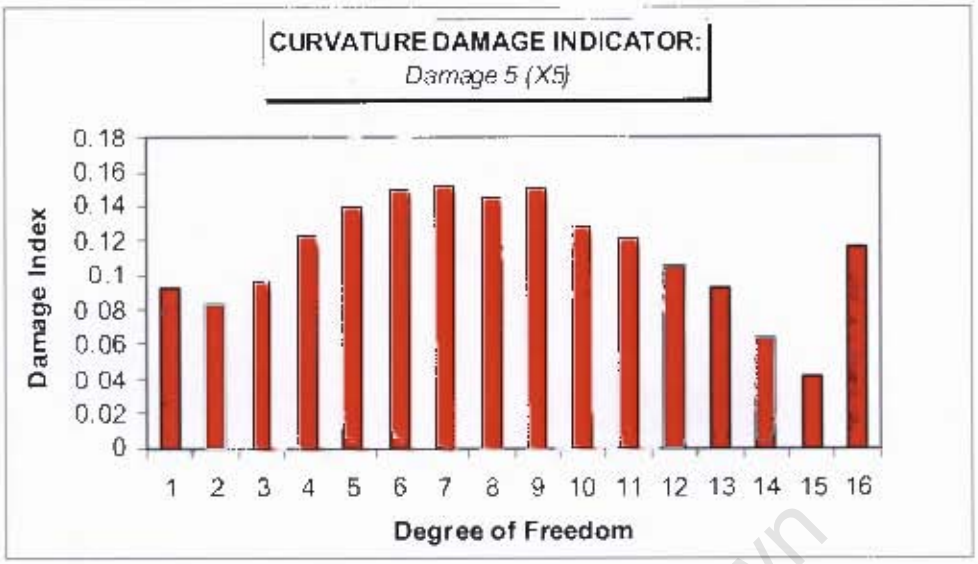

(a)

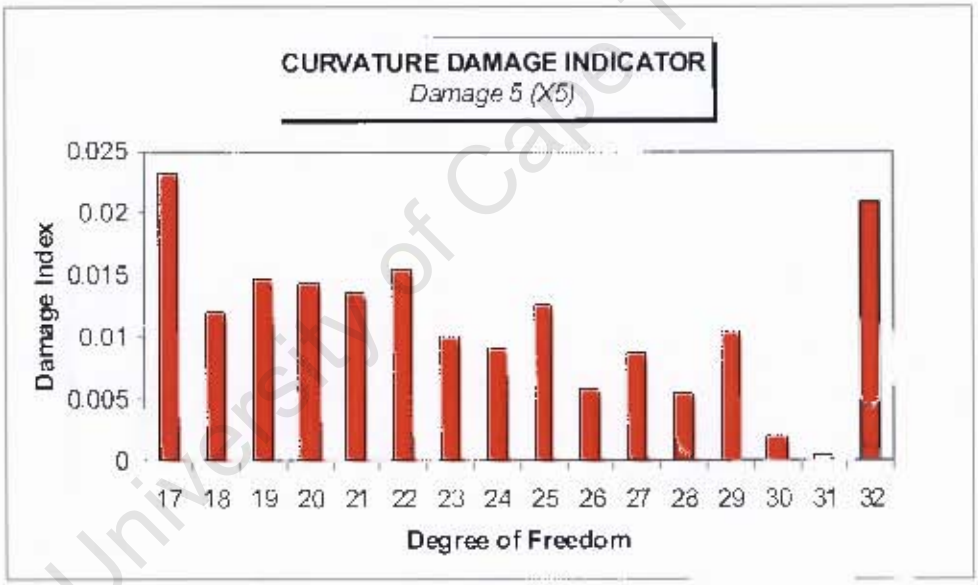

(b)

Fig 5.17: *Curvature Damage Index values for damage five*

Calculated CDI values for severe damage five are shown in Fig 5.17. The CDI values for the outer beam shows a similar pattern to the ones calculated for other damage cases presented earlier in section 5.4.2.2. Maximum values were observed at the centre over six shear connector positions and decreased gradually to the edges. This accounts for 40% of the loosened shear connectors. It is difficult however to tell the critical CDI values that might be due to damage. As can be seen in the graph (beam one), there is gradually decrease in CDI values and one wonders what optimum value should be used to screen these values.

Shown also in Fig 5.17 are CDI values calculated for an inside beam on this damage. Maximum values were recorded at support positions of the beam. The middle values were relatively small and this indicates that no damage was present in these positions. This was however incorrect. This observation shows the non-sensitivity of CDI values as damage becomes severe.

Based on the above observations, the CDI technique was able to identify some of the loosened shear connectors on the structure. Some false identification was also observed and some loosened shear connectors could not be located. In summary, one has to use this technique with great engineering intuition.

The other technique investigated is the flexibility change method. The next section describes this technique.

5.4.2.3 Flexibility Change Method

The modal flexibility matrix of the system was calculated for both the undamaged and the damaged structures. This was estimated from equation 2.8a-2.8c.

The calculated flexibility change values for various structural systems are shown in Fig 5.18 and Fig 5.19. Flexibility values increased from the supports towards the centre for the first to the third damage cases as shown in Fig 5.18. It was difficult to distinguish if the displayed trend was as a result of loosened shear connectors or the expected system flexibility characteristic. Any system that is simply supported shows maximum flexibility at the centre and minimum displacements at the supports. Maximum flexibility values were increasing from the intact system to the damage case three. The maximum flexibility value of eleven was calculated for the intact structure whereas a maximum value of twelve was calculated for the second and third damage scenarios. This might be due to the effect of loss in composite action caused by loosening shear connectors. Surprisingly, this seems to be a global characteristic and there is no localisation of the loosened connectors.

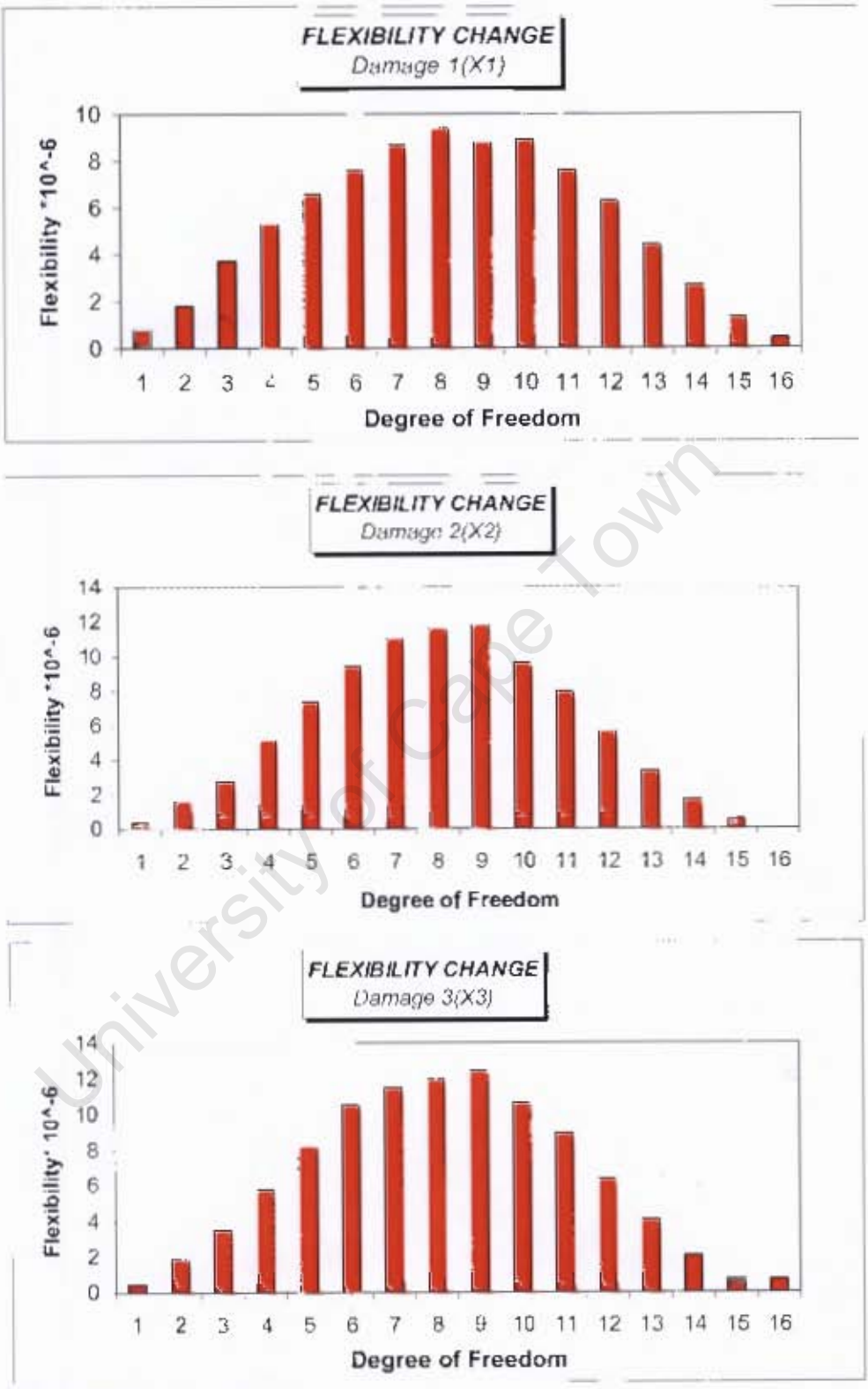

Figure 5.18: *Flexibility plots for damage scenarios one, two and three*

Observations for the fourth and fifth damage cases are shown in Fig 5.19. Maximum flexibilities were recorded at midspan for both damage scenarios. The flexibility values on positions 5 to 10 show some pattern that is different from others for the fourth damage case. This shows the damaged region clearly. The same observation was displayed on

positions 36 to 44 for severe damage five. Similarly this is the region where the shear connectors were loosened. Minimum values were recorded on six shear connector positions near the supports. These shear connectors were not loosened.

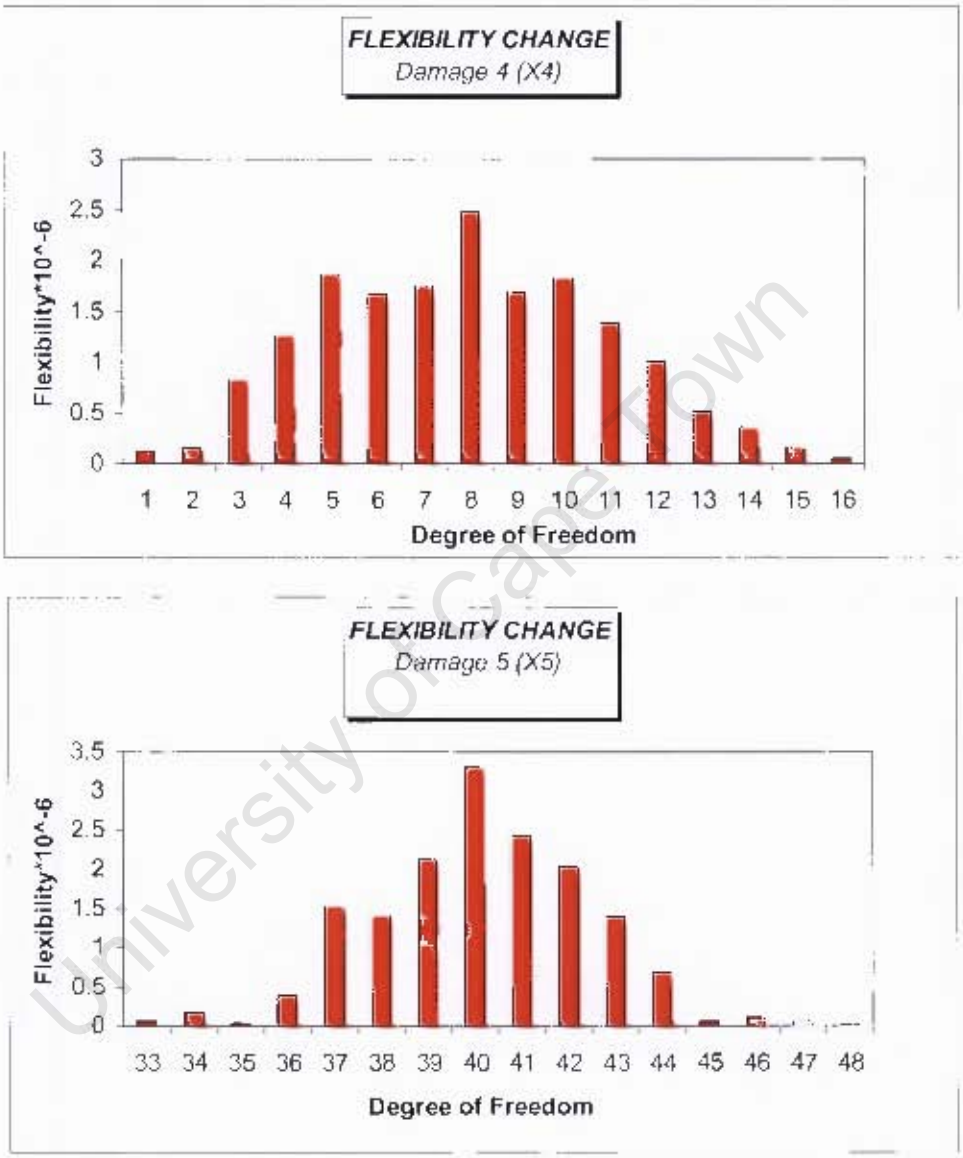

Figure 5.19: *Flexibility plots for damage scenarios four and five*

Based on these observations, the flexibility technique is effective when more than 35% of the shear connectors are damaged. Such a percentage is however unlikely for a structure under serviceability limit state conditions. This means that the loss in composite action in a concrete beam and slab bridge may remain undetected using this technique until such a time when it is difficult to repair or catastrophic failure has occurred.

This research also investigated the use of change in stiffness technique to locate the damaged shear connectors in a bridge structure.

5.4.2.4 Change in Stiffness Method

The modal stiffness is the inverse of flexibility of the structure. The modal stiffness for different damage scenarios was estimated from equation 2.9a t0 2.9f.

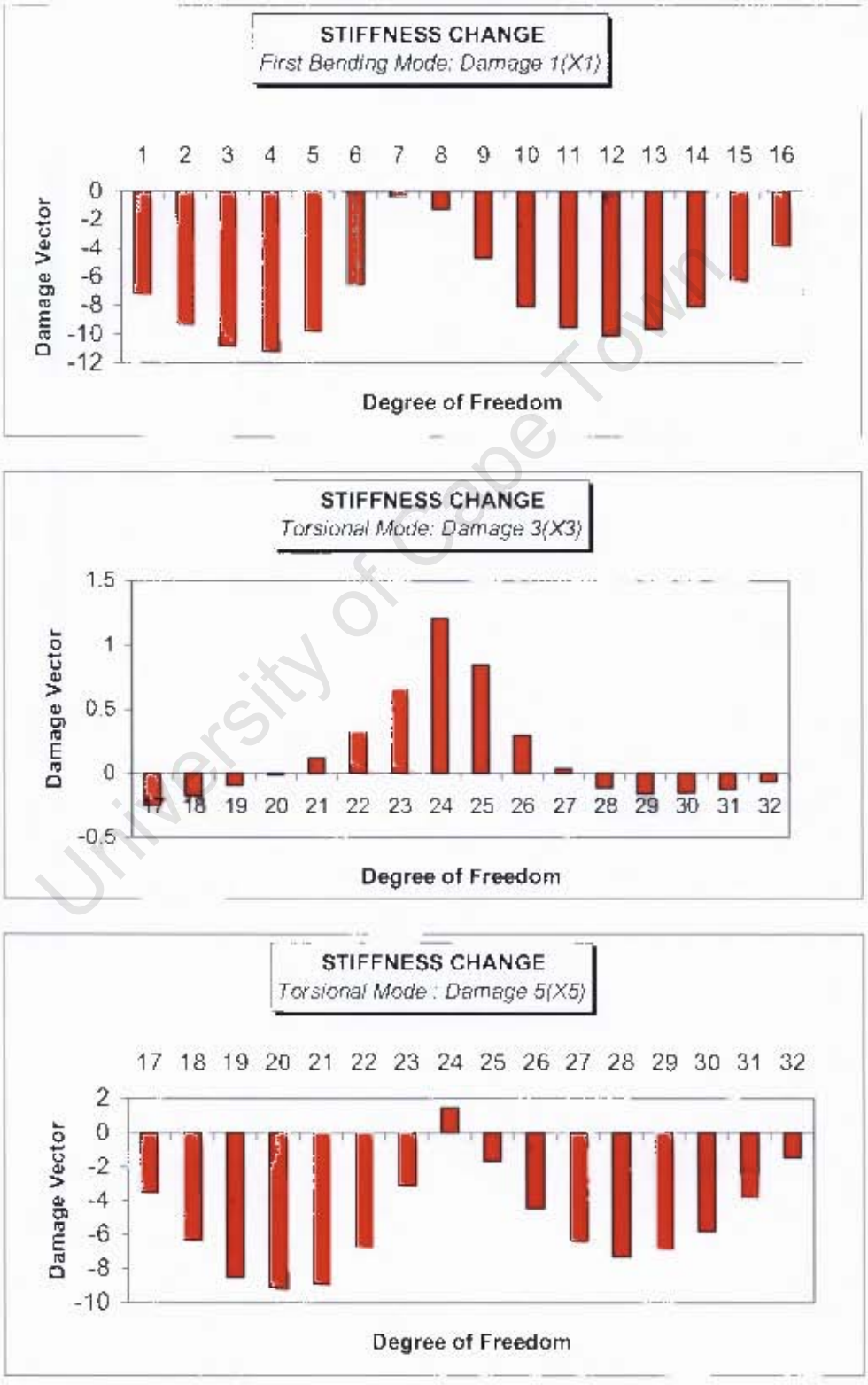

Figure 5.20: Change in stiffness technique applied on different damage scenarios

Fig 5.20 shows the calculated damage vectors for damage scenarios one *(X1)*, three *(X3)* and five *(X5)*. The damage vectors for cases two *(X2)* and four *(X4)* resemble those for damage cases one and three respectively. The calculated damaged vectors for damage case one *(X1)* show the same trend for all the five mode shapes extracted. The vectors were calculated for only the outside beam. Minimum amplitudes of vibrations were recorded at the midspan of the beam. The same trend was displayed for damage scenario five. This however does not show any relation to the inflicted damage.

The damage vectors for damage scenario three are also shown in the same figure. Maximum amplitudes of vibrations are recorded at the central positions of the beams. These values locate the damage region effectively. However these maximum values may also be due to high flexibility of the system at this position.

As explained earlier, this research integrates both the experimental and FE analysis to investigate how the loss in composite action in concrete beam and slab bridges could be detected. Results from the FE investigations are discussed in the next section.

5.5 NUMERICAL RESULTS

An FE model of the system was developed using Automatic Dynamic Incremental Nonlinear Analysis (ADINA) software. This model was fine tuned manually so that its natural frequencies could match the experimental ones. The results are outlined below.

5.5.1 Global modal parameters

Modal frequencies and mode shapes where obtained from modal analysis of the fine tuned system. The MAC values were then computed using the mode shape vectors. The following sections give an outline of the results.

5.5.1.1 Numerical modal frequencies and MAC values

Natural frequencies and MAC values are shown in Table 5.4 and Table 5.5. As mentioned in chapter 4, the initial model used rigid connectors to simulate shear connectors. The ends of the beams were fixed. The frequencies obtained from this system were relatively high and it was impossible to match them to the frequencies obtained experimentally. These frequencies are shown in Table 5.4. The rigid connectors were then replaced with non-linear spring elements. Spring elements were also used to simulate the rubber bearings supporting the model. To correlate the experimental and theoretical results, the spring

stiffnesses representing the rubber bearing and the shear connectors were adjusted manually. The resulting spring stiffnesses are as shown on Table 5.6. These springs stiffness's also take into account the effect of friction between the beams and slab.

***Table 5.4**: Natural frequencies obtained from a model using rigid connectors to simulate shear connectors*

Type of Mode	*Frequency, Hz*
1: First Bending	47.18
2: Torsional	49.42
3: Second Bending	137.60
4: Combined bending and torsion	146.30
5: Transverse	113.60

Natural frequencies for a model using spring elements to simulate shear connectors are shown in Table 5.5. The frequencies showed a decreasing trend from the intact state to the severe damage case except for the transverse mode on the extreme damage case. This indicates a global reduction of system stiffness with loosening of shear connectors. This was however expected as early observations from experimental work showed the same trend.

Surprisingly, mode shapes between the intact and all the damage states correlate well as shown by MAC values of unit in the table. This cannot be the case especially for severe damage. This shows the non-sensitivity of these values to this damage.

Table 5.6 give the resulting final spring properties used.

***Table 5.5**: FE frequencies and MAC values*

Mode	*Case*	*Frequency, Hz*	*% Change based on X0 Frequency*	*MAC Values*
1st Bending Mode	*X0*	19.76	-	-
	X1	19.75	0.05	1.0
	X2	19.72	0.20	1.0
	X3	19.57	0.96	1.0
	X4	19.22	2.73	1.0
	X5	15.88	19.64	1.0
Torsional mode	*X0*	31.61	-	-
	X1	31.01	1.90	1.0
	X2	30.45	3.67	1.0
	X3	29.67	6.14	1.0
	X4	29.00	8.26	1.0
	X5	27.62	12.62	1.0
2nd Bending mode	*X0*	63.90	-	
	X1	63.73	0.23	1.0
	X2	63.56	0.53	1.0
	X3	63.02	1.38	1.0
	X4	63.80	0.16	1.0
	X5	48.41	24.24	1.0
Combined Bending and Torsion	*X0*	79.91	-	
	X1	79.84	0.09	1.0
	X2	79.56	0.44	1.0
	X3	79.32	0.74	1.0
	X4	78.20	2.14	1.0
	X5	75.41	5.63	1.0
Transverse mode	*X0*	92.94	-	
	X1	92.00	1.01	1.0
	X2	89.00	4.23	1.0
	X3	78.78	15.24	1.0
	X4	73.32	21.11	1.0
	X5	148.90	+60.21	1.0

***Table 5.6**: Spring stiffness: Bearings and Shear connectors*

Bearings		***Shear Connectors***	
Spring Property	Stiffness	Spring Property	Stiffness
X-Translation	3 x 10^8 N/m	X-Translation	3 x 10^8 N/m
Y-Translation	3 x 10^8 N/m	Y-Translation	3 x 10^8 N/m
Z-Translation	3 x 10^8 N/m	Z-Translation	3 x 10^8 N/m
X-Rotation	1.8 x 10^6 Nm/rad	X-Rotation	1 x 10^5 Nm/rad
Y-Rotation	8 x 10^5 Nm/rad	Y-Rotation	7 x 10^8 Nm/rad
Z-Rotation	3 x 10^8 Nm/rad	Z-Rotation	3 x 10^8 Nm/rad

***Table 5.7**: Comparisons of numerical and experimental natural frequencies*

Mode	*Case*	*Numerical Frequency, Hz*	*Experimental Frequency, Hz*	*Percentage Difference*
1st Bending Mode	*X0*	19.76	19.71	-0.3
	X1	19.75	19.59	-0.8
	X2	19.72	19.67	-0.3
	X3	19.57	19.30	-1.4
	X4	19.22	18.90	-1.7
	X5	15.88	18.01	+13.4
Torsional mode	*X0*	31.61	28.86	-8.7
	X1	31.01	27.93	-9.9
	X2	30.45	28.38	-6.8
	X3	29.67	27.91	-7.7
	X4	29.00	27.38	-5.5
	X5	27.62	25.65	-7.1
2nd Bending mode	*X0*	63.90	67.69	+5.8
	X1	63.73	66.47	+4.3
	X2	63.56	66.47	+4.5
	X3	63.02	60.13	-4.5
	X4	63.80	52.71	-17.4
	X5	48.41	50.54	+4.4
Combined Bending and Torsion	*X0*	79.91	77.85	-2.6
	X1	79.84	75.36	-5.6
	X2	79.56	74.35	-6.4
	X3	79.32	71.77	-9.5
	X4	78.20	69.19	-11.5
	X5	75.41	59.57	-15.8
Transverse mode	*X0*	92.94	86.51	-6.9
	X1	92.00	83.93	-8.7
	X2	89.00	88.41	-5.9
	X3	78.78	86.71	+10.1
	X4	73.32	79.68	+8.7
	X5	148.90	67.62	-

The comparison of experimental and numerical frequencies are shown in Table 5.7. On average, a 10% difference was observed. This is a significant difference. It is assumed that the large difference was due to handling cracks observed on the physical model. These were not simulated in the analytical model

5.5.1.2 Mode shapes

The mode shapes extracted are shown in Figure 5.21. Interestingly, the analytical mode shapes clearly show the positions of the loosened shear connectors from the second damage scenario upwards without further analysis. The curvature of the shapes change instantly at positions where the spring elements were reduced to zero to simulate damaged shear connectors. Nevertheless, this representation deviates from the actual setup on the

ground where the damaged shear connectors might still impact some stiffness on the composite action.

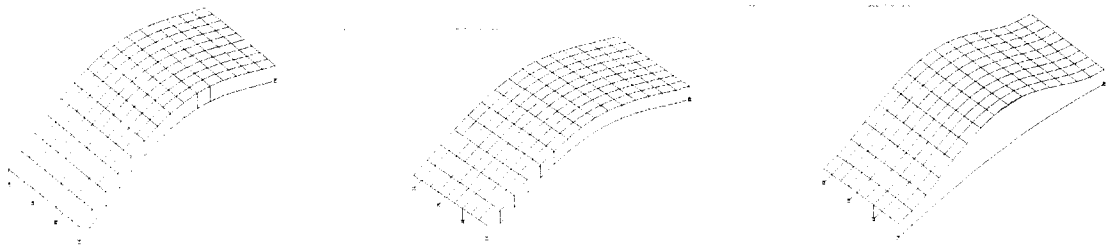

First Bending modes

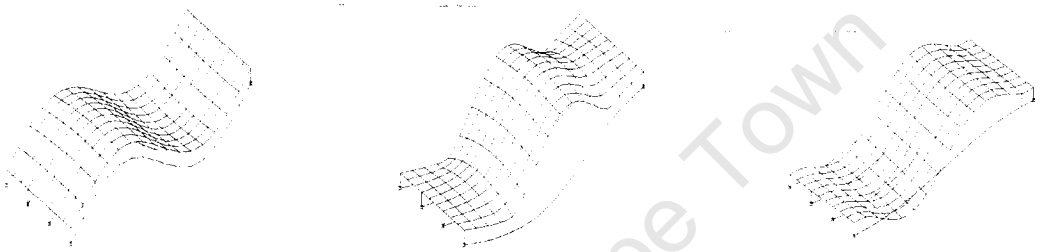

Second Bending modes

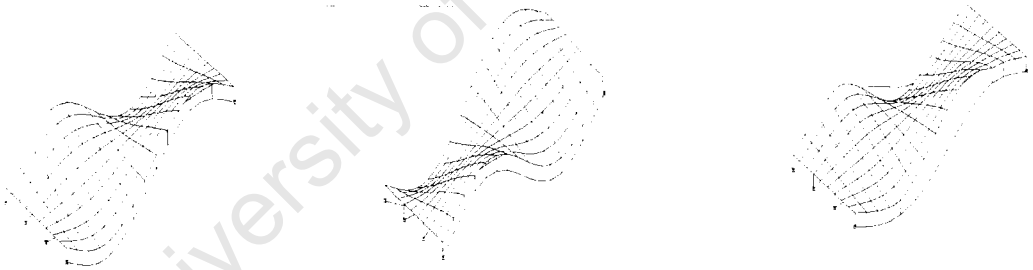

Combined Bending and Torsion modes

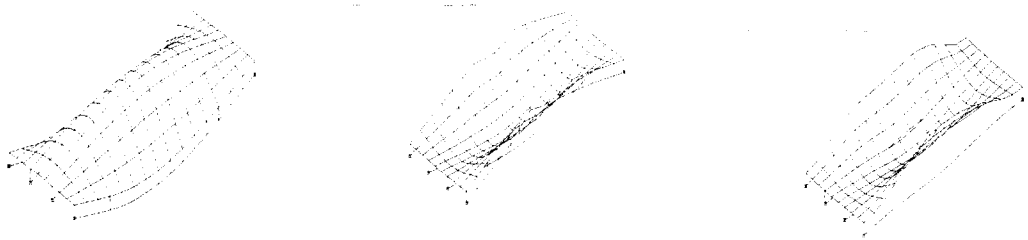

Transverse modes

***Fig 5.21**: Mode shapes extracted from the FE model*

The plots of these modes after scaling are shown in the following figures. In the same way as calculations are done using experimental data, the data from the undamaged mode structure was used for scaling other modes.

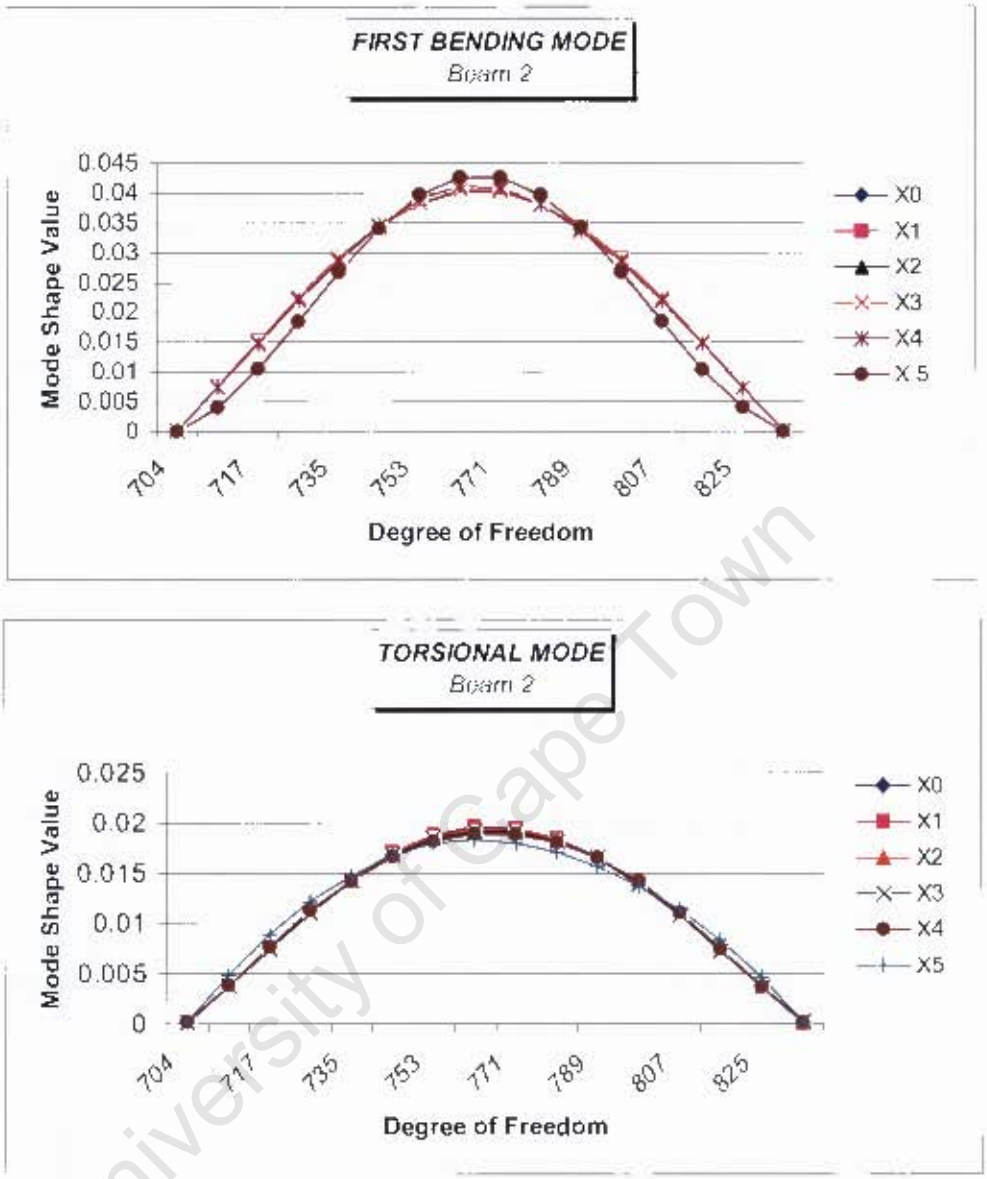

Fig 5.22: *First bending and torsional modes*

The plots of the first bending and torsional modes along one of the beams are shown in Figure 5.22. The mode curvatures for damage one to four started to deviate from the undamaged mode curvature on five connector positions. This deviation was more pronounced at mid-span of the beam. The modes from the second and third damage cases are superimposed together i.e. there was very little difference in damage. In-fact, only two shear connectors were loosened for damage two to three. A different scenario was observed on the fifth mode where 75% of shear connectors were loosened. There was no correlation between this damage mode and all the other damaged modes shapes.

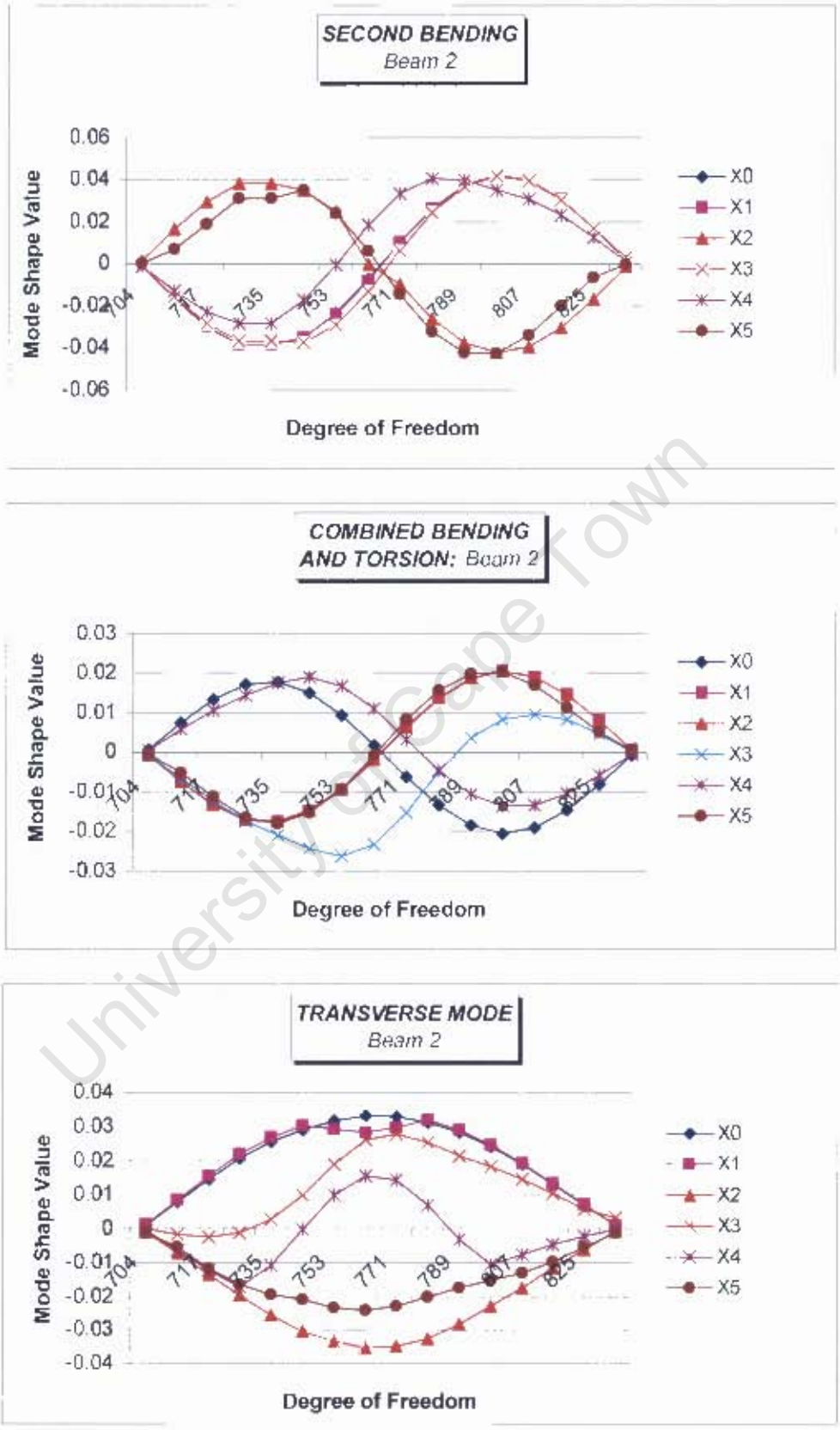

Figure 5.23: *Plot of second bending, combined bending and torsion and transverse modes*

It should be noted that different numbering for experimental and numerical modes where used. This however does not result in conflicting explanations.

Phase changes between modes of different damage cases for the second bending were observed. The undamaged *(X0)*, damage one *(X1)*, damage three *(X3)* and damage four *(X4)* mode shapes were all in phase whereas damage two *(X2)* and damage five *(X5)* mode shapes where out of phase from the other mode shapes. Besides this information, there was no indication relating the modes to the inflicted damage.

The same trend observed in the second bending modes was displayed in combined bending and torsion mode plots. The undamaged and damage four mode shape plots were in phase whereas all the other plots were out of phase with these two plots.

Interesting results were observed on the transverse mode plots. A smooth transverse mode was observed for an undamaged structure. Some deviation between this curve and the one for damage case one *(X1)* on positions where shear connectors were removed was clear. A different scenario was observed on the mode plot for damage case two (X2) .The curvatures was smooth along the entire beam. There was indication of the loosened connectors as seen on the mode for damage case one *(X1)*. The mode shapes for damage cases three *(X3)* and four *(X4)* clearly locate positions of loosened shear connectors as shown by an abrupt change in the mode gradients at these positions. Surprisingly, the mode from severe damage five *(X5)* shows very little indication of the damaged region. Only reduced amplitudes of the mode could be noticed for this damage.

Based on scaled mode data used in above comparisons, local damage indicator algorithms used on section 5.4.2.2 were used in the localisation of this damage.

5.5.2 Vibration-based algorithms

Similar local damage techniques as those applied on experimental data were also applied on the analytical data. These are:

(i) Coordinate Modal Assurance Criterion (COMAC)

(ii) Mode shape curvature method

(ii) Change in flexibility method and

(iii) Change in stiffness method

Phase changes between modes of different damage cases for the second bending were observed. The undamaged *(X0)*, damage one *(X1)*, damage three *(X3)* and damage four *(X4)* mode shapes were all in phase whereas damage two *(X2)* and damage five *(X5)* mode shapes where out of phase from the other mode shapes. Besides this information, there was no indication relating the modes to the inflicted damage.

The same trend observed in the second bending modes was displayed in combined bending and torsion mode plots. The undamaged and damage four mode shape plots were in phase whereas all the other plots were out of phase with these two plots.

Interesting results were observed on the transverse mode plots. A smooth transverse mode was observed for an undamaged structure. Some deviation between this curve and the one for damage case one *(X1)* on positions where shear connectors were removed was clear. A different scenario was observed on the mode plot for damage case two (X2) .The curvatures was smooth along the entire beam. There was indication of the loosened connectors as seen on the mode for damage case one *(X1)*. The mode shapes for damage cases three *(X3)* and four *(X4)* clearly locate positions of loosened shear connectors as shown by an abrupt change in the mode gradients at these positions. Surprisingly, the mode from severe damage five *(X5)* shows very little indication of the damaged region. Only reduced amplitudes of the mode could be noticed for this damage.

Based on scaled mode data used in above comparisons, local damage indicator algorithms used on section 5.4.2.2 were used in the localisation of this damage.

5.5.2 Vibration-based algorithms

Similar local damage techniques as those applied on experimental data were also applied on the analytical data. These are:

(i) Coordinate Modal Assurance Criterion (COMAC)

(ii) Mode shape curvature method

(ii) Change in flexibility method and

(iii) Change in stiffness method

5.5.2.1 COMAC Values

Equation 2.6 was used to calculate the COMAC values at each degree of freedom and plots of these are shown in Fig 5.24 and Fig 5.25.

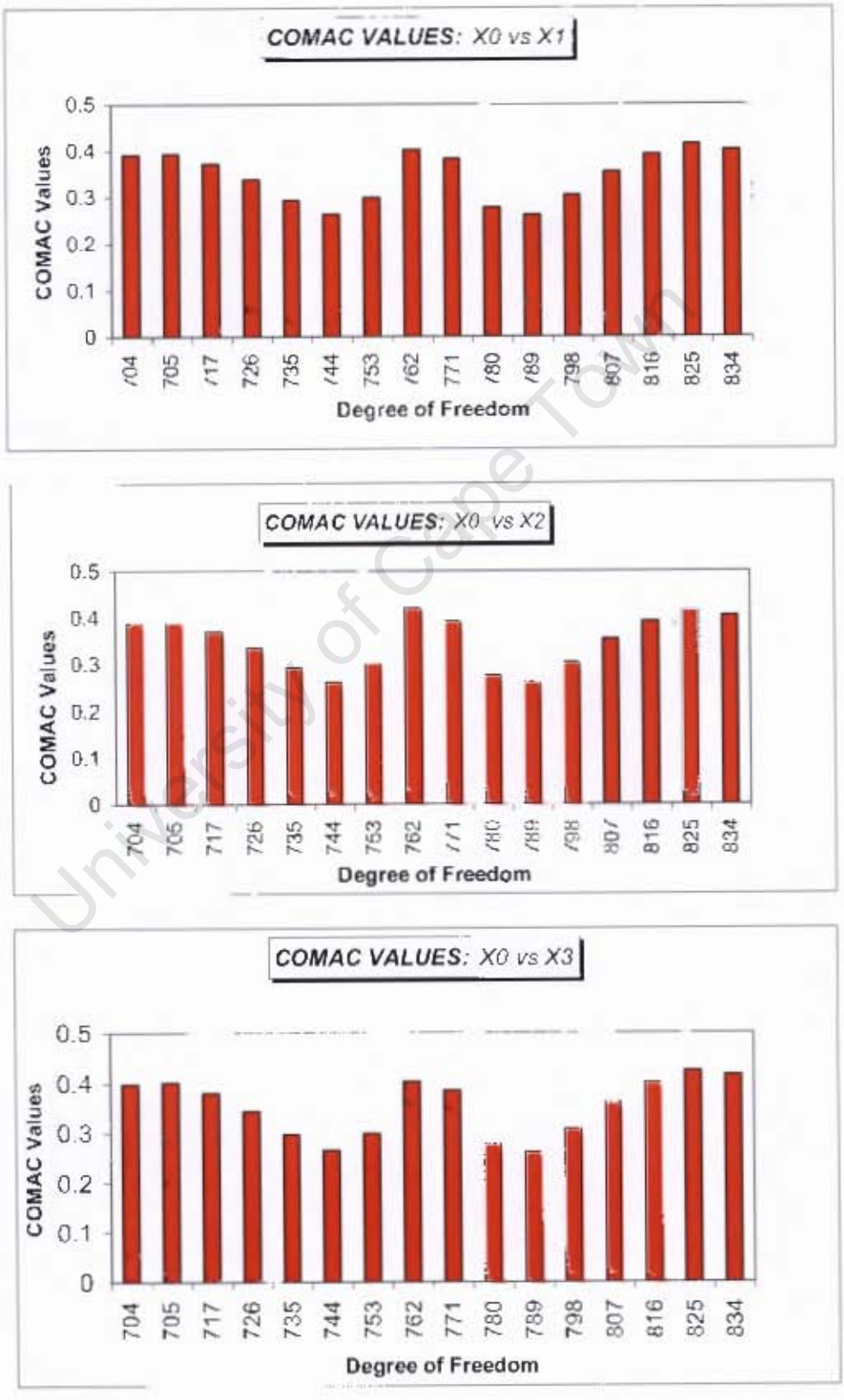

Fig 5.24: COMAC values for undamaged structure vs different damage states

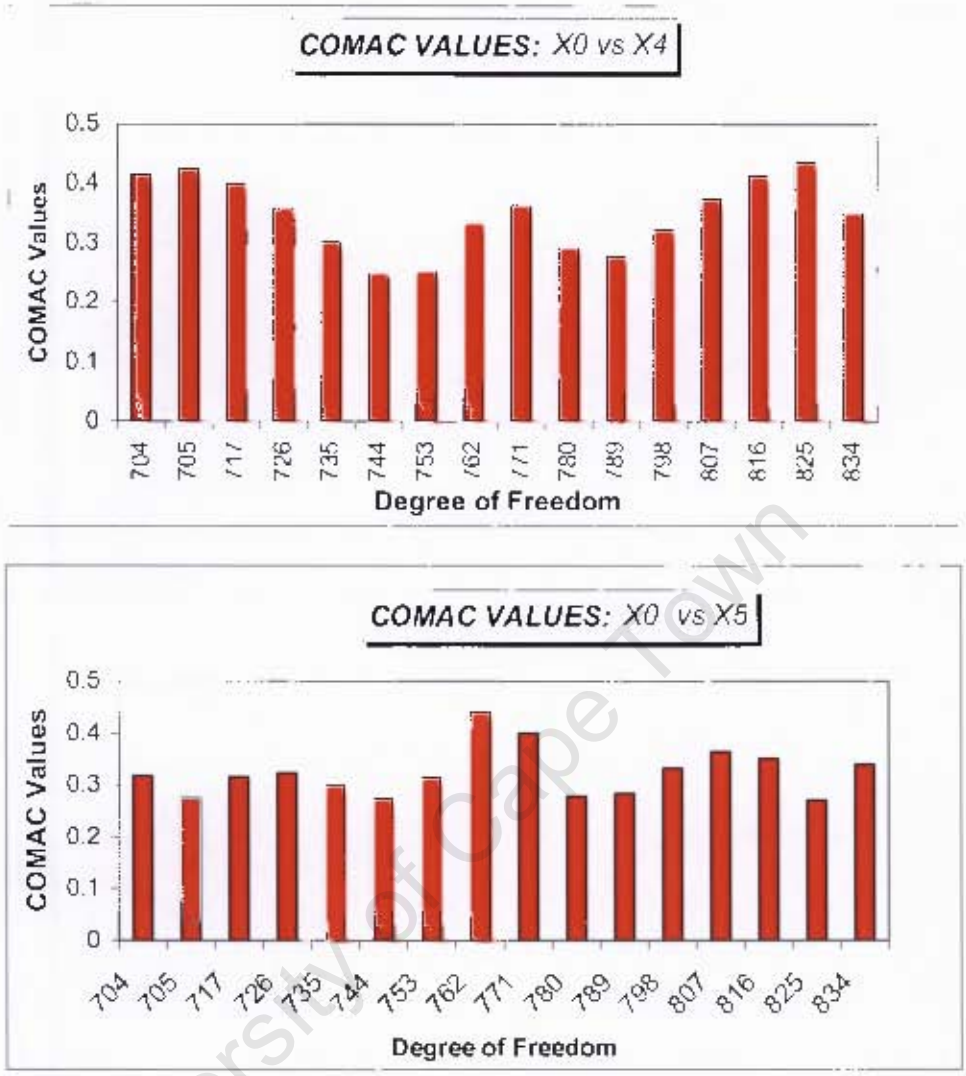

Fig 5.25: *COMAC values for undamaged structure modes vs different four and five*

The calculated COMAC values were below 0.9. This indicates that there was no correlation between the undamaged and damaged modes. Maximum COMAC values were recorded on the middle of the span. Surprisingly, this was the region were shear connectors were loosened for all damage scenarios and one would have expected this region to have the lowest COMAC values. As observed in section 5.4.2.2, this indicates the non-sensitivity of this technique to detect damage of this nature.

5.5.2.2 Mode shape curvatures and curvature damage indicators.

Equation *5.2* was used to compute the curvatures. Based on the curvature values, a curvature damage index (CDI) was also computed using equation *5.3*. The computed curvatures are plotted in Fig 5.26 and Fig 5.27.

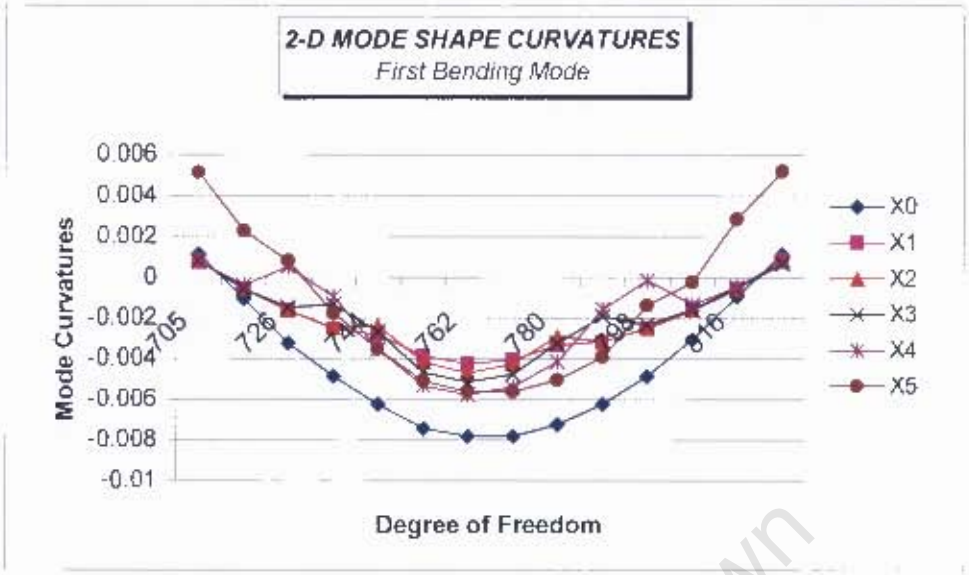

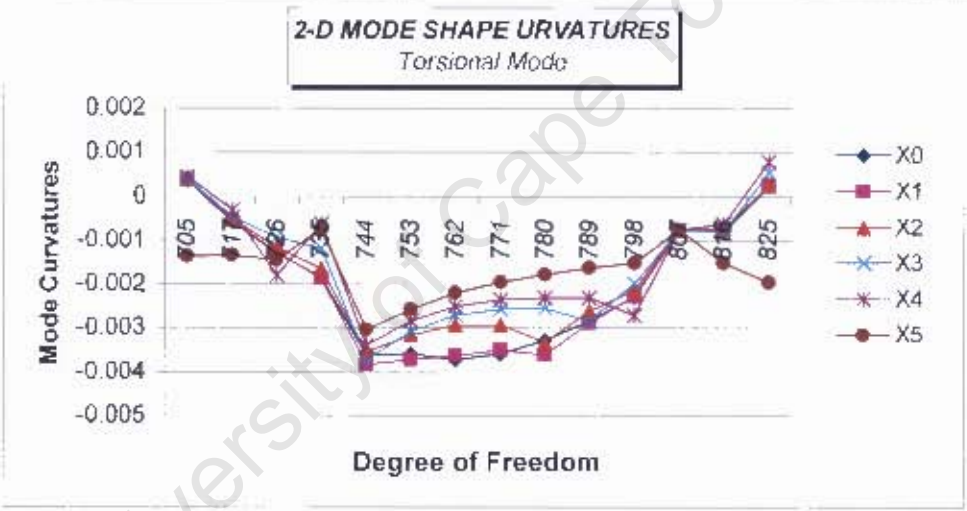

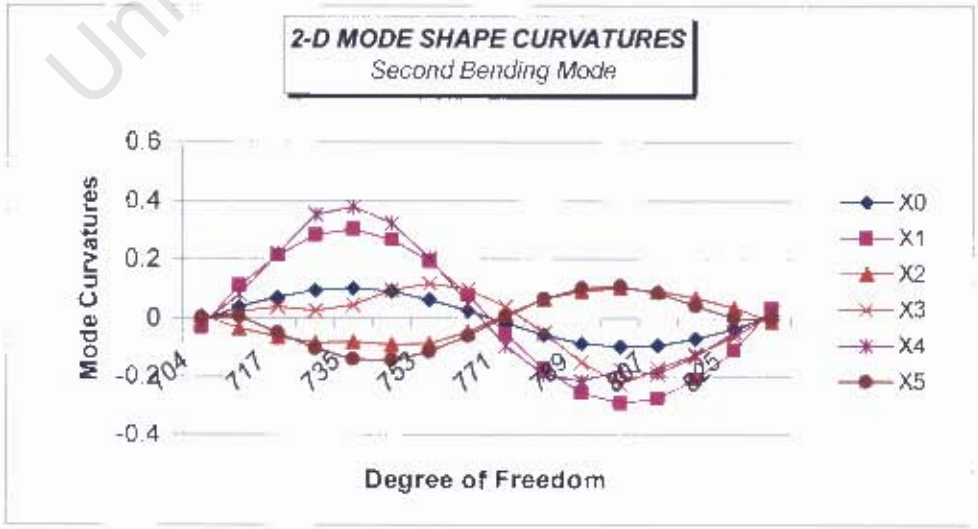

Fig 5.26: Mode shape curvatures: First bending, torsion and second bending

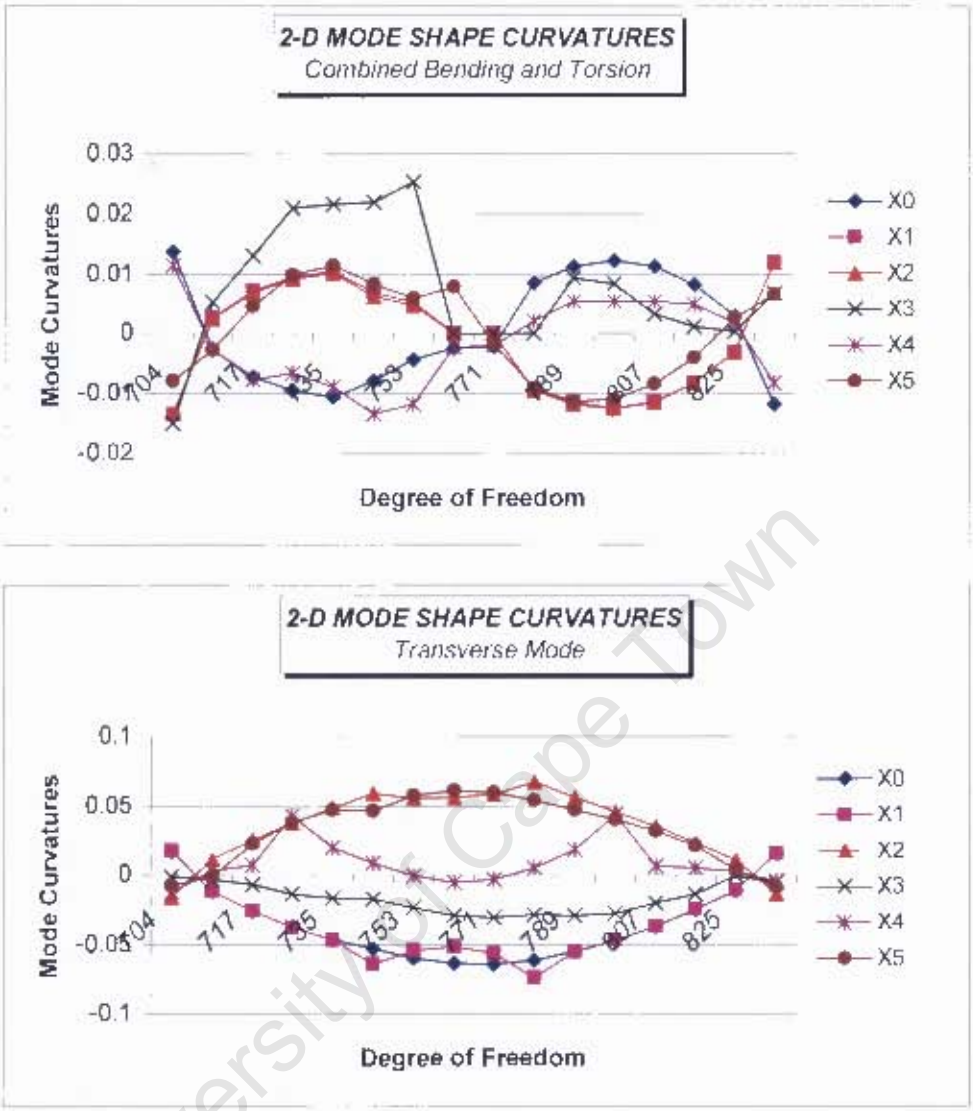

Fig 5.27: Mode shape curvature: combined bending and torsion and transverse

The first bending mode curvatures computed for different damage states showed interesting results. Firstly, a reduction of the curvature values from the undamaged to the severe damage scenario was observed. In this case, a smooth curvature for undamaged structure, as expected, was observed. Secondly, curvature changes at loosened shear connectors were observed. In addition the curvature changes were more pronounced on the second, third, fourth and fifth damage scenarios.

Surprisingly very little could be observed on the torsional mode plots. It was difficult to capture the effect of damage on this mode. This was also the case for combined bending and torsional mode curvatures. Similarly, it was difficult to distinguish between the curvatures for the second bending mode.

The curvature plots for the transverse modes are shown also in Fig 5.26. There were noticeable curvatures changes on the damaged regions of the systems, especially for damage scenarios one, four and five.

The calculated curvature damage indexes between the undamaged and different damage scenarios are shown in Fig 5.28 and Fig 5.29.

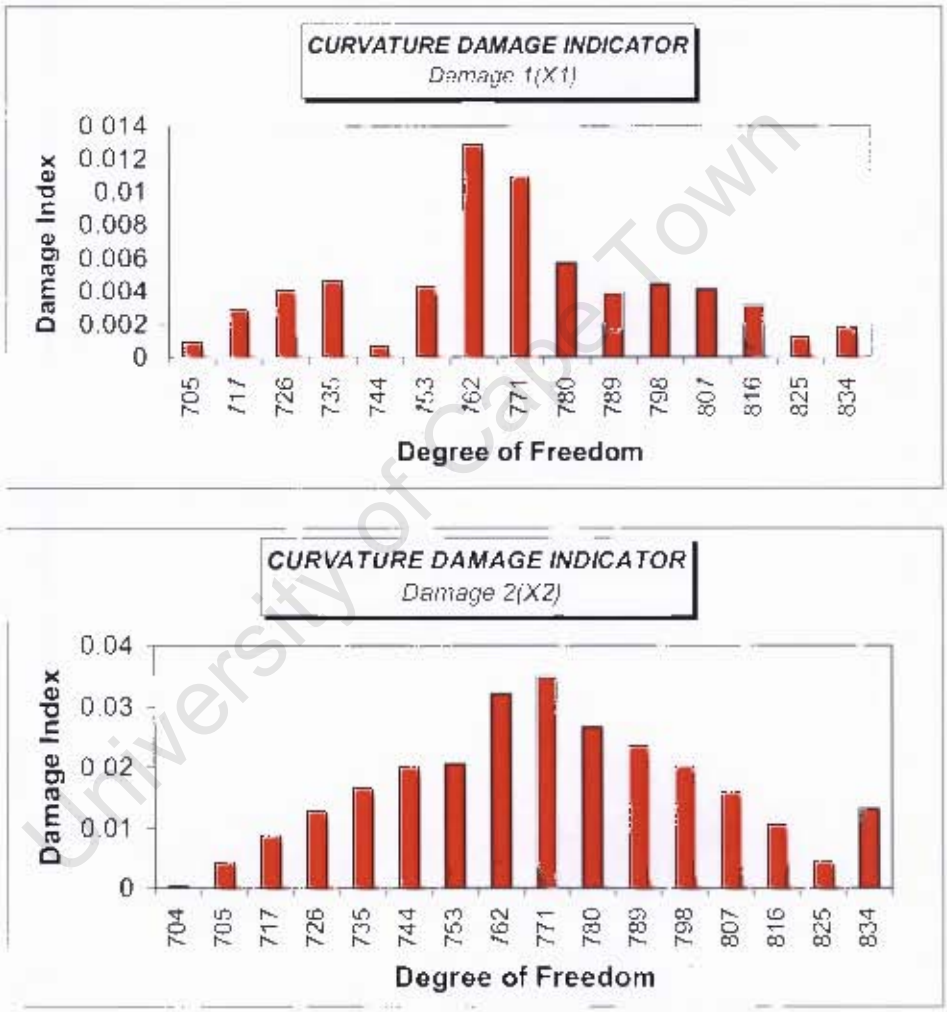

***Fig 5.28**: Curvature Damage Indexes: Damage one and two*

Higher damage indexes were observed on the central positions of the beam on damage case one *(X1)*. This detects the two damaged shear connectors at this location. The third loosened shear connector could not be detected. The damage indexes on the other positions were much lower with the least values recorded at the supports.

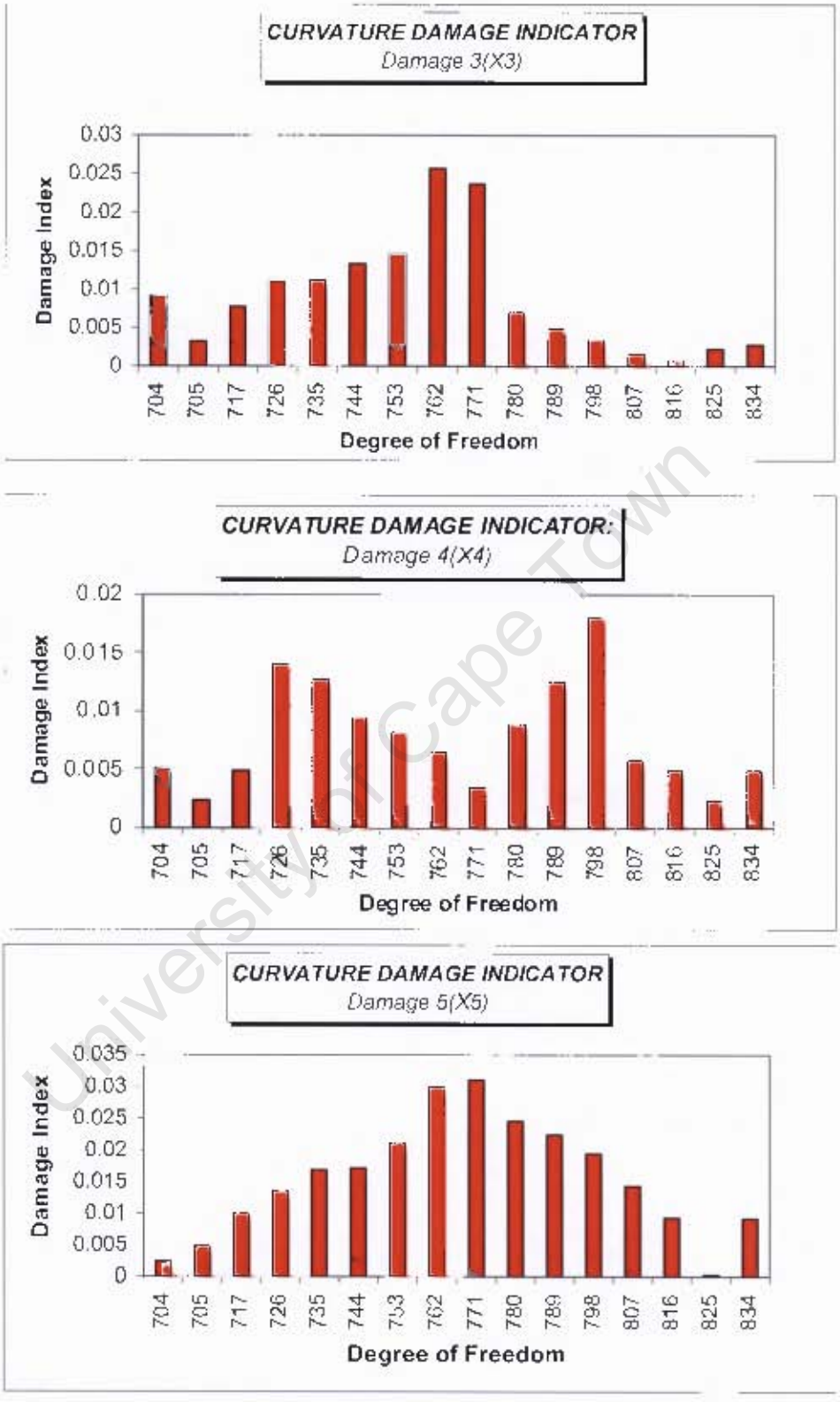

***Fig 5.29**: Damage indexes: Damage three, four and five*

Damage indexes for damage case two also show the same trend as those for the first damage case. Although two loosened shear connectors were identified on this damaged scenario, four connectors were loosened.

Maximum damage indexes could be observed in the mid-span for the third damage scenario. Similarly, only two central loosened shear connectors were identified. The other five could not be identified.

Two peak damage indexes were recorded on the eighth and ninth positions of the shear connectors for the fourth damage investigated. Between these two positions, the indexes reduced and the minimum was recorded at mid span. The indexes for damage case five follow those on the second damage case where two maximum values were recorded at the centre.

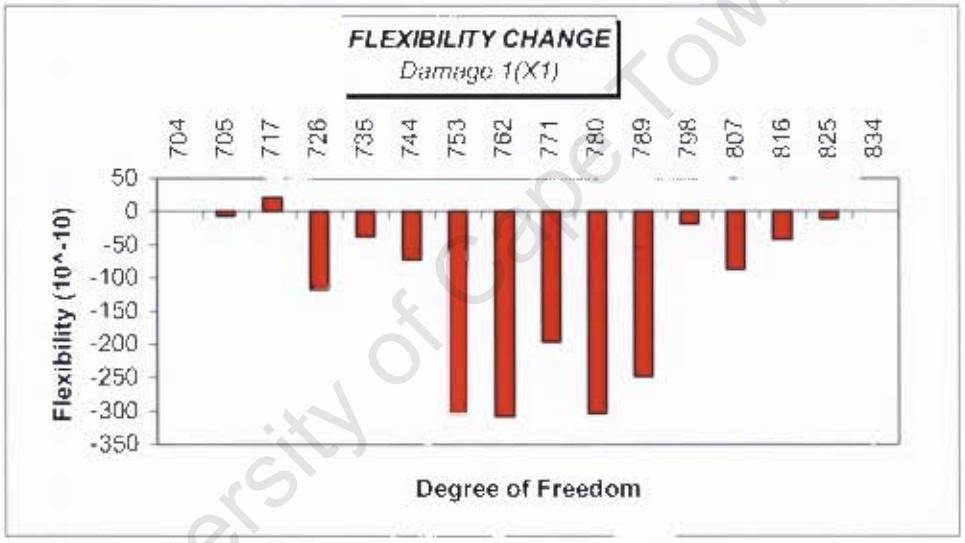

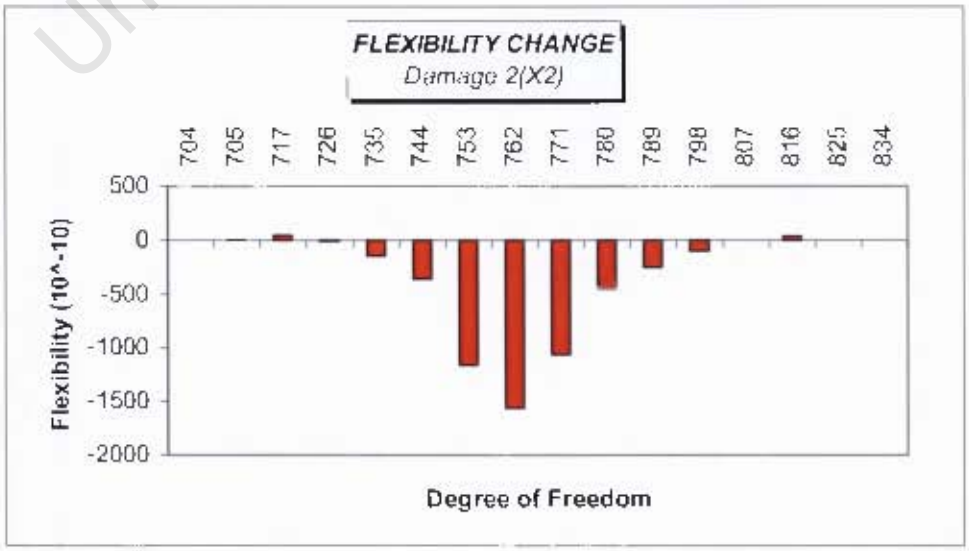

Fig 5.30: *Change in Flexibility: Damage one and two*

5.5.2.3 Flexibility Change Technique

Modal flexibility of the systems was computed from mode data based on equations 5.4 to 5.7. The results are displayed in Fig 5.30, Fig 5.31 and Fig 5.32. The flexibility values for the first damage case identified four positions as the damaged region. The technique managed to detect all loosened connectors. The technique also located 75 percent of the loosened connectors on second damage scenario as shown in Fig 5.30.

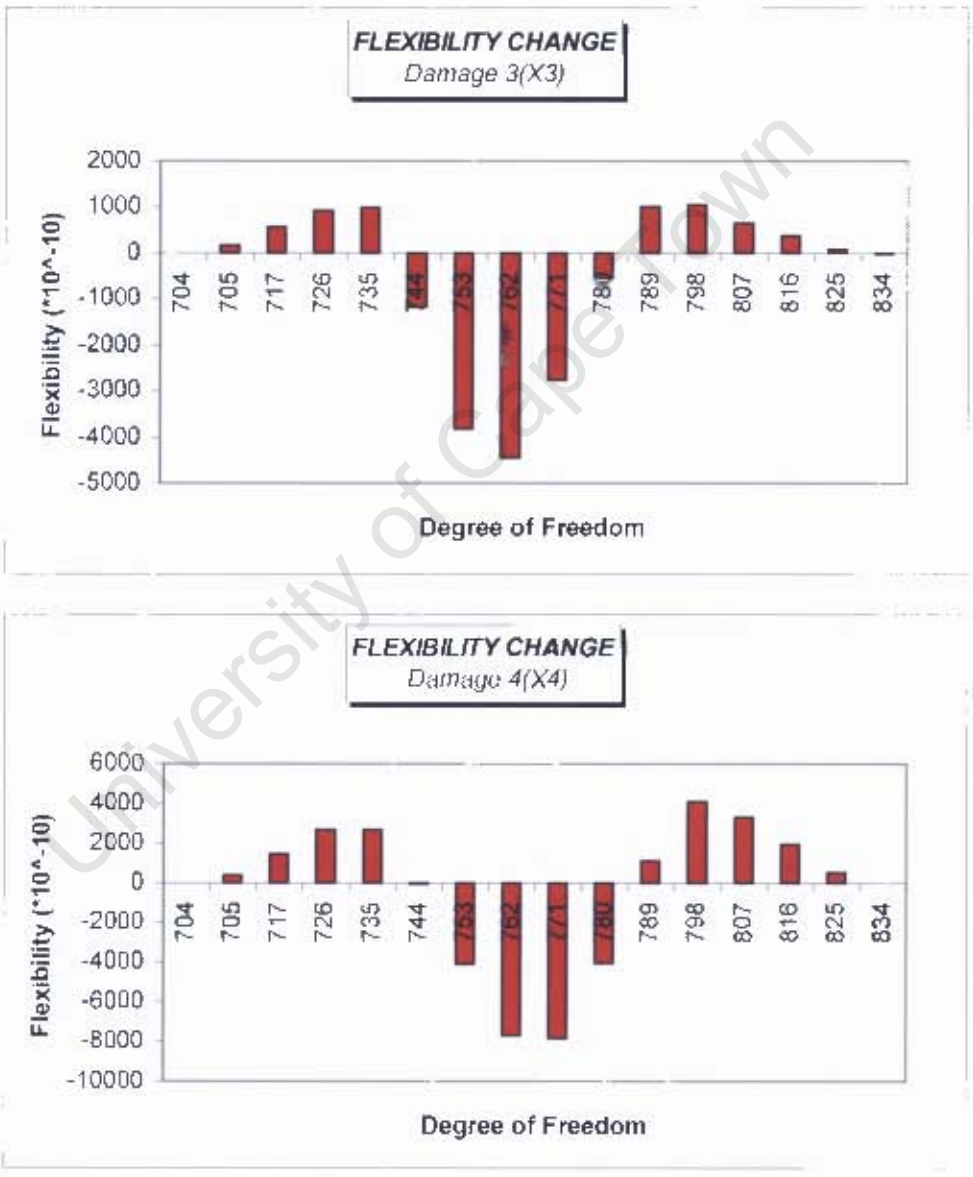

Fig 5.31: Flexibility change: Damage three and four

The results for the third and fourth damage scenarios displayed in Fig 5.31 reveal interesting results. Negative flexibility values were observed on 75% of the damaged region. The flexibility phase shift and peak values shown on this damage clearly show the

sensitivity of the technique to the damage inflicted. Similar observations are shown in Fig 5.32 for severe damage. In this scenario, all the loosened shear connectors were identified.

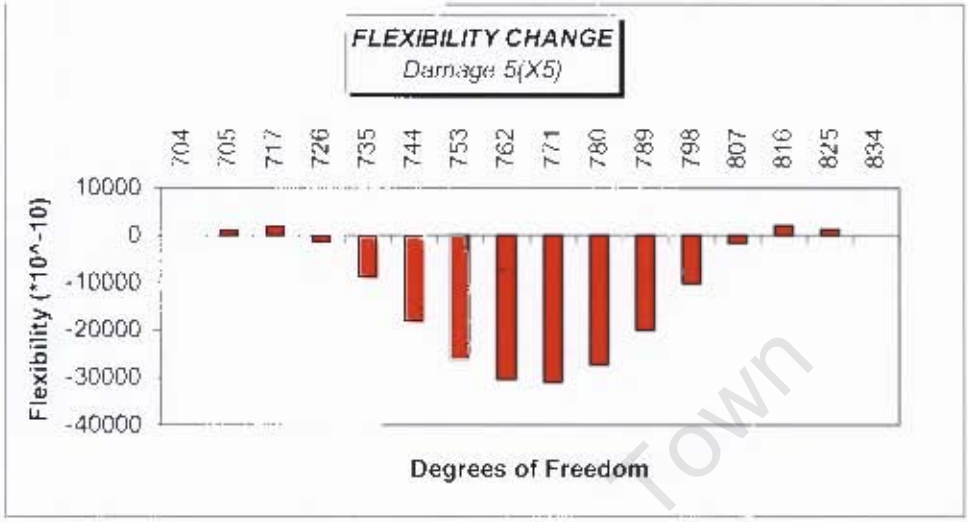

***Figure 5.32**: Flexibility change for damage scenario five*

In conclusion, this technique was able to locate the damaged region for all the cases investigated. This clearly shows the importance of using a robust FE model in damage detection works. This model can only be obtained through integration of both dynamic testing and numerical models.

The mode shape data obtained from the fined tuned model after analysis was used also to compute the modal stiffness of the systems. Details of this work are described in the next section.

5.5.2.4 The Stiffness Change method

Stiffness algorithms used in section 5.4.2.4 still hold and are used latter on mode shapes data. The modal stiffness is a good indicator of the damaged shear connectors as this technique computes stiffness at each point of interest. The damaged displacement vectors for different modes are then computed from the stiffness values. The higher the displacement vector, the less stiff is the point. These values are computed for each mode for different damage cases. The computation of damaged values is advantageous as this investigates the effect of this damage on different modes. This research seeks to identify the effective way to detect this damage. As such, identification of the modes that are sensitive to this damage is critical.

Damaged vectors for first bending mode are shown in Fig 5.33 for light damage. The results indicate that all the damaged connectors were all identified.

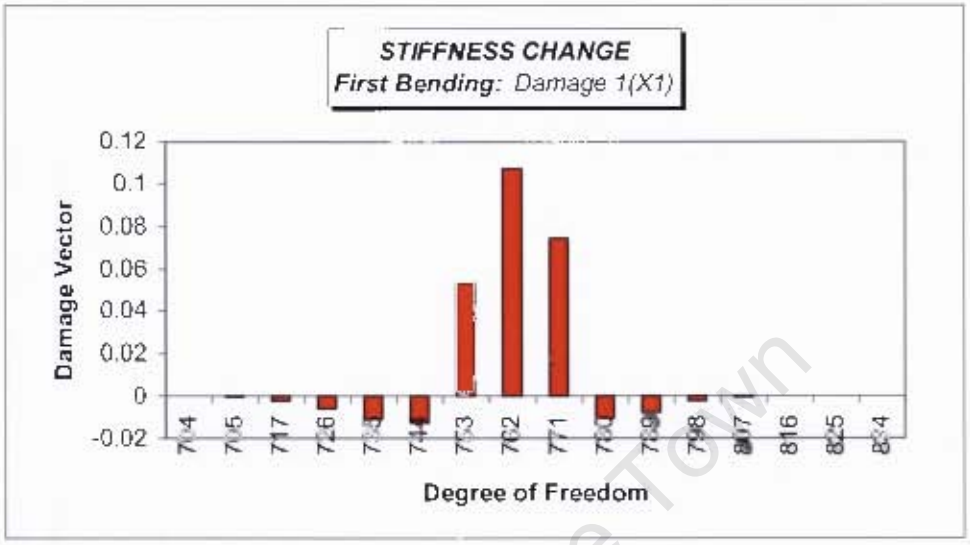

***Fig 5.33**: Damage vectors (X1): First bending mode*

The damaged vectors computed for the torsional mode also give similar observations. The maximum values could be easily identified for the loosened shear connectors. This is shown in Fig 5.34.

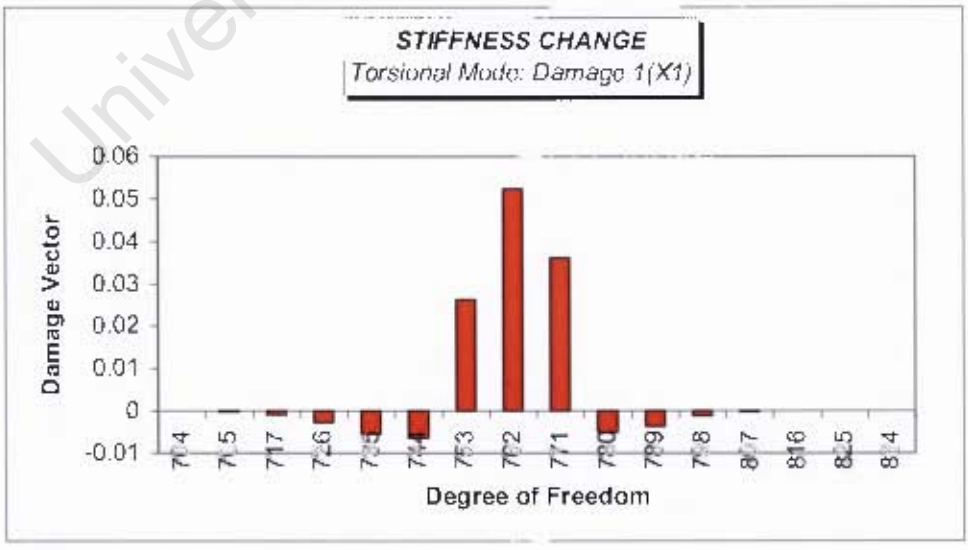

***Fig 5.34**: Damage vectors (X1): Torsional mode*

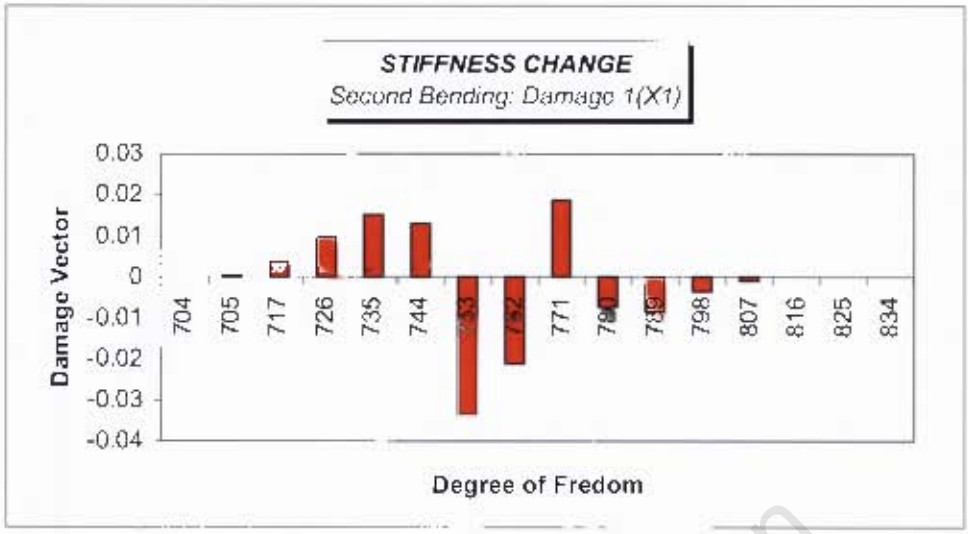

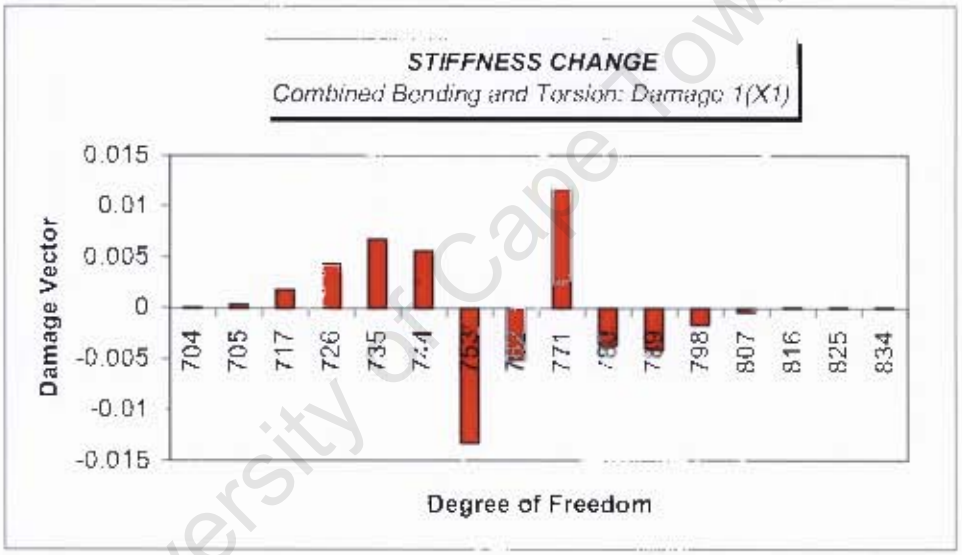

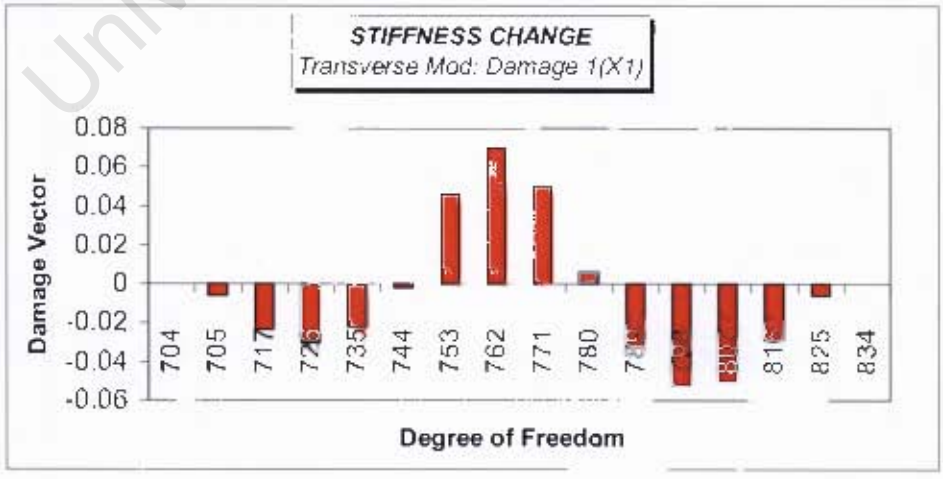

Fig 5.35: Damage vectors (X1): Second bending, combined bending and transverse modes

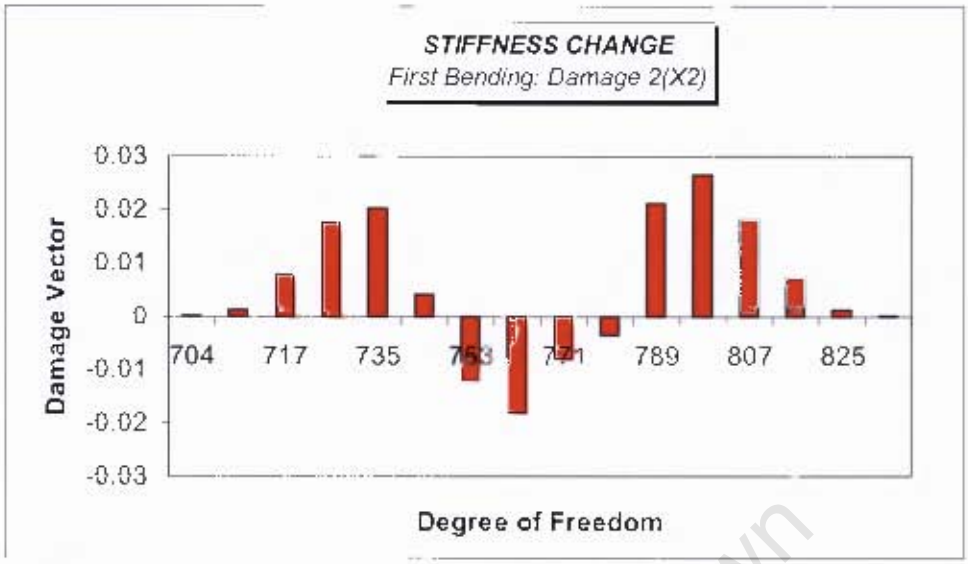

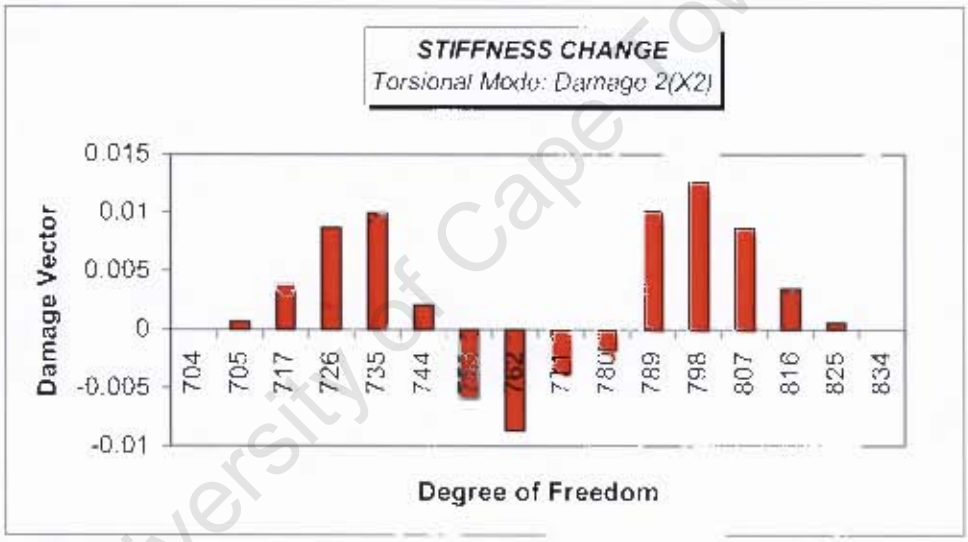

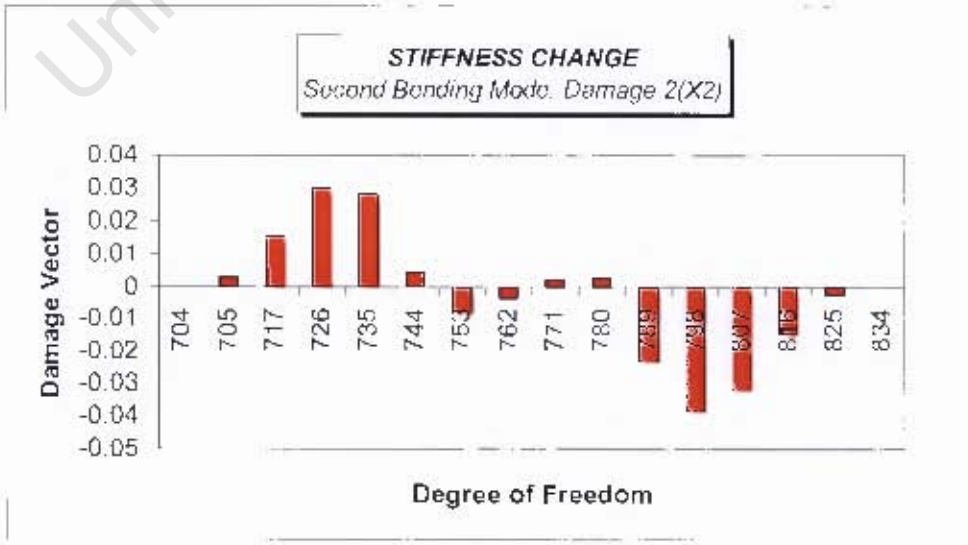

Fig 5.36: Damage vectors (X2): First Bending, Torsion and Second bending modes

The second bending, combined bending and transverse modes damage vectors are shown in Fig 5.35. One damaged shear connector was located on the second bending and combined bending and torsion mode vectors. All the three shear connectors loosened are shown on damage vector plots for the transverse modes.

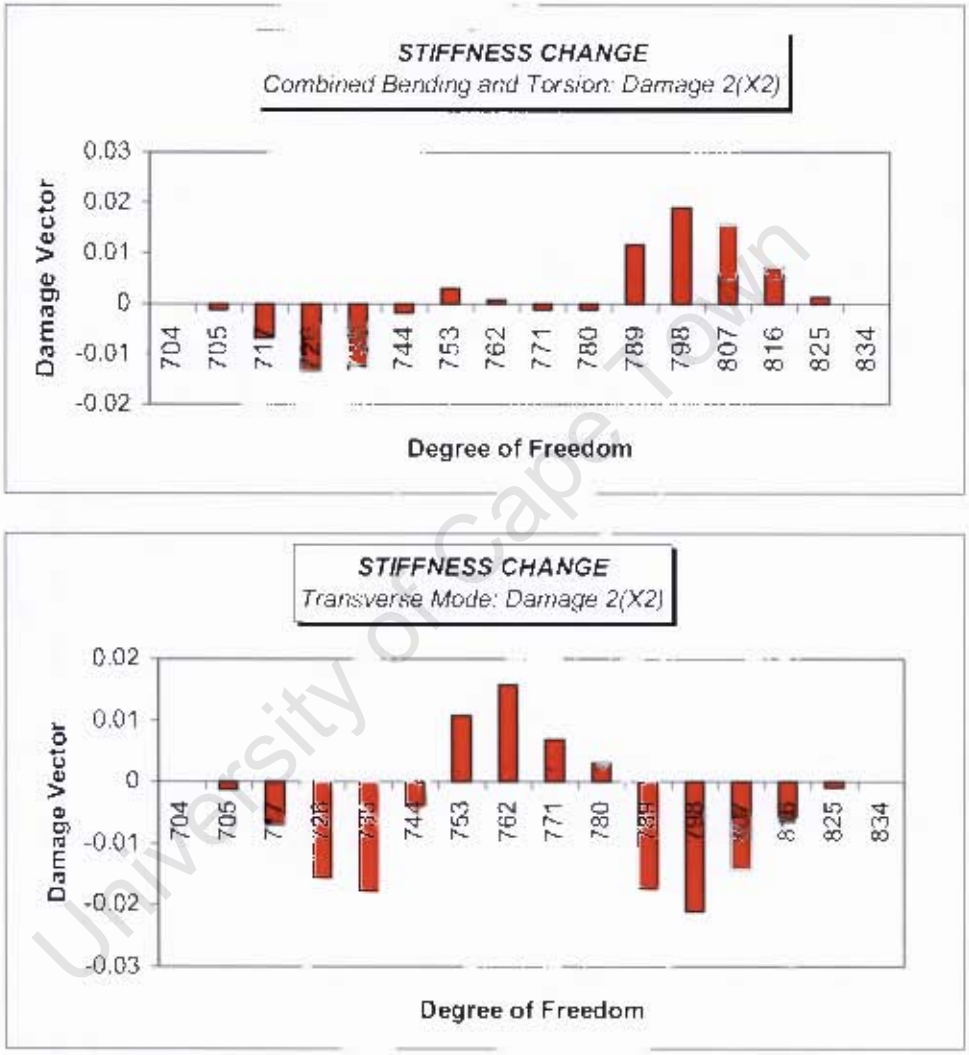

***Fig 5.37**: Damage vectors (X2): Combined bending and torsion and transverse modes*

Based on these observations, one may identify the modes of interest for this work. It is clear that loss in composite action could be identified on first bending, torsional and transverse mode interrogations. The vectors computed for the second damage are shown in Fig 5.36 and Fig 5.37.

A phase change was observed on loosened shear connectors for all vectors for different modes on damage two. The peak damage vectors were necessarily not at the loosened

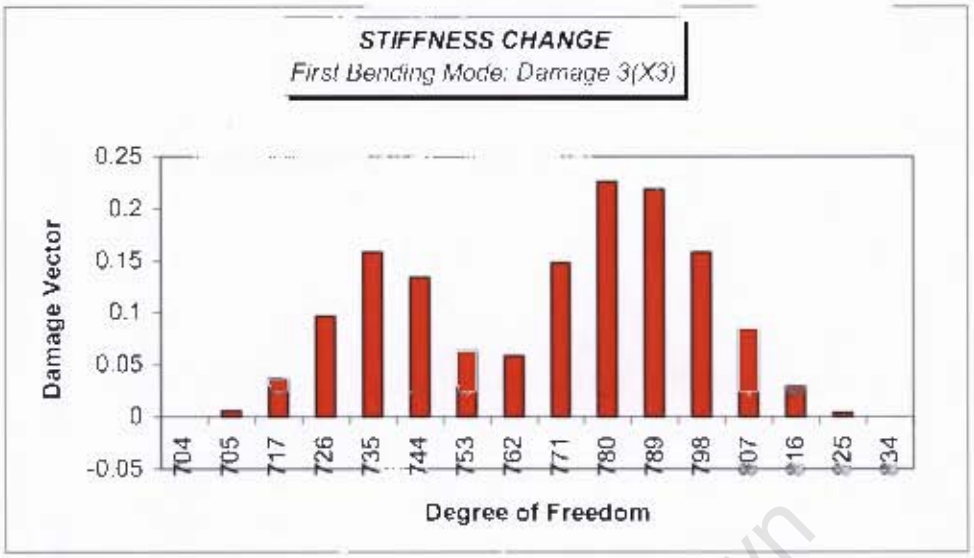

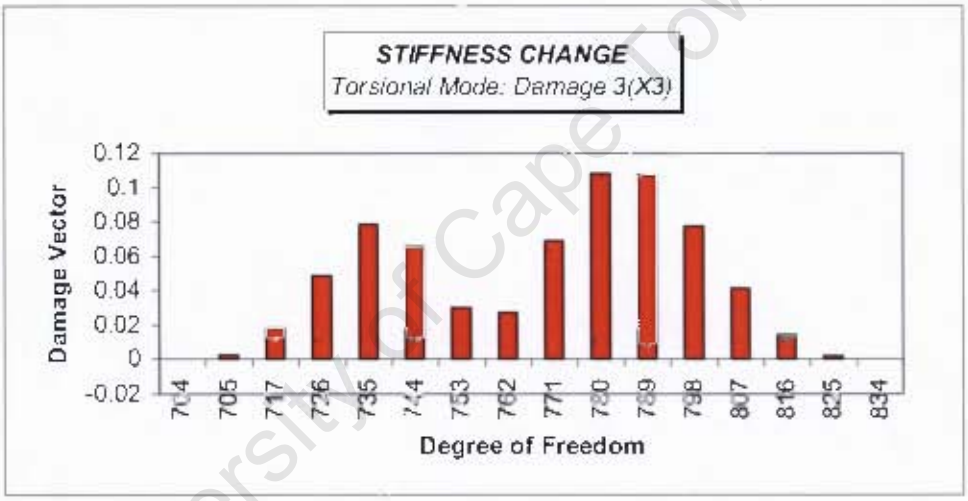

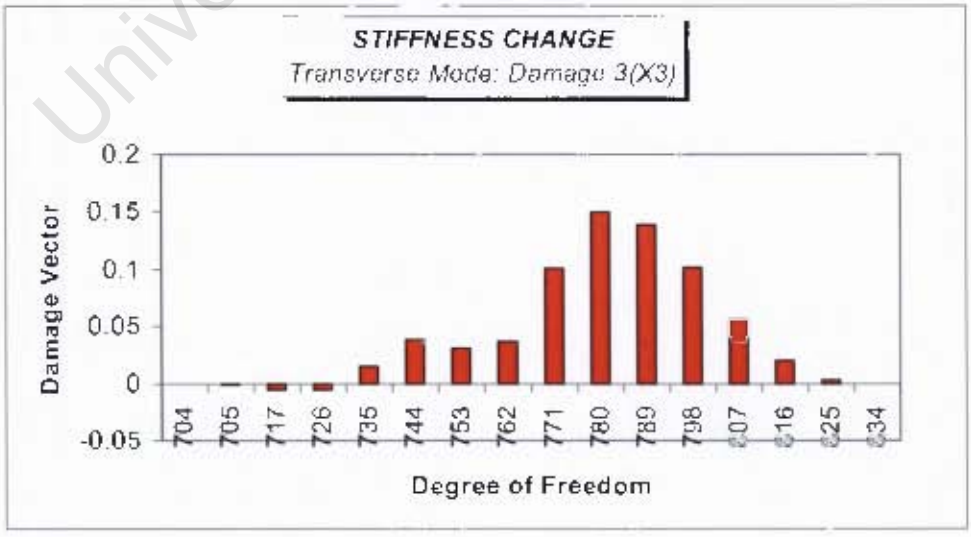

Fig 5.38: Damage vectors (X3): damage scenario three

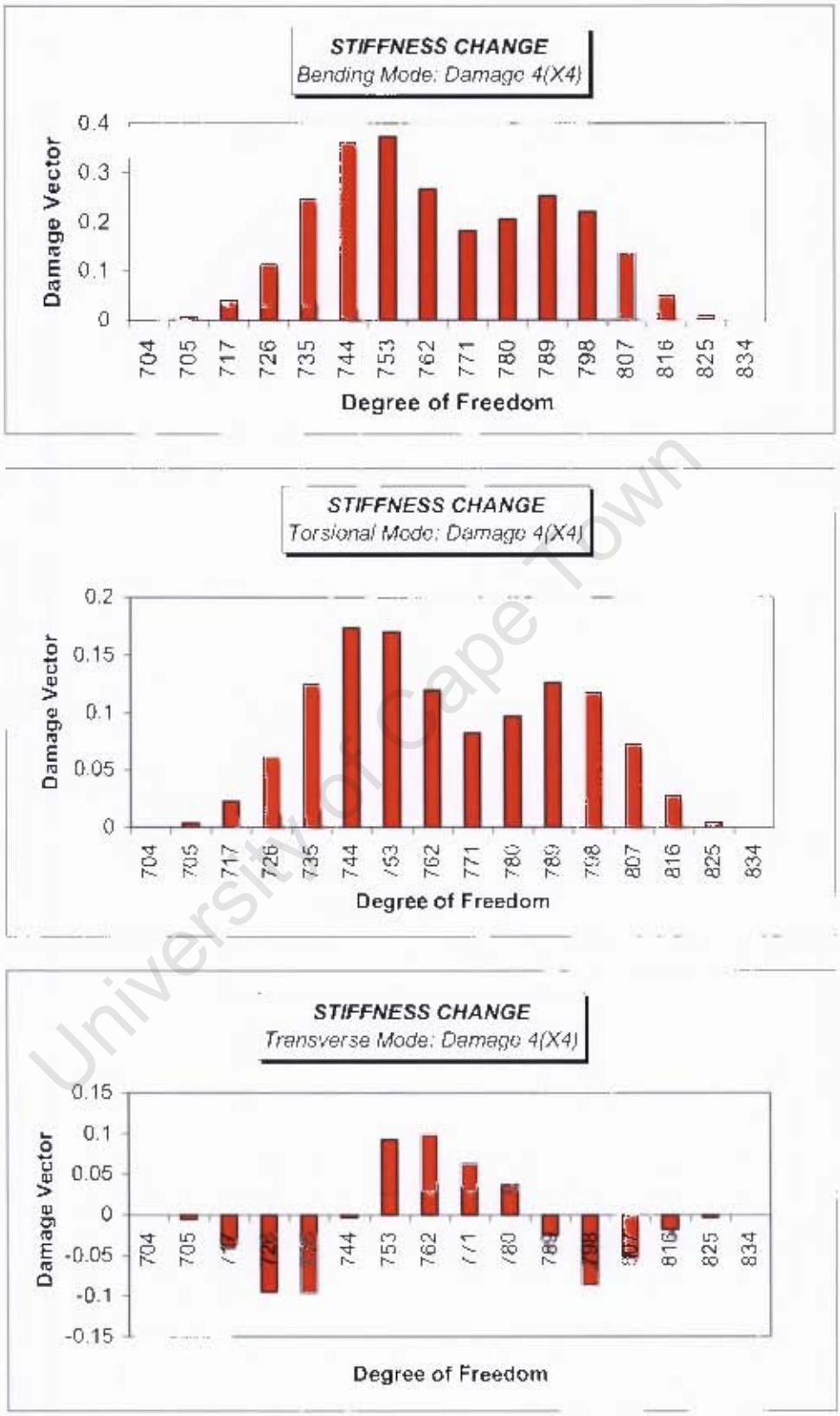

Fig 5.39: Damage vectors (X4): First bending, torsional and transverse modes

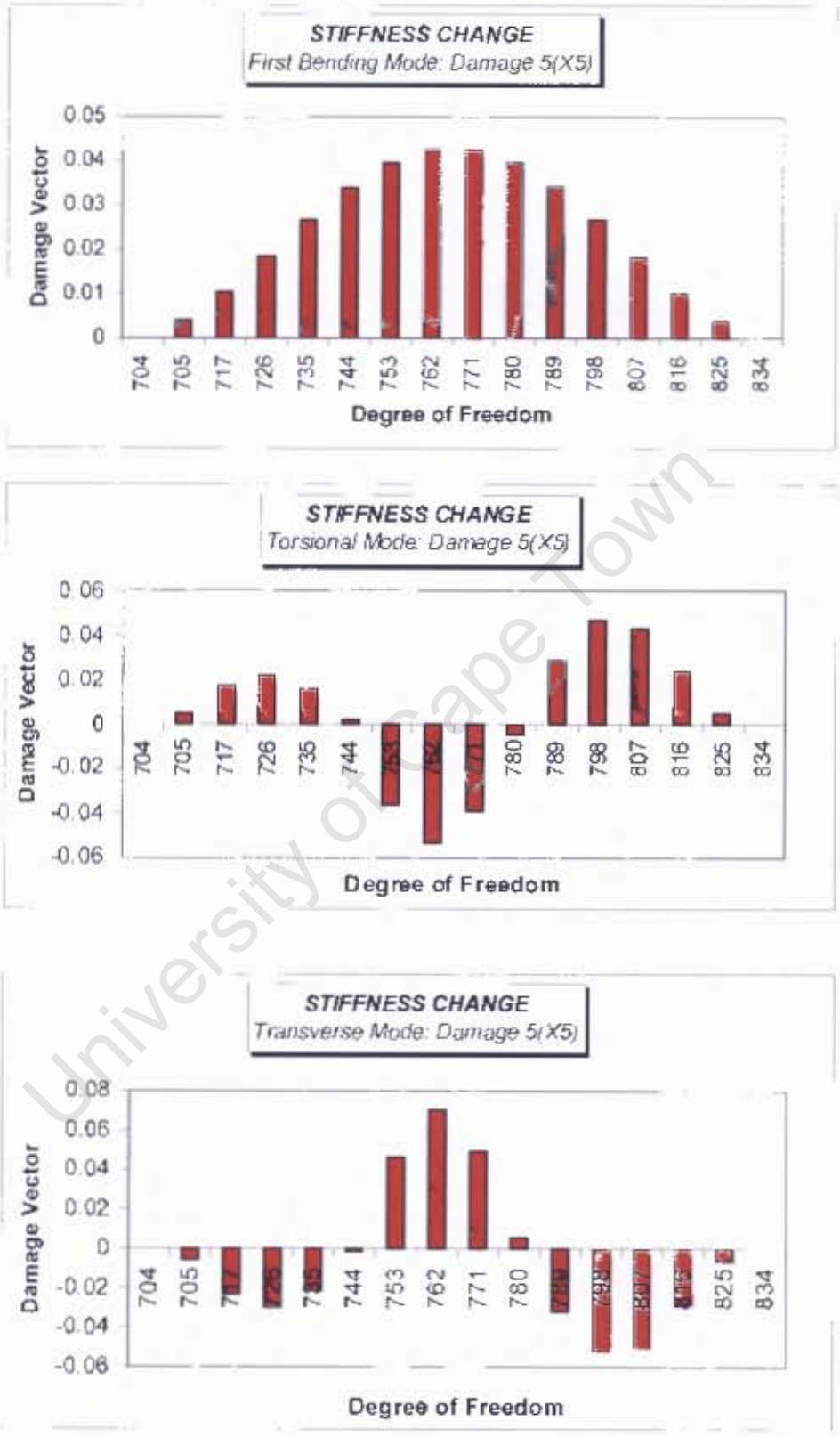

Fig 5.40: Damage vectors (X5): First bending, torsional and transverse modes

shear connectors as shown. Also observed are relatively lower vectors on second bending and on combined bending and torsional modes. The same observations could be seen in Fig 5.37 for the combined bending and transverse mode vectors.

Damaged vectors calculated for third and fourth damage scenarios are shown in Fig 5.38 to Fig 5.40 respectively. The first two modes show the same trends in the damaged vectors of the structure for both damage scenarios. Nevertheless, the transverse mode of damage scenario four shows some trends that can be linked to the damage. This trend follows that obtained from the earlier scenarios.

5.6 Summary

The application of vibration-based damage detection techniques using experimental and numerical data has been presented. Both global and local techniques were investigated. Table 5.8 and Table 5.9 give summaries of damage detection results using experimental and numerical modal data respectively. The adequacy of each method in detecting damage was based on variation of quantities for damaged and undamaged structure. However threshold values are used in most engineering problems to draw conclusions.

***Table 5.8**: Summary of damage detection results based on experimental modal data*

Method	***Damage Scenarios***				
	X1	***X2***	***X3***	***X4***	***X5***
Frequency Change	√	√	√	√	√
Mode Shapes	$\sqrt{}^{B}$ $\sqrt{}^{T}$	$\sqrt{}^{T}$	$\sqrt{}^{B}$ $\sqrt{}^{T}$	$\sqrt{}^{B}$ $\sqrt{}^{T}$	$\sqrt{}^{B}$ $\sqrt{}^{T}$
MAC Values	X	X	X	X	X
COMAC Values	X	X	X	X	X
Mode curvatures	X	X	X	$\sqrt{}^{B}$	$\sqrt{}^{B}$
Flexibility Change	X	X	X	√√	√√
Stiffness Change	X	X	$\sqrt{}^{B}$	X	X

√ - Damage detected; $\sqrt{}^{B}$ - Damage detected and localised using first bending mode $\sqrt{}^{T}$ - Damage detected and localised using torsional mode; X- Damage not detected (Or localised; √√- Damage detected and localised

Frequency changes were consistent in detecting damage due to loosening of shear connectors. The first bending and torsion modes were also sensitive to this damage. However, this was not the case with higher modes. Examination of MAC and COMAC values showed that these modal properties are poor indicators of damage. This observation verifies other investigators findings. The other damage localising algorithms showed mixed sensitive to this damage. The flexibility change technique was able to localise damage when more than 35% of shear connectors were loosened. The change in stiffness method was only sensitive for the third damage scenario (24% damage). Higher damage scenarios could not be located.

***Table 5.9**: Summary of damage detection results based on numerical modal data*

Method	***Damage Scenarios***				
	X1	***X2***	***X3***	***X4***	***X5***
Frequency Change	√	√	√	√	√
Mode Shapes	$\surd\surd^{B}$ $\surd\surd^{T}$ $\surd\surd^{TR}$	$\surd\surd^{T}$	$\surd\surd^{B}$ $\surd\surd^{T}$ $\surd\surd^{TR}$	$\surd\surd^{B}$ $\surd\surd^{T}$ $\surd\surd^{TR}$	$\surd\surd^{B}$ $\surd\surd^{T}$ $\surd\surd^{TR}$
MAC Values	X	X	X	X	X
COMAC Values	XX	XX	XX	XX	XX
Mode curvatures	√√	√√	XX	XX	XX
Flexibility Change	XX	√√	√√	√√	√√
Stiffness Change	$\surd\surd^{B}$ $\surd\surd^{T}$ $\surd\surd^{SB}$ $\surd\surd^{TR}$	$\surd\surd^{B}$ $\surd\surd^{T}$ $\surd\surd^{TR}$	XX	$\surd\surd^{TR}$	$\surd\surd^{T}$ $\surd\surd^{TR}$

√ - Damage detected; $\surd\surd^{B}$. Damage detected and localised using first bending mode
$\surd\surd^{T}$ - Damage detected and localised using torsional mode; X- Damage not detected (Or localised; $\surd\surd^{TR}$ - Damage detected and localised using transverse mode
√√- Damage detected and localised; XX- Damage not localised

The numerical results also show that frequency changes were consistent in detecting this damage. The MAC and COMAC values based on numerical data revealed also their non-

and *X2*. Using the flexibility change algorithm, 90% of loosened shear connectors were located as shown on Table 5.9. Based on stiffness change algorithm, damage was located using the first bending, torsion, second bending and transverse modes. However the sensitivity of this algorithm reduced as more damage was introduced on the structure.

From these findings, it is clear that integrating experimental and FE analysis yields better results. An improved ability to detect and locate the damage using numerical modal data is shown in Table 5.9. Nevertheless an engineering judgement is important for an accurate and interpretation of these results.

CHAPTER 6

PRACTICAL APPLICATION OF VIBRATION TESTING AND FE MODELLING

6.1 Introduction

This section presents the application of vibration-based techniques on Van der Kloof Bridge, South Africa. The bridge was closed to traffic after structural cracks were observed on the deck slab during visual inspections. The road users were also experiencing excessive vibration under traffic loading (Ronne, 2008). The condition of shear connectors between the beams and slab was also of interest. A thorough investigation of the bridge was therefore necessary. The investigations were based on vibration testing. An FE model for the system was also required. This model could be used as reference for future investigations of the structure. This chapter therefore focuses on the development of an accurate FE model for the bridge. This assesses the accuracy of modelling shear connectors in a physical bridge using spring elements. The effectiveness of the refurbishment scheme could also be assessed using the updated FE model. Thorough investigation of condition of the structure was also provided during vibration testing. Vibration testing was done before and after rehabilitation of the bridge.

The following sections give a description of the bridge and results of the investigation.

6.2 Description of Van der Kloof Bridge

Van der Kloof bridge is a concrete-concrete composite structure that consists of precast pre-stressed beams and a cast in-situ deck slab. The bridge is curved in plan and has a total length of 204 m comprising of 15 simply supported spans. Each span has a length of 13 m. The

beams have a straight alignment and the horizontal curvature is achieved by concrete infill at pier locations. The superstructure consists of 9 precast prestressed concrete beams with an in-situ cast deck slab which is 130 mm thick. 20 mm fibre cement plates were used as permanent formwork for casting the *in-situ* deck slab. The beams were spaced at 1.25 m. The superstructure was supported on piers founded on the concrete dam wall. A pictorial view of the bridge is shown in Fig 6.1.

***Fig 6.1**: Van der Kloof Bridge, South Africa*

The general layout of the structure is shown in Fig 6.2. The shear connection between the beams and slab was provided by extended beam web reinforcement as shown in the figure.

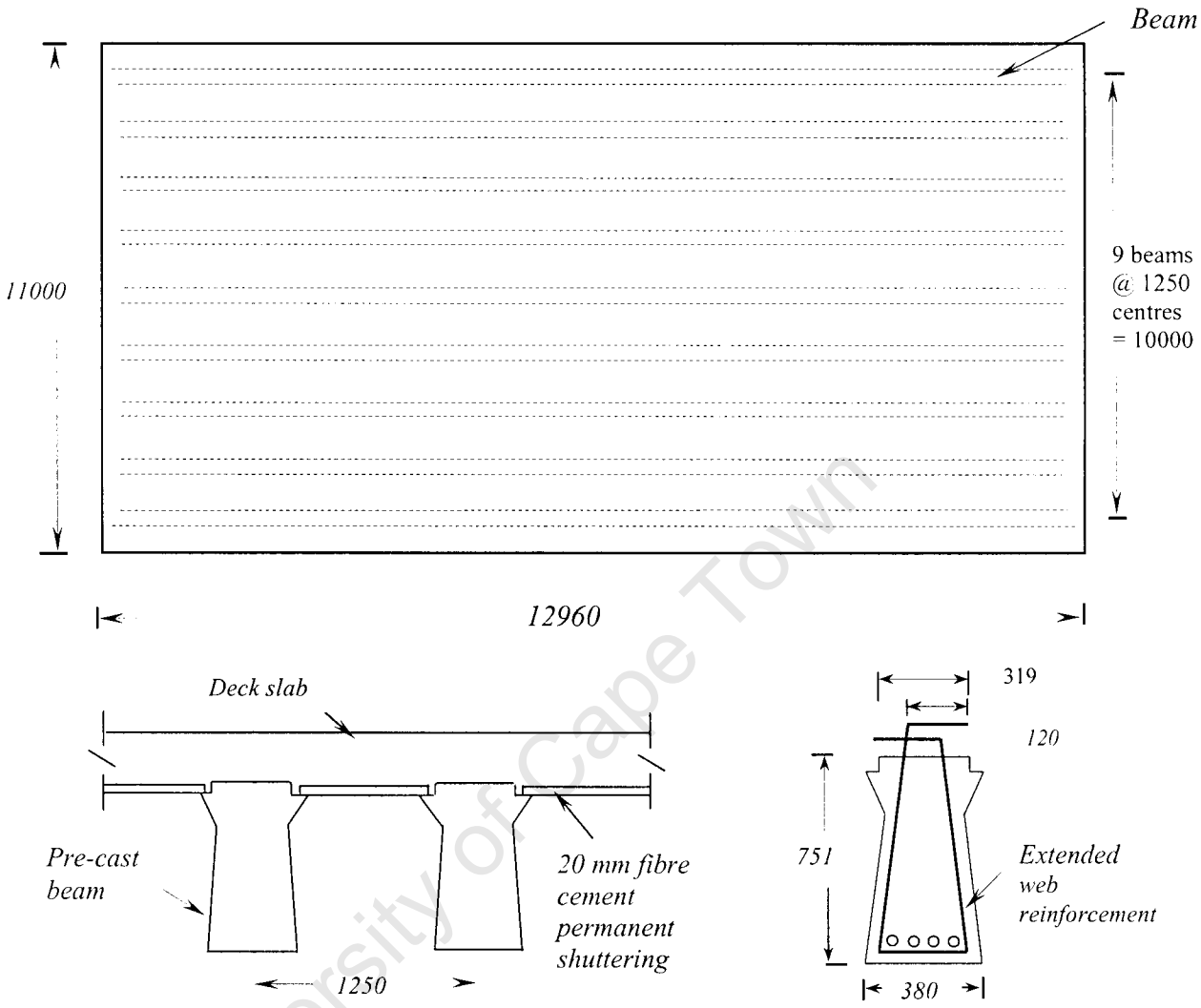

***Fig 6.2**: Plan, section and beam details for one of the spans (All units in mm)*

6.3 Scope of work

As mentioned in the introductory section, a thorough investigation on the condition of structural elements of the system not accessible during visual inspections was required. A robust FE model of the bridge was also required. Vibration testing was done on the bridge to extract the modal parameters. These were the modal frequencies and mode shapes. The mode shapes were used to assess the stiffness distribution of the structure and also the condition of bearings of the structure. The bearings could not be assessed using visual techniques due to accessibility problems. The frequencies were used later to assess the effectiveness of the

retrofitting scheme. The extracted frequencies could also be used as damage indicators in the structure, in future. Moreover, the frequencies were used for validation of the FE model.

It is worth noting that the condition of the shear connectors could not be assessed at this stage. The reason being that assessment of these connectors is a long term process that relies on comparing modal parameters extracted at different times. The modal parameters extracted at this stage could be used as reference data in future.

6.3.1 Vibration-based assessment

Vibration measurements were taken from one of the spans on the spillway of the dam. A shaker was used to energise the structure. The response of the structure was measured directly over the beams and in- between the beams.

6.3.2 FE modeling of the system

ADINA software was used for modeling the system. A typical mesh of the structure is shown in Fig 6.3. The deck slab was modeled using shell elements. The beams were modeled using beam elements. The shear connectors were initially modeled using rigid connectors. However the frequencies obtained were much higher than the actual frequencies measured on the structure. The rigid connectors were then replaced by 6-D non-linear spring elements.

Fig 6.3: *Typical mesh of the system*

The extracted frequencies and mode shapes are displayed in the next section.

6.4 Test results before rehabilitation

6.4.1 Frequencies

The following tables show the natural frequencies of the system before rehabilitation. The measured and theoretical frequencies are presented. Table 6.1 shows the comparisons of measured and theoretical frequencies for a system using rigid connectors to model shear connectors. The comparisons of the measured and theoretical frequencies for a model using spring elements to model shear connectors are shown in Table 6.2. The resulting spring stiffness after fine tuning are shown in Table 6.3.

***Table 6.1**: Identified frequencies for a system using rigid connectors to model shear connectors: Pre-retrofitting*

	Mode	*Measured frequency (Hz)*	*Theoretical frequency (Hz)*	*% Difference in frequency*
1	Bending	8.8	14.0	59.0
2	Torsion	10.9	15.0	37.6
3	Transverse 1	13.1	17.2	31.1
4	Transverse 2	17.2	21.0	22.1
5	Transverse 3	22.9	26.5	15.7

***Table 6.2**: Identified frequencies for a system using spring elements to model shear connectors: Pre-retrofitting*

	Mode	*Measured frequency (Hz)*	*Theoretical frequency (Hz)*	*% Difference in frequency*
1	bending	8.8	9.0	+0.02
2	torsion	10.9	10.1	-0.93
3	Transverse 1	13.1	12.8	-0.98
4	Transverse 2	17.2	17.4	+0.01
5	Transverse 3	22.9	23.9	+0.04

***Table 6.3**: Spring stiffness: Bearings and Shear connectors*

Bearings		***Shear Connectors***	
Spring Property	Stiffness	Spring Property	Stiffness
X-Translation	3×10^8 N/m	X-Translation	3×10^8 N/m
Y-Translation	3×10^8 N/m	Y-Translation	3×10^8 N/m
Z-Translation	3×10^8 N/m	Z-Translation	3×10^8 N/m
X-Rotation	1.8×10^9 Nm/rad	X-Rotation	9×10^{19} Nm/rad
Y-Rotation	1.8×10^8 Nm/rad	Y-Rotation	1.7×10^9 Nm/rad
Z-Rotation	3×10^8 Nm/rad	Z-Rotation	3×10^8 Nm/rad

6.4.2 Mode shapes

Table 6.4 shows the experimental and theoretical modes. Five mode shapes were extracted from the bridge. This includes the bending, torsion and three successive transverse modes. The transverse modes displayed double curvature changes. This was observed also on theoretical modes. This could be explained in terms of stiffness distribution within the structure.

6.5 Discussion of results and conclusions

The comparisons of measured and theoretical frequencies show that the FE system using spring elements produce an accurate model after updating. A maximum difference of 0.98% was recorded between experimental and theoretical frequencies. This model therefore depicts the physical system as accurate as possible. For an FE model using rigid connectors, frequency difference as high as 59% were recorded. This shows that the use of rigid connectors to model shear connectors results in a relatively stiffer system. This does not represent the actual structure.

The use of spring elements in an FEM simulation for shear connectors is therefore the correct way of representing the shear connectors. This allows control of stiffness of the boundary conditions. The resulting FE model simulates the physical structure, after fine tuning, and can therefore be used in future to assess the condition of shear connectors. This can be done following the steps proposed in Fig 7.1 (Chapter 7).

Table 6.4: *Experimental and theoretical mode shapes*

Mode	***Experimental Mode***	***Theoretical mode***
Bending		
Torsion	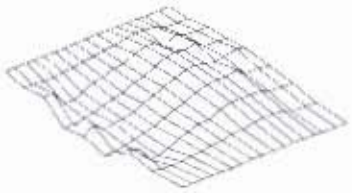	
Transverse		
Transverse	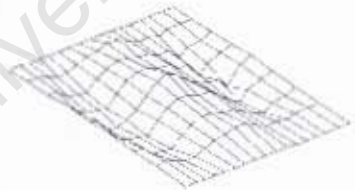	
Transverse	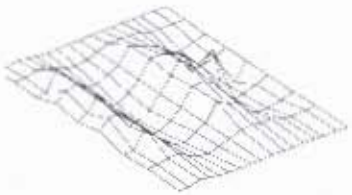	

The mode shapes of the bridge, particularly the transverse shapes indicate a very low transverse stiffness of the bridge. Double curvatures were observed on transverse modes of the structure. The low transverse stiffness may result in poor load distribution of the bridge. Additional transverse beams were therefore required. The mode shapes also reveal malfunctioning of the bearings of the bridge. This was shown by a flat slope of the mode shapes near the boundaries.

The above findings clearly show that vibration testing is an important tool that can be used to assess the condition of a structure. The results of vibration testing are also important to produce an accurate FE model of a structure. An updated FE model can help minimize testing costs if properly developed and integrated with measurement tests from the structure.

CHAPTER 7

CONCLUSIONS AND RECOMMENDATIONS

7.1 Conclusions

Highway bridges constitute significant and critical components of transportation systems and are among the most expensive investment asset of any country's infrastructure. However, there is a growing number of damaged bridge structures owing to ageing of these structures and increase in allowable axle loads. One of the most common types of bridges, which have been in service for over two decades for short to medium spans in South Africa and worldwide is the concrete-concrete composite structure consisting of pre-cast pre-stressed beams and cast in-situ slab. The slab is connected to the beams using shear connectors. These connectors are responsible for the composite action and therefore the efficiency of the structure.

Despite the technological advancement, most Bridge Management Systems still rely on visual inspections for condition assessment of these structures. This means damage in inaccessible parts of the structure may go undetected until it is expensive to repair or catastrophic failure occurs. However, during the past few decades vibration-based damage detection techniques have emerged as promising tools in assessing and detecting damage in structures. Nevertheless, these techniques have not been used to detect damaged shear connectors on bridges based on modal data measured from the surface of the deck slab. This research therefore investigated the use of vibration techniques based on experimental and FE analysis.

Most of the vibration-based localising algorithms investigated were able to localise loosened shear connectors using the analytical first bending, torsion and transverse modes data. The application of local indices of vibration-based methods on experimental data did not give convincing localising results. Some false damage was detected. On average less than 30% of loosened shear connectors were localised using experimental modal data. However, the localising techniques were able to localise most of the loosened shear connectors using the analytical modal data. Over 70% of loosened shear connectors were located.

The use of spring elements to model shear connectors was also applied on an existing bridge. The bridge was closed to traffic due to excessive vibrations under loading. Cracks were also observed on the deck slab. The condition of shear connectors of the bridge also needed to be assessed. However, the assessment of the connectors is a long term process. Only the FE model and baseline modal data were developed for this bridge. The FE model produced was able to produce frequencies that were close to the measured ones. A maximum difference of 0.98% was recorded between frequencies. The model developed could be used to assess the condition of shear connectors using the steps proposed in Fig 7.1.

These observations show the importance of integrating experimental modal analysis and robust FE models to detect and localise damage in such bridges. Some engineering judgement is however needed to distinguish between actual and false damage. Nevertheless, these techniques can be used to detect and locate damaged shear connectors in concrete-concrete bridges if correct engineering judgement is applied.

Most practising engineers in the field of structural assessment and rehabilitation are not familiar with modal analysis and vibration testing of structures. This is because the modal analysis and testing courses are specialised courses and not taught at undergraduate level. It is therefore of great importance to give simple steps that may be followed if vibration-based techniques are to be used to assess and detect the condition of shear connectors in concrete-concrete composite bridges. This is presented in the following paragraphs.

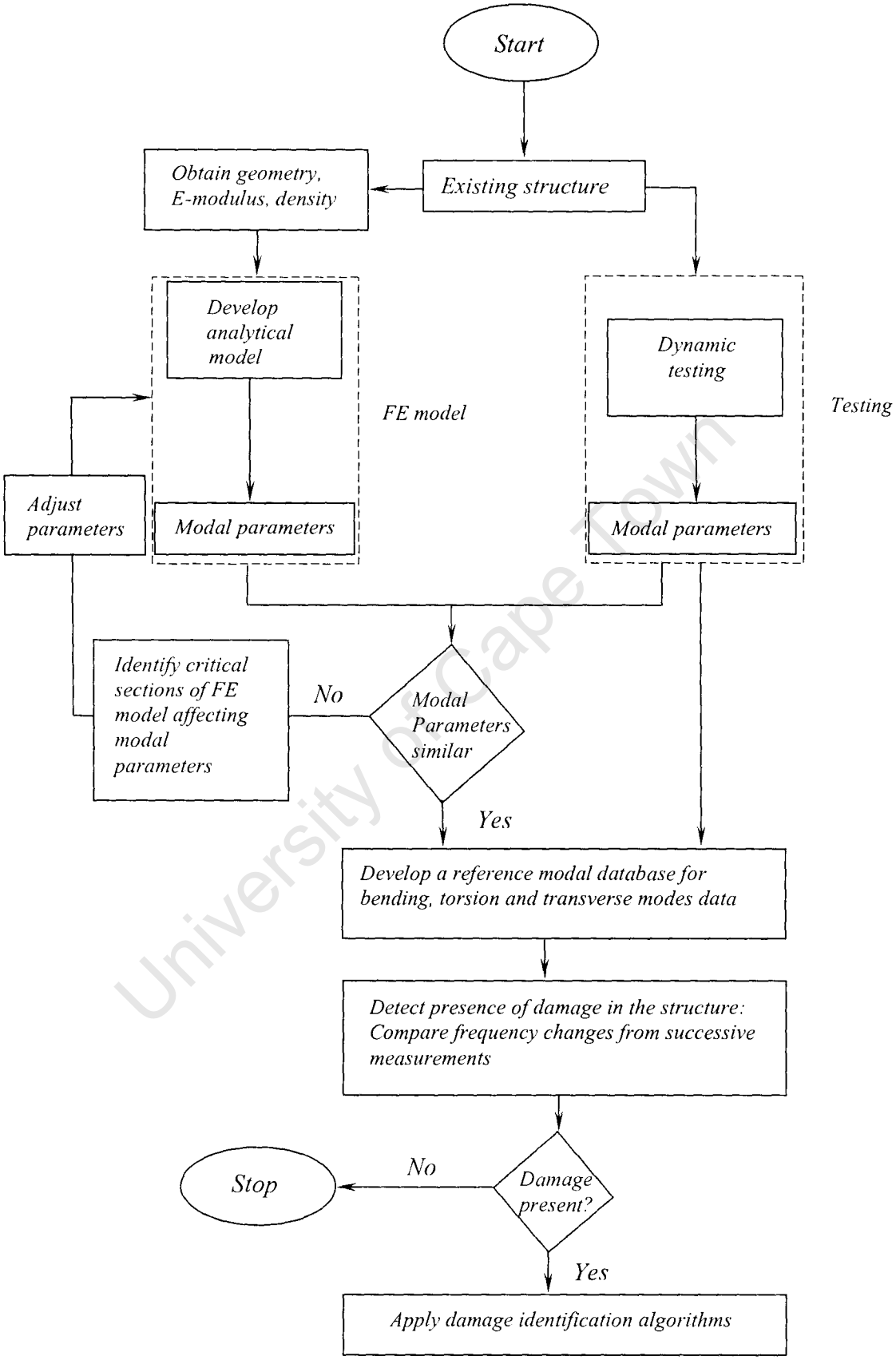

***Fig 7.1*: Proposal for a typical procedure for detecting damaged shear connectors in concrete bridges**

The flow chart in Fig 7.1 proposes a sequence of steps that can be followed for a dynamic investigation to assess, detect and locate damaged shear connectors in composite concrete-concrete bridges. The process is based on long term dynamic monitoring of the structure to create a modal database. Using the database, the indices of vibration-based methods can then be used to localise the damaged region of the structure.

The proposed steps take into account the fact that in most cases, FE models of these bridges do not exist and therefore need to be developed. This is because most of these structures were built a long time ago when powerful modelling softwares were not available. In addition, vibration assessment or modal testing of civil infrastructure such as bridges is relatively new and is not widely understood by practising forensic engineers that are responsible for the repair of bridges. Nevertheless, modal data of a structure is needed if an accurate FE model that can be used for further investigation need to be developed.

The first step is to characterise the material properties of the structure. This may be done by taking core samples from the structure that could be tested for compressive strength, tensile strength and elastic modulus. The geometry of the structure can easily be measured. The geometry and material properties are needed to develop an FE model of the system.

The modal parameters of the system can be measured and these are needed to fine tune the FE model of the structure. These parameters are also needed for comparing with future measured modal data.

It was shown in chapter five that damage of shear connectors in concrete-concrete composite bridges affects mainly the first bending, torsion and transverse modes. Conversely, application of damage location algorithms on modal data from these modes are used in the flow-chart (Fig 7.1). However not all the modes of the structure can be used to detect the presence of damaged shear connectors in the structure.

The process detailed in Fig 7.1 needs to be repeated at time intervals that may coincide with inspection periods of these structures. In short, these structures have to be continuously monitored or tested if vibration-based techniques are to be used to assess the condition of shear connectors that govern the efficiency of these bridges.

7.2 Recommendations

This research was limited to assessing reliability and practicality of vibration-based methods to detect damaged shear connectors in concrete-composite bridges. An appropriate way of modelling this system was also developed. However, it is worthy noting that this work did not produce solutions for some of the problems. The remaining sections not critically dealt with are recommended for future investigations.

There is great need to develop statistical analysis procedures that can establish confidence limits on different damage techniques investigated. This helps to clarify if the changes in parameters such as flexibility, stiffness and curvatures are due to actual damage and not other factors such as experimental errors and weather changes.

The effects of loss in composite action on the load carrying capacity of the structure need also to be investigated. This is vital to determine the stage when repairs are needed as a result of loss in composite action.

A manual FE updating process was used in this research to correlate the analytical and experimental modal parameters. However it would be interesting to develop a scientific updating process or an updating algorithm based on spring parameters. This will give a complete and robust FE model that can be used to assess and locate damaged shear connectors in these bridges.

Finally, the vibration techniques need to be integrated with strain measurements to investigate the effect of loss in composite action. The integration of the two promises to give a more robust assessment technique to prolong the service life of these bridges.

REFERENCES

Ackerman, C.A. (2007), "A vibration based model that rates bridge structural deterioration in a bridge management system." *Ph.d Thesis*. Tshwane University of Technology, Pretoria, South Africa. Available online:http//:www.libserv5.tut.ac.za:7780/pls/eres/wpj_docload.download_file (17 January 2008).

Addis, B. (2001), "Strength of hardened concrete, in *Fulton's concrete technology*." 8th Ed, 2001, Midrand, South Africa.

ADINA R&D Inc. (2008), "User Interface Primer: Report ARD 08-06," Watertown, USA.

Agilent Technologies (2000), "The fundamentals of modal testing." USA. Available on line: http//:cp.literature.agilent.com/litweb/pdf/5954-7957 (21 January 2008).

Agilent Technologies (2000), "The fundamentals of signal analysis." USA. Available on line: http//:cp.literature.agilent.com/litweb/pdf/5954-7957 (21 January 2008).

Alvandi, A., Cremona, C. (2005), "Assessment of vibration-based damage identification techniques." *Journal of Sound and Vibration*, 292, 179-202.

Brownjohn, J.M.W., Moyo, P., Omenzetter, P., Lu, Y. (2003, "Assessment of highway bridge upgrading by dynamic testing and finite-element model updating." *Journal of Bridge Engineering*, 8(3), 162-172.

Brownjohn, J.M.W. (2008), "Structural effects of vibration problems." *Informal Discussion*, 10/08, 2008. Cape Town.

BVM-Epelem. Ltd. (2006), "Building better bridges." *Science Grid This Week Magazine*, Available online: *www.interactions.org/../1018/concret .mor .html (5 June 2007).*

Chen, S. (2008), "Discussion of long-term analysis of steel-concrete composite beams: FE modelling for effective width evaluation." *Journal of Engineering Structures*, 28, 1110-1121.

Clubley, S.K., Moy, S.S.J., Xiao, R.Y. (2002), "Shear strength of steel-concrete-steel composite panels. Part I – testing and numerical modelling." *Journal of Construction Steel Research*, 59, 781-794.

Committee of State Road Authorities. (1989), "*Code of practice for the design of highway bridges and culverts in south Africa.*" THM 7, Part 3.

Dennis, L. (2007), "Capacities of headed stud shear connectors in composite steel beams with precast hollow slabs." *Journal of construction steel research*, Available online: http://www.sciencedirect.com/locate/jcsr (5 August 2007).

Dutta, A., Talukdar, S. (2002), "Damage detection in bridges using accurate modal parameters." *Finite Element Analysis and Design*, 40, 287-304.

Liang, Q.Q., Uy, B., Bradford, M.A., Ronagh, H.R. (2005), "Strength analysis of steel-concrete beams in combined bending and shear." *Journal of Structural Engineering*, 131(10), 1593-600.

Estes, A.C., Frangopol, D.M. (2003), "Updating bridge reliability on bridge management system using visual inspection results." *Journal of Bridge Engineering*, 8(6), 374-382.

Ewins, D.J. (2003), "Modal Testing: theory, practice and application." 2nd Edn, London, England.

Farrar, C.R., Jauregui, D.A. (1997), "Comparative study of damage identification algorithms applied to a bridge: 1. Experiment." *Smart Material Structures*, 7, 704-719.

Flavia, M.S.J., Ibrahim, A.E.M.S., Lidia, C.D.S. (2006, "Shear strength of pre-cast pre-stressed composite beams with discontinuous connections made of cast-in-place shear keys." *Materials and Structures*, 39, 353-364.

Friswell, M.I., Mottershead, J.E. (1995). "*Finite element model updating in structural dynamics*." Netherlands: Kluwer Academic Publishers.Gajanan, M.S. (1979). "*Handbook of composite Construction engineering*." 1st Ed, Melborne, London.

Galambos, T.D. (2007), "Mississippi bridge collapse." *Informal Discussion*, 14 October 2007. University of Cape Town.

Gattesco, N. (1999), "Analytical modelling of nonlinear behaviour of composite beams with deformable connection." *Journal of Constructional Steel Research*, 52, 195-218.

Ghosn, M. (1999). "*Modelling of bridge dead and live loads, in bridge safety and reliability*." Edited by Frangopol, D.M, 1st Ed, American Society of Civil Engineers, USA.

Hobbs, D.W., (1994), "Worldwide durability problems with concrete and trends in prevention." *Concrete Society of Southern Africa Silver Jubilee Commemoration National Convention*, Sun City. 18-21 September. *Cited by*: Ackerman, C.A. (2007), "A vibration based model that rates bridge structural deterioration in a bridge management system." *PhD Thesis*. Tshwane University of Technology, Pretoria, South Africa.

Huang, Z., Burgess, I.W., Plank, R.J. (1999), "The influence of shear connectors on the behaviour of composite steel –framed buildings in fire." *Journal of Construction Steel Research*, 51, 219-237.

Jin-Hee, A., Chungwook, S., Young-Ju, J., Sang-Hyo, K. (2008), "Fatigue behaviour and statistical evaluation of the stress category for a steel-concrete composite bridge deck." *Journal of Construction Steel Research*, 411-712.

John.P., Cook, P.E. (1977), "*Composite construction methods*." 1st Ed, Canada.

Kuan-Chen, F., Feng, L. (2003), "Nonlinear finite element analysis for highway bridge superstructures." *Journal of Bridge Engineering*, 8(3), 173-179.

Kumar, A. (1988), "Composite concrete bridge superstructures." 1st Ed, British Cement Association.

Larose, K., Elwood, K.J. (2006), "Performance of headed shear studs clusters for precast concrete bridge decks." *Paper prepared for presentation at the Bridges for the 21st century (B) session of the 2006 annual conference of the Transportation Association of Canada*, Charlottetown, Prince Edward Island.

Law, S.S., Chan, T.H.T., Wu, D. (2000), "Efficient numerical model for the damage detection of large scale." *Journal of Engineering Structures*, 23, 436-451.

Li, T.Q., Choo, B.S., Nethercot, D.A, "Connection element method for the analysis of semi-rigid frames." *Journal of Constructional Steel Research*, 32, 143-171.

Macorini, L., Fragiacomo, M., Amadio, C., Izzuddin, B.A, "Long-term analysis of steel-concrete composite beams: FE modelling for effective width evaluation." *Journal of Engineering Structures*, 28, 1110-1121.

Maeck, J., Wahab, M.A., Peeters, B., De Roeck, G., De Visscher, J., De Wilde, W.P., Ndambi, J.M., Vantomme, J. (2000), "Damage identification in reinforced concrete structures by dynamic stiffness determination." *Engineering Structures*, 22, 1339-1349.

Maeck, J. (2003), "Damage assessment of civil engineering structures by vibration monitoring." *PhD Thesis*, Katholieke Universiteit Leuve.
Available: http//:www.kuleuven.ac.be/bwm/paper/maec03a.pdf (22 April 2008).

Maia, N.M.M., Silva, J.M.M, He, J., Lieven, N.A.J., Lin, R.M., Skingle, G.W., To, W.M., Urgueira, A.P.V. (1997), "*Theoretical and experimental modal analysis*." Edited by: Nuno, M.M, Maia, J.M and Silva, M. 1st Edn, Research Studies Press Ltd, Baldock, England.

McCann, D.M., Forde, M.C. (2001). "Review of NDT methods in the assessment of concrete and masonry structures." *NDT & International*, 34, 71-84.

Moyo, P. (2008): UCT Civil Engineering senior lecturer, "Problems in Vander-Kloof and Gariep bridges." *Informal Discussion*, 9/2, 2008. Vander-Kloof

Moyo, P., Alexander, M.G. (2006), "Condition assessment of bridges in South Africa: Challenges and opportunities." In Concrete repair, rehabilitation and retrofitting, Edited by: Alexander, M.G., Beushausen, H.D., Dehn, F., Moyo, P.1st Edn, London.

Ndambi, J.M., Vantomme, J., Harri, K. (2002), "Damage assessment in reinforced concrete beams using eigen-frequencies and mode shapes derivatives." *Engineering Structures*, 24, 502-515.

Nigel, R.H. (2003), "*Pre-stressed concrete bridges,' design and construction.*" 1st Ed, Thomas Telford, London.

Parkash, S., Goel, R., Kumar, R. (2006), "Fatigue performance of pre-stressed concrete bridges: State-of-the art." *Advances in Bridge Engineering*, 24(25), 479-486.

Queiroz, F.D., Vellasco, P.C.G.S., Nethercot, D.A. (2007), "Finite element modelling of composite beams with full and partial shear connection." *Journal of Construction Steel Research*, 63(4), 505-521.

Richardson, M., Schwarz, B. (2003), "Modal parameter estimation from operating data." *Sound and Vibration.*

Ronne', D.P, (2008), "Problems in Vander-Kloof and Gariep bridges." *Informal Discussion*, February 2008. Vander-Kloof,

Ryall, M.J., Parke, G.A.R Harding, J.E. (2003), "*Manual of Bridge Engineering.*" Thomas Telford Publishing, London.

Sameh, S., Badie, P.E., Tadros, P.E., Maher, K., Hussam, F.K., Darlin, L.S. (2002), "Large Shear Studs for Composite Action in Steel Bridge Girders." *Journal of Bridge Engineering*, Vol.7, No.3, 2002, 195-203.

Seracino, R., Lee, C.T., Lim, T.C., Lim, J.Y. (2004), "Partial interaction stresses in continuous composite beams under serviceability loads." *Journal of Construction Steel Research*, 60, 1525-1523.

Somerville, G., Tiller, R.M. (1975), "*Cement and Concrete Association: Standardised bridge beams for spans from 7 m to 36 m.*" 1st Edtn, London.

Sowman, R., Poree, N., (2000), "Situation report on heavy freight vehicle overloading control in South Africa." *Automobile Association of South Africa*, Kyalami. Cited by: Ackerman, C.A. (2007), "A vibration based model that rates bridge structural deterioration in a bridge management system." *PhD thesis*. Tshwane University of Technology, Pretoria, South Africa.
Available:http//:www.libserv5.tut.ac.za:7780/pls/eres/wpj_docload.download_file (17 January 2008).

Tailor, R. (1979), "*Composite reinforced concrete.*"1st Edn, Thomas Telford Limited, London.

Thambiratnam, D.P., Brameld, G.H. (1995), "Free vibration analysis of bridges." *Engineering Structures*, 17(10), 705-713.

Tamberg, K.G. (1968), "Aspects of torsion in concrete structure design, In *Torsion of concrete structures.*" 1st Edtn, ACI Publications, Michigan, USA.

Wahab, M.M.A., De Roeck, G. (1999), "Damage detection in bridges using modal curvatures: Application to a real damage scenario." *Journal of Sound and Vibration*, 2(227), 217-235.

Vibrant Technology, Inc (2007), "Visual Modal Educational, ME'scopeVES software." Version 4.0.0.96.

Wang, A.J., Chung, K.F. (2008), "Advanced finite element modelling of perforated composite beams with flexible shear connectors." *Journal of Engineering Structures*, 1000-1016.

West, R. (1971*), "Cement and Concrete Association: Recommendations on the use of grillage analysis for slab and pseudo-slab bridge decks.*" 1st Edn,, London.

Wium, D.J.O., Aucamp, G.H.P., Ullmann, M., Duncan, K.K.A.B., Nordengen, P.A. (1994), "The effect of an increase in the permissible heavy vehicle loads on road bridges." *Research Report RR 91/004*, Department of Transport, Pretoria. *Cited by*: Ackerman, C.A. (2007), "A vibration based model that rates bridge structural deterioration in a bridge management system." *PhD thesis*. Tshwane University of Technology, Pretoria, South Africa.

Womack, K.C., Halling, M.W. (1999). "Forced vibration testing of I-15 South Temple Bridge." A research report submitted to the Utah Department of Transportation, Available on line: http://www.udot.utah.gov/main/uconowner.gf (08 February 2008).

Xia, Y., Hong, H., Deeks, A.J. (2007), "Dynamic assessment of shear connectors in slab-girder bridges." *Engineering Structures*, 29, 1475-1486.

APPENDICES

Appendix A- Material Properties

Determining E-Modulus for the Beams

Sample No. 1

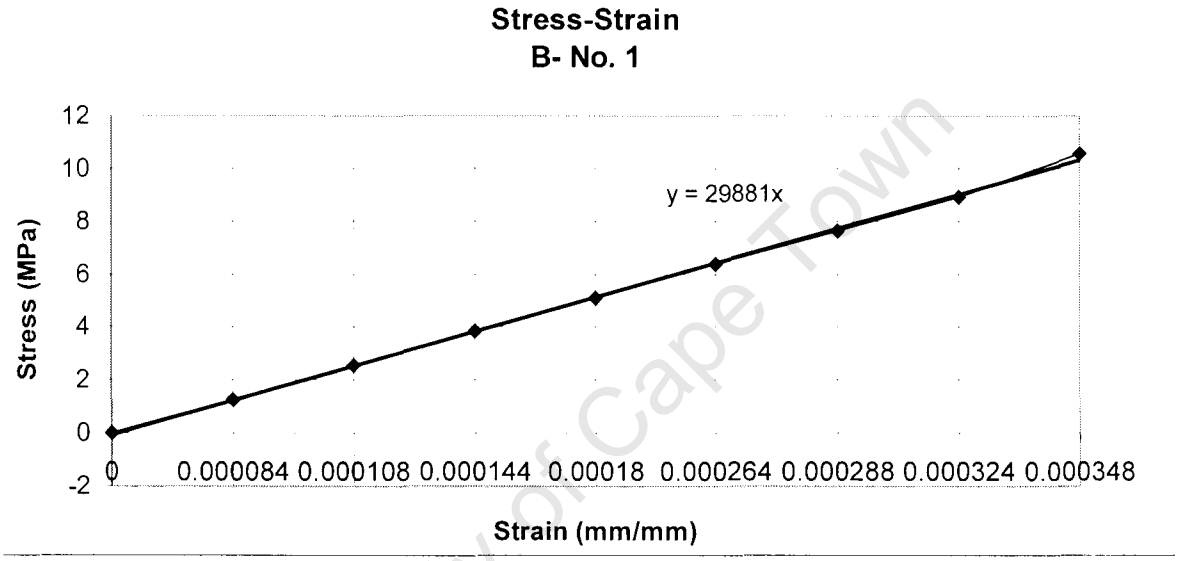

Sample No. 2

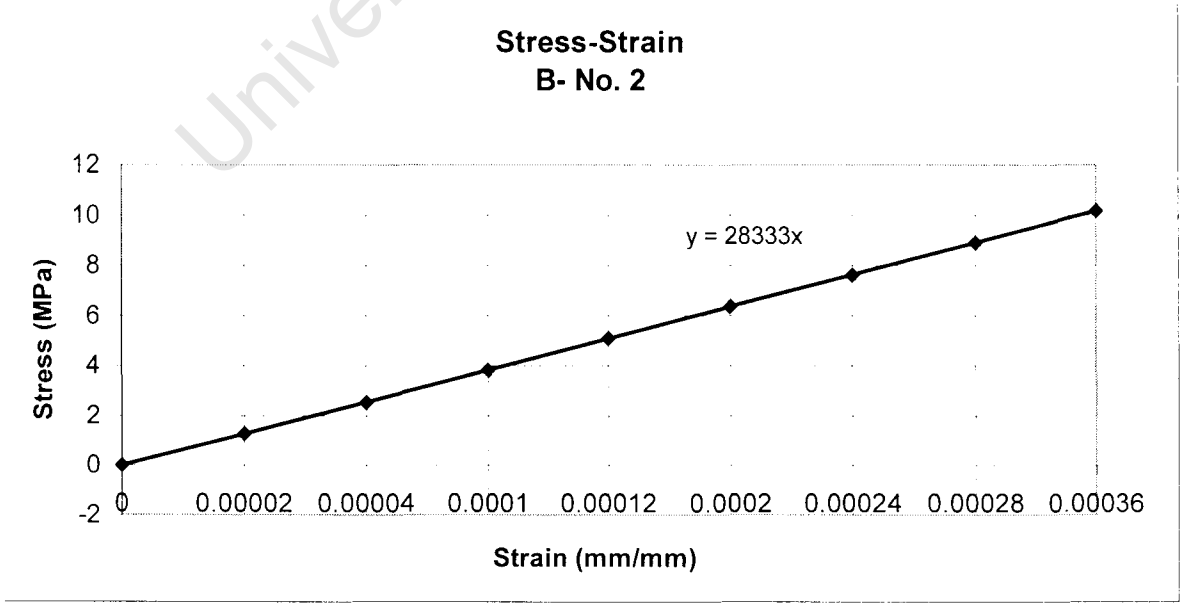

Appendix A cont…

Sample No. 3

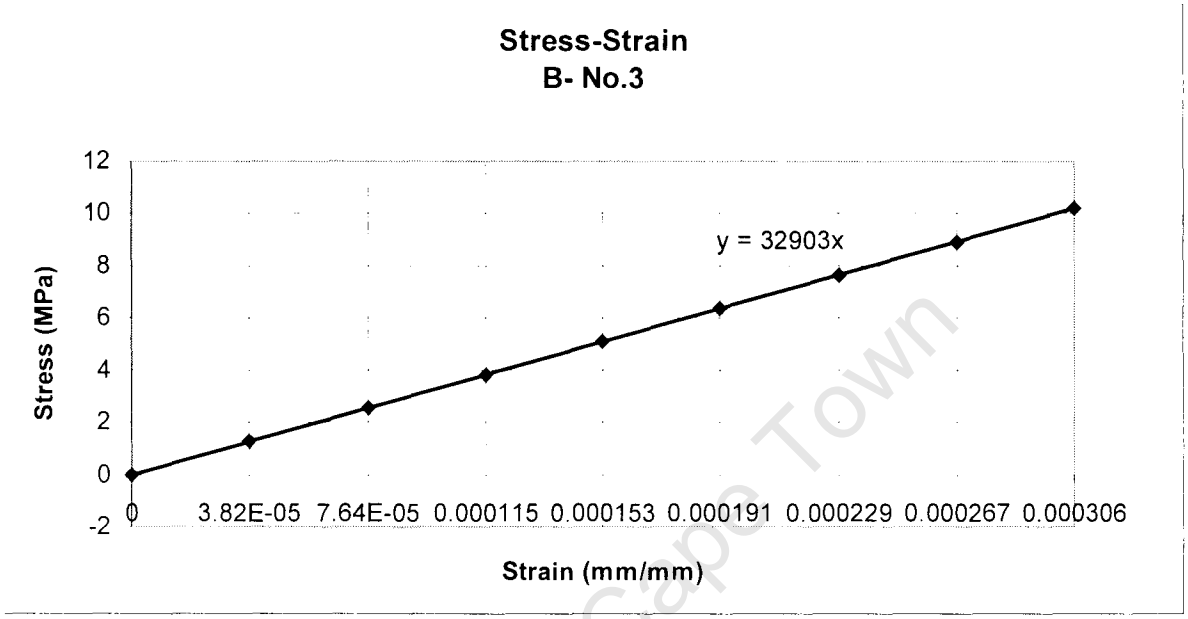

Determining E-Modulus for the slab

Sample No. 1

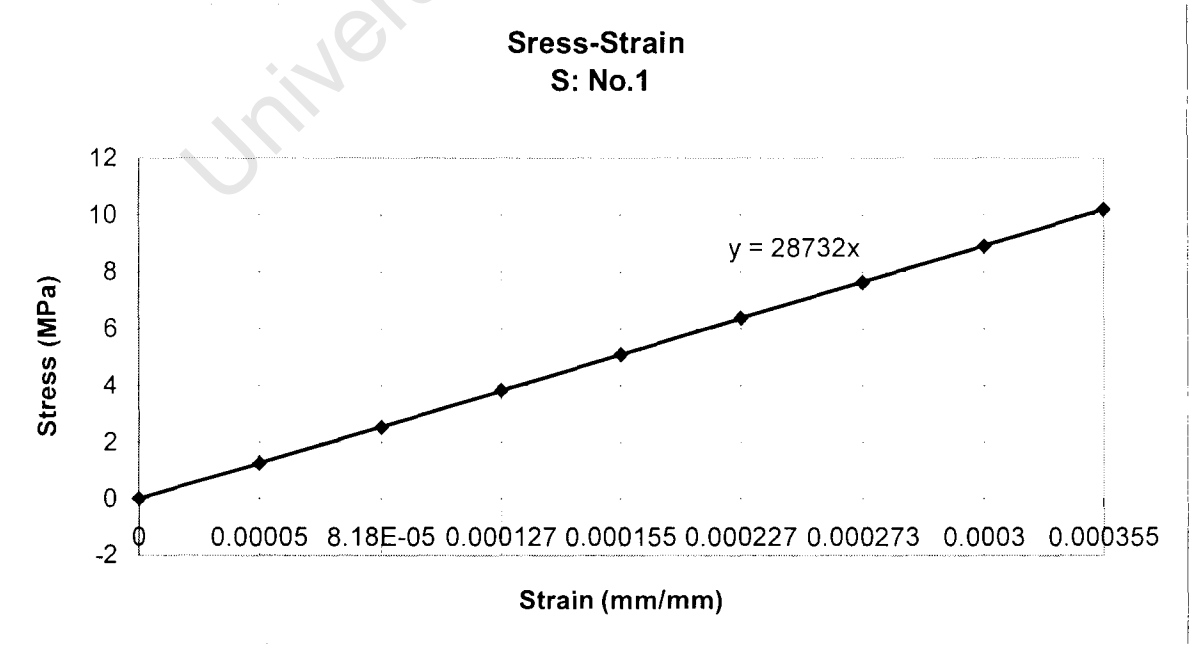

Appendix A cont…

Sample No. 2

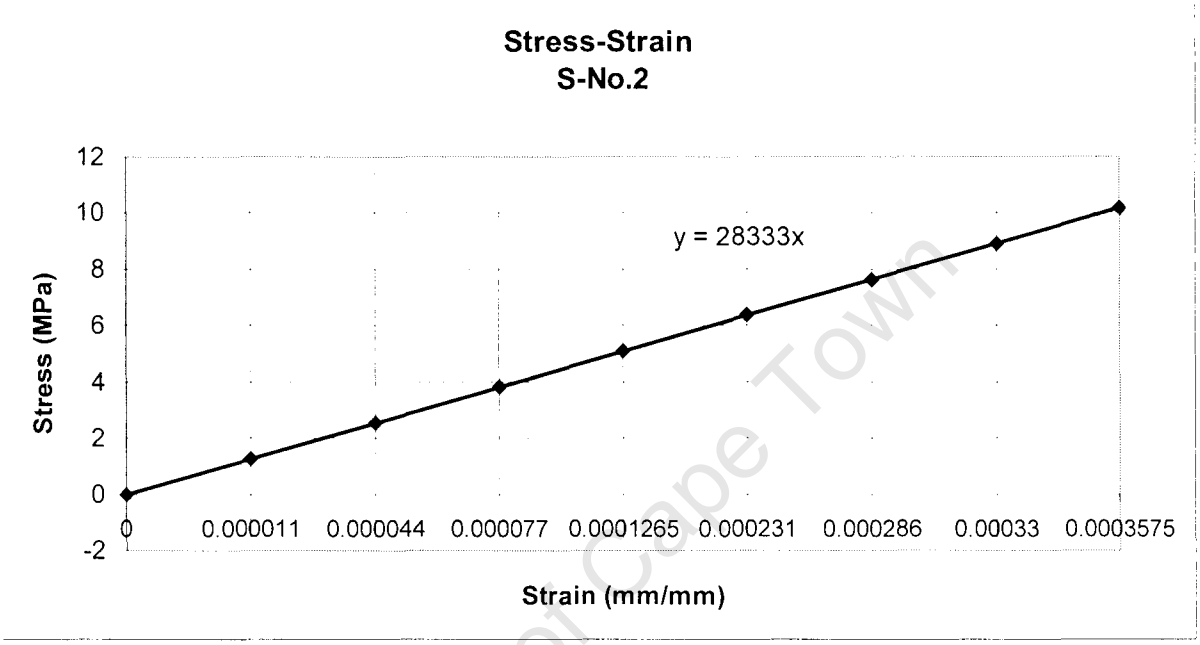

Sample No. 3